The Study of Nanostructured Solar Selective Coatings

This thesis is submitted in partial fulfillment of the requirements for

Master of Science (By Research) in Electronics Engineering

Yuyi Yang

Department of Electronics

University of York

March 2012

Abstract

In this thesis, nanostructured solar selective coatings used in solar thermal collectors are explored. The nanostructured stainless steel-aluminum nitride (SS-AlN) solar selective coating, a typical solar absorber, has been studied in terms of surface morphology, optical characterization, heat treatment and calculation optimization. Additionally, the potential of using the Fe_3O_4 nanoparticles coating as a solar absorber has been investigated. A green chemical method of co-precipitation is employed to prepare the Fe_3O_4 nanoparticles. The coating of Fe_3O_4 nanoparticles is formed on the copper substrate using dip-coating process. The effects of the thickness, substrate roughness and heat treatment on the performance of the Fe_3O_4 nanoparticles coating have been then analyzed.

The nanostructured SS-AlN solar selective coatings were deposited by sputtering on the glass substrates. The detailed structure of the sample as confirmed by the TEM images is as follows: AlN (73nm)/ SS-AlN (LMVF) (20nm)/ SS-AlN (HMVF) (30nm)/ AlN (8nm)/ Cu. The absorptance denoted by a and the emittance denoted by ε are 0.9033 and 0.1317, respectively, as measured by spectrometers. After being annealed below 500℃ for 1 hour, the SS-AlN solar selective coating has a higher absorptance and a lower emittance compared to the unannealed sample. Especially when annealed between 200℃ and 300℃， its absorptance increases while the emittance decreases, as a result a is 0.9378 and ε is 0.11. However, an annealing process above 500℃ was found to cause considerable damage on the SS-AlN samples. By using Matlab's simulation tool, the structure of SS-AlN solar selective coating is optimized as: SiO2 (40nm)/AlN (30nm)/SS-AlN (f2=0.25, d2=30nm)/SS-AlN (f3=0.33, d3=50nm)/AlN (8nm)/Cu. We found that a double antireflective layer helps to improve the absorptance.

The Fe_3O_4 nanoparticles prepared by co-precipitation are needle-like with an average

size estimated around 20 nanometers. With the number of dip times increasing, the thickness of Fe_3O_4 nanoparticles coating is enhanced which, however, leads to an unfavorable detach of the film. In terms of the effects of substrate roughness, we found that: 1) the Fe_3O_4 nanoparticles coating bonded better with rough copper substrate; 2) the coating on a polished copper substrate has higher reflectance in infrared region than that on a rough copper substrate, which contributes to reduce thermal emittance. The thermal emittance of the Fe_3O_4 nanoparticles coating reduces after the heat treatment at 100℃, 200℃, and 300℃. We found that the optical properties of coating have been significantly improved when annealed at 100℃, i.e. a=0.926, ε=0.378. Annealed above 200℃, however, the absorptance of the coating decreases.

Contents

List of Figures ..... **VI**

List of Tables ..... **IX**

Acknowledgements ..... **X**

Declaration ..... **XI**

Chapter 1 Introduction **1**

1.1 Background 1

1.2 Project Objectives 3

1.3 Project Outlines 3

Chapter 2 Literature Review **4**

2.1 Theoretical Background of Solar Selective Surface 4

2.1.1 Electromagnetic Radiation 4

2.1.2 Characterization of the Solar Selective Surface 6

2.2 Development of the Solar Selective Surface 9

2.2.1 Types of the Solar Selective Surfaces 9

2.2.2 Fabrication Techniques 13

2.3 Metal-Dielectric Composite Solar Selective Coating 16

2.3.1 Effective Medium Theory 16

2.3.2 Thin Film Optics 18

2.3.3 M-AlN Solar Selective Coating 21

Chapter 3 Experimental Methods **23**

3.1 Sample Preparation 23

3.1.1 Co-precipitation of Particles 23

3.1.2 Dip-Coating 23

3.1.3 Sputtering of Thin Films 24

3.2 Heat Treatment 25

3.3 Optical Characterization 26

3.3.1 Filmetrics F10-RT Spectroscopy....26
3.3.2 Equinox 55 Fourier Transform (FT-IR) spectroscopy....27
3.4 Non-Optical Characterization....28
3.4.1 Scanning Electron Microscopy （SEM） 28
3.4.2 Transmission Electron Microscopy (TEM)....29
3.4.3 Alpha-step Profiler....32
3.5 Simulation of the Multilayer Solar Selective Coating....33
3.5.1 Calculation of the Multilayer Solar Selective Coating....33
3.5.2 MATLAB Simulation Program....34
Chapter 4 Nanostructured SS-AlN Solar Selective Coating....39
4.1 Morphology and structure....40
4.2 Optical Characterization....45
4.3 Heat Treatment....46
4.3.1 Surface Morphology....46
4.3.2 Optical properties....48
4.4 Calculation Optimization....52
4.5.1 Optimization of the Absorbing Layers....54
4.5.2Optimization of the Antireflection Layer....57
4.6 Summary....59
Chapter 5 Fe_3O_4 Nanoparticles Solar Selective Coatings....60
5.1 Fe_3O_4 Nanoparticles Synthesis and Film Formation....60
5.2 Characterization of Fe_3O_4 Nanoparticles....62
5.3 Thickness Analysis....63
5.3.1 Thicknesses Measurement of Coatings with Different Dip Times....63
5.3.2 Surface Morphology....64
5.4 Substrate Roughness Analysis....66
5.4.1 Surface Morphology....66
5.4.2 Optical Characterization....68

5.5 Heat Treatment 69
5.5.1 Surface Morphology 70
5.5.2 Optical Characterization 71
5.6 Summary 72
Chapter 6 Conclusions and Future Work 73
6.1 Summary and Conclusions 73
6.2 Future work 74
Bibliography 75

List of Figures

Figure1.1 Three forms of solar energy conversion [2].....1

Figure2.1 Solar hemispherical spectral irradiance for AM1.5 and blackbody radiation spectra calculated from Planck's law for three different temperatures (100 ℃，200 ℃，300 ℃) [15]. 7

Figure2.2 Spectral performance of an ideal selective solar absorber [6].....8

Figure2.3 Schematic design of semiconductor coating 9

Figure 2.4 Schematic design of Multilayer absorbers.....10

Figure2.5 Schematic design of metal-dielectric composite coatings [6]. 11

Figure2.6 Schematic design of texture surfaces [6]. 12

Figure2.7 Schematic design of selectively solar-transmitting coating on a blackbody like absorber 13

Figure2.8 Microstructures of (a) separated-grain, (b) aggregate structure for a two component composite, (c) and (d) are the random unit cells to derive the effective dielectric function of Maxwell-Garnett model (separated-grain structure) and Bruggeman model(aggregate structure), respectively [15]. 17

Figure2.9 Reflection and refraction at a plane interface [15]. 18

Figure2.10 A multilayer stack scheme of K layers on a metallic substrate [15].....20

Figure2.11 3-target DC current magnetron sputtering system [48] 22

Figure3.1 Thermal Oxidation Furnace used for heat treatment 25

Figure3.2 Filmetrics F10-RT spectroscopy.....27

Figure3.3 Equinox 55 Fourier Transform (FT-IR) spectroscopy 28

Figure3.4 Layout of components in a basic TEM [65] 30

Figure3.5 Tungsten filament electron source [66]. 31

Figure3.6 Tencor alpha-step profiler.....32

Figure3.7 Working environment of MATLAB software.....35

Figure3.8 A structure of SS-AlN solar selective coating 35

Figure4.1 Pieces of the sunshore's all-glass evacuated solar collector tubes with SS-AlN solar selective coating. 40
Figure4.2 Structure scheme of the sunshore's SS-AlN solar absorber. LMVF is low metal volume fraction, HMVF is high metal volume fraction. 40
Figure4.3 SEM images of SS-AlN solar absorber 41
Figure4.4 TEM cross-section image of SS-AlN solar absorber.....42
Figure4.5 EDS images in A, B, C layers of SS-AlN solar absorber. 44
Figure4.6 Estimated Structure of SS-AlN samples based on its TEM image.....44
Figure4.7 Measured reflectance spectrum of sunshore's SS-AlN solar absorber. 45
Figure4.8 SEM images of SS-AlN solar absorbers after annealing at different temperatures.....48
Figure4.9 Reflectance spectra of unannealed and annealed SS-AlN coatings with different annealing temperature (100 ℃, 200 ℃, 300 ℃, 400 ℃) 49
Figure4.10Transmittance spectra of annealed SS-AlN sample at 500 ℃, 600 ℃ and 700 ℃. 50
Figure4.11 Images of unannealed and annealed sample at 500 ℃, 600 ℃ and 700 ℃.51
Figure4.12 Structure (a) and calculated reflectance spectrum (b) of the SS-AlN solar absorber sample 53
Figure4.13 Calculated spectra of SS-AlN soalr absorbers with different thickness of the absorbing layers. 54
Figure4.14 Calculated spectra of SS-AlN solar absorbers with different thickness of HMVF SS-AlN layer. 55
Figure4.15 Calculated spectra of SS-AlN solar absorrs with different thickness of LMVF SS-AlN layer 56
Figure4.16 Optimized structure of SS-AlN solar absorbers with double antireflection layers.....57
Figure4.17 Optimized reflectance spectrum of SS-AlN solar absorber with double antireflection layers (m) and reflectance spectrum of SS-AlN solar

absorber with single antireflection layer (l).....58
Figure5.1 Fe_3O_4 Nanoparticles preparation 61
Figure5.2 The TEM image of Fe_3O_4 nanoparticles.....62
Figure5.3 The thicknesses of Fe_3O_4 nanoparticles coatings on polished copper substrate with different dip times. (a) one dip, (b) two dips, (c) three dips. They are measured by Alpha-step Profiler. 64
Figure5.4 SEM images of Fe_3O_4 nanoparticles coatings on polished copper substrate with different dip times. (a) coating with one dip, (b) coating with two dips, (c) coating with three dips. 65
Figure5.5 Images of polished and rough copper substrates 66
Figure5.6 SEM images of Fe_3O_4 nanoparticles coatings on polished copper substrate (a) and rough copper substrate (b). 67
Figure5.7 Measured reflectance Spectra of Fe_3O_4 nanoparticles coatings on polished and rough copper substrates. 68
Figure5. 8 Images of Fe_3O_4 nanoparticles coatings on polished copper substrates: (a) unannealed, (b) annealed at 100 ℃ for 1 hour, (c) annealed at 200 ℃ for 1 hour, (d) annealed at 300 ℃ for 1hour. 69
Figure5.9 SEM images of Fe_3O_4 nanoparticles coatings on polished copper substrates. (a) unannealed, (b) annealed at 100 ℃ for 1 hour, (c) annealed at 200 ℃ for 1 hour, (d) annealed at 300 ℃ for 1 hour. 70
Figure5. 10 Measured reflectance spectra of Fe_3O_4 nanoparticles coating on polished copper substrate and that after annealing at 100 ℃, 200 ℃, 300 ℃ for 1 hour. 71

List of Tables

Table4.1 Absorptance and emittance of unannealed and annealed SS-AlN coatings with different annealing temperature (100 ℃, 200 ℃, 300 ℃, 400 ℃).....49

Table4.2 Absorptance and emittance of calculated SS-AlN coating with different thickness of absorbing layer. 54

Table4.3 Absorptance and emittance of calculated SS-AlN coating with different thickness of HMVF SS-AlN layer. 55

Table4.4 Absorptance and emittance of calculated SS-AlN coating with different thickness of LMVF SS-AlN layer. 56

Table4.5 Absorptance and emittance of calculated SS-AlN coating with single antireflection layer and double antireflection layers 57

Table5.1 Absorptance and emittance of Fe3O4 nanoparticles coatings on polished copper substrates and that after annealing. 72

Acknowledgements

I would like to first express my sincere gratitude to my supervisor, Prof. Yongbing Xu, for his support and encouragement during my MSc (by research) study.

I would like to thank Dr. Eugene (Evgeny) Avrutin and Dr. Jing Wu for their helpful suggestions on Optics. I am grateful to Dr. Iain Will for his technical support and guidance. I also appreciate the help from Prof. Jianguo Zheng for TEM images and Mr. Paul Elliott for spectrometers. I would also like to thank my collaborator: Mark Williams for his kind assistance and all the members of our group: Dr. Daxin Niu, Xuefeng Hu, An Ding, Cong Lu, Yang Yang, and Jiazhuo Chen, etc.

During the MSc study, my parents provide me tremendous encouragement and persistent support. Their encouragement gave me the confidence to overcome all challenges in the life in UK. I would like to thank them for their deep love and support. Also, I am grateful to Jingjing Liu for his support and help.

Declaration

I declare that this thesis is my own work and has not been submitted in any form for another degree or diploma at any university or other institution of tertiary education. Information derived from the published or unpublished work of others has been acknowledged in the text and a list of references is given.

Yuyi Yang

March 2012

Chapter 1 Introduction

1.1 Background

Nowadays, energy demands are continually increasing due to the rapid industrial development. However, the use of fossil fuel to deal with this problem is extremely limited and has brought a series of environmental problems. One of these problems is the release of carbon dioxide resulting in the depletion of ozone layer and affecting the balance of the global environment. Therefore, looking for alternative green energy resources becomes a central issue and has drawn a lot of interests in research.

Solar energy, as a green and renewable resource, is abundantly available over most of the planet world. It is reported that the amount of solar energy delivered to the earth every year is up to 1×10^{18} kW ħ, which is almost ten thousand times that of the energy humanity uses annually [1]. As illustrated in Figure 1.1, solar energy can be converted into three forms of energy, i.e. electricity, chemical fuel, and heat. Sunlight is converted into electricity by exciting electrons in a solar cell. Also, it can produce chemical fuel by natural photosynthesis in green plants or artificial photosynthesis in human-engineered systems. Finally, the thermal devices are used to collect and convert solar energy into heat for direct use at lower temperature (T<300 ℃) or creating steam for further electricity generation at high temperatures [2].

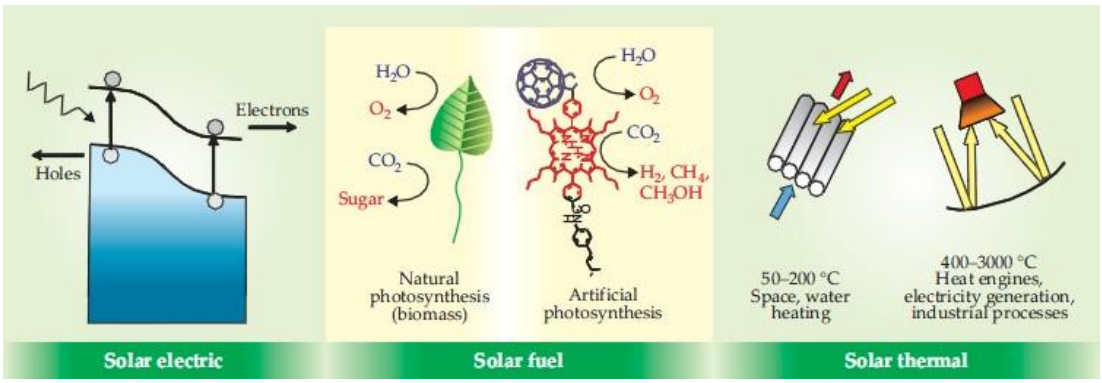

Figure1.1 Three forms of solar energy conversion [2].

Solar thermal energy has been widely studied and applied in many areas, e.g. water heating, space heating, space cooling and process heat generation [3]. The common types of solar thermal devices used for heating water are flat plate collectors and evacuated tube collectors [4]. The most important part of solar collectors is solar selective coatings, which directly affect the efficiency of the solar-to-thermal energy conversion. A selective solar absorber should exhibit high solar absorptance in the solar energy spectrum (0.3-2.5μm) to capture maximum solar energy, and low emittance in the infrared region (2.5-20μm) to reduce energy losses.

The solar selective coating was first investigated by Tabor in 1955 [5]. It was a tandem surface with a top absorbing layer deposited on an infrared reflective metal substrate. With the onset of the oil crisis, varieties of solar selective coatings have been researched, such as semiconductor coatings, multilayer absorbers, metal-dielectric composite coatings, and texture surfaces. Several techniques can be used to produce these solar selective coatings, generally divided into physical vapour deposition: electrochemical methods, painting, and sol-gel process [6]. The metal-aluminum nitride (M-AlN) composite coatings are produced on a large scale by physical vapour deposition. For example, the stainless steel –aluminum nitride solar selective coatings made by a company (Sunshore) in China are produced by magnetron sputtering. Generally speaking, thicker M-AlN solar selective coatings have higher the thermal emittances. Thus, the M-AlN composite coating is usually nanostructured and the total thickness is less than 1μm [7]. Furthermore, particle-size in the absorbing layer plays an important role in achieving optimal spectral selectivity. It is widely accepted that the smaller particles avoid scattering [8]. The solar selective coatings of nanoparticles have been researched, such as coatings of Fe_3O_4 nanoparticles. However, the work on solar selective coatings of nanoparticles is very limited [8]. Therefore, the nanostructured solar selective coatings are studied in this thesis.

1.2 Project Objectives

- Learn various techniques to characterize the structural, optical and morphological properties of solar selective coatings
- Study the typical nanostructured SS-AlN solar selective coatings and, in particularly, the effects of annealing.
- Research the potential of Fe_3O_4 nanoparticles coating as a solar absorber.

1.3 Project Outlines

- Chapter 2 Literature Review

  This chapter introduces theoretical background electromagnetic radiation and characterization of solar selective coatings. It also summarizes the development of solar selective coatings. The calculation theories of metal-dielectric coatings are also explained.
- Chapter 3 Experiment Methods

  Chapter 3 deals with experimental methods including sample preparation, optical measurement, non-optical characterization and simulation of SS-AlN solar selective coating by MATLAB program.
- Chapter 4 Nanostructured SS-AlN Solar Selective Coatings

  Chapter 4 studies the structural, optical and morphological properties of the commercial SS-AlN solar selective coatings. It then studies the properties of SS-AlN absorber samples after heat treatment and finally the structure of SS-AlN as optimized by simulation program.
- Chapter 5 Fe3O4 Nanopaticles Solar Selective Coatings

  A green chemical method of co-precipitation and dip-coating are employed to prepare the Fe_3O_4 nanoparticles coatings on the copper substrate. The effects of the thickness, substrate roughness and heat treatment on Fe_3O_4 nanoparticles coatings are further studied.
- Chapter 6 Conclusion

Chapter 2 Literature Review

2.1 Theoretical Background of Solar Selective Surface

2.1.1 Electromagnetic Radiation

Electromagnetic Phenomena are recognized as electromagnetic fields produced by a distribution of electric charge and current. J. C. Maxwell was the first to propose a theory of Classical Electromagnetism in 1865 and predicted that light is a form of electromagnetic radiation. Electromagnetic radiation is classified based on its frequency. Specifically, as parts of Electromagnetic spectrum, solar radiation of λ=0.3~2.5μm and Thermal radiation of λ=2.5~50μm are important for solar energy applications.

2.1.1.1 Thermal Radiation

Thermal Electromagnetic Radiation is emitted from any objects with a temperature above absolute zero. The wavelength and intensity of the radiation are determined by the temperature of the body and its optical properties. A blackbody is an ideal physical body that absorbs all incident radiation and emits the maximum amount of energy for a given temperature. It is usually used as a reference to compare with the properties of real surfaces. Plank's law [9] gives the spectral blackbody radiation as:

$$B(\lambda, T) = c_1 \lambda^{-5} (e^{\frac{c_2}{\lambda T}} - 1)^{-1} \qquad (2.1)$$

where $c_1 = 3.7405 \times 10^8\ W\mu m^4/m^2$ and $c_2 = 1.43879 \times 10^4\ \mu mK$ are the first and second of Planck's radiation constants. The wavelength λ is given in μm and the spectral blackbody radiation $B(\lambda, T)$ in $W/m^2\mu m$ at a certain temperature T. The Stephan-Boltzmann law quantitatively defines the relation between the blackbody radiation and temperature as:

$$B(T) = \sigma T^4 \qquad (2.2)$$

where $\sigma = 5.6696 \times 10^{-8}\,\mathrm{W/(m^2K^4)}$ is the theoretical Stephan-Boltzmann constant, similar to the experimental result $\sigma_{exp} = 5.729 \times 10^{-8}\,\mathrm{W/(m^2K^4)}$ [10]. The law shows that the blackbody radiation is proportional to the fourth power of the absolute temperature. In other words, increasing the temperature by a factor of 2 could increase the radiation by a factor of 16.

2.1.1.2 Solar Radiation

The sun is approximately $1.496 \times 10^{11}\,\mathrm{m}$ away from the earth and emits over $3.8 \times 10^{23}\,\mathrm{kW}$ of solar radiation generated by nuclear fusion. The spectrum of the solar radiation is distributed from the long wavelength of infrared to the very short wavelength of gamma radiation. However, most of solar radiation is absorbed or scattered by atmospheric components such as oxygen, nitrogen, ozone, carbon-dioxide, water vapour. The actual solar irradiance incident on the earth throughout the year tends to a constant of $G_{sc} = 1367 \pm 1\%\,\mathrm{W/m^2}$, which is called as the solar constant [11]. About 8.03% of solar radiation to the earth is in the UV region, 46.41% in the visible region and the rest 46.40% in NIR region. Also, the effective blackbody temperature of the sun can be calculated from the solar constant through this equation [12]:

$$T = \left[\frac{G_{sc}}{\sigma}\left(\frac{r_0}{r_s}\right)^2\right]^{\frac{1}{4}} \qquad (2.3)$$

where G_{sc}, r_0 and r_s are the solar constant, the sun-earth distance and the mean radius of the solar. From the equation, the effective blackbody temperature of the sun is 5777K.

The different level of irradiance experienced on the earth's surface results from the variation of the solar azimuth found at different latitudes. By measuring the solar position, it is possible to calculate the air mass [12]. The air mass is defined as the ratio of optical mass in the direct optical path to that of the vertical path [13]. The variation

of air mass mainly effects the solar radiation density at short wavelengths. At a larger air mass number, more radiation is absorbed or scattered much stronger at the short wavelength, which alters the total density of the solar radiation. Generally, without absorbing and scattering, the solar radiation outside the atmosphere is referred to AM0. The air mass of 1.5(AM 1.5) is employed in order to characterize the optical properties of solar selective surfaces. AM1.5 is commonly used especially at higher latitudes [14].

2.1.2 Characterization of the Solar Selective Surface

The performance of the solar selective surface can be characterized by the absorptance and the thermal emittance. The solar absorptance is defined as the ratio of the absorbed radiation to the total incident radiation. Considering a opaque material with Kirchoff's Law, the spectral absorptance can be expressed in terms of total reflectance $R(\lambda, \theta)$,

$$\alpha(\lambda, \theta) = 1 - R(\lambda, \theta) \qquad (2.4)$$

where λ is the wavelength, θ is the incident angle of light, and $R(\lambda, \theta)$ includes the diffuse and collimated reflectance, which also depends on the temperature T. The solar absorptance can be obtained by combining this with the wavelength dependent solar spectrum $G(\lambda)$,

$$\alpha(\theta) = \frac{\int_{\lambda_1}^{\lambda_2} [1 - R(\lambda, \theta)] G(\lambda) d\lambda}{\int_{\lambda_1}^{\lambda_2} G(\lambda) d\lambda} \qquad (2.5)$$

where λ_1, λ_2 are minimum and maximum solar wavelengths, respectively. Using standard spectrophotometers, solar reflectance is usually measured in the 0.3-2.5μm wavelength range at near-normal ($\theta = 0$) angle of incidence [15].

The thermal emittance is another parameter that characterizes the performance of the solar selective surface in the infrared wavelength range. The thermal emittance can be described as the fraction of emitted radiation from the heated body as compared to the blackbody radiation at the same temperature. Because the thermal radiation is emit

from all directions, hemispherical thermal emittance is assumed [15]. Using Kirchhoff's law, for an opaque object, the thermal emittance relates to the absorptance as follows:

$$\varepsilon(\lambda, T) = 1 - R(\lambda, T) \qquad (2.6)$$

and the total hemispherical emittance at a given temperature T can be calculated from

$$\varepsilon(T) = \frac{\int_{\lambda_1}^{\lambda_2} [1 - R(\lambda, T)] B(\lambda, T) d\lambda}{\int_{\lambda_1}^{\lambda_2} B(\lambda, T) d\lambda} \qquad (2.7)$$

where $B(\lambda, T)$ is the blackbody radiation spectrum given in Equation(2.1). The emitted radiation from a body at low temperatures are mainly found in the infrared range, and thus 2.5μm and 50μm are used for λ_1 and λ_2. The thermal emittance of ideal blackbody is unity. For a solar selective surface, it is between 0 and 1.

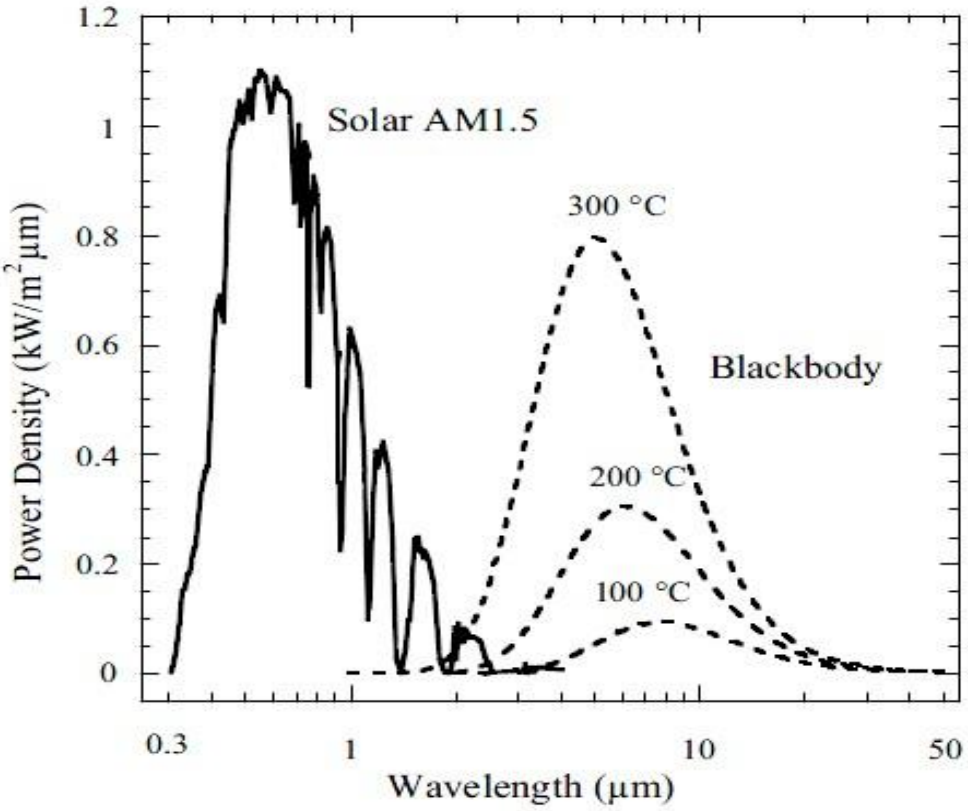

Figure2.1 Solar hemispherical spectral irradiance for AM1.5 and blackbody radiation spectra calculated from Planck's law for three different temperatures (100 ℃，200 ℃，300 ℃) [15].

The solar spectrum and blackbody spectra at three different temperatures are shown in Figure 2.1. From the figure, we can see that the solar spectrum is mainly distributed from 0.3-2.5μm, which does not overlap with the blackbody spectra. It also shows blackbody spectra at three different temperatures calculated by Planck's law. With the increase of the temperature, the amount of blackbody radiation increases and the peak wavelength shifts to the shorter wavelength. Using this knowledge, it is a possible to design a solar selective surface which absorbs as much solar radiation as possible and emits lowest thermal radiation. The solar selective surface was first proposed by Tabor [16], which has high absorptance (low reflectance) in the solar spectrum and the low emittance (high reflectance) in the infrared region. As an ideal solar selective surface, the reflectance is near zero in the solar spectrum and unity in the blackbody spectrum at a given temperature, as in Figure2.2. For a real solar selective surface, the absorptance $\alpha < 1$ and the thermal emittance $\varepsilon > 0$. A solar selective surface with high absorptance and low emittance is desirable.

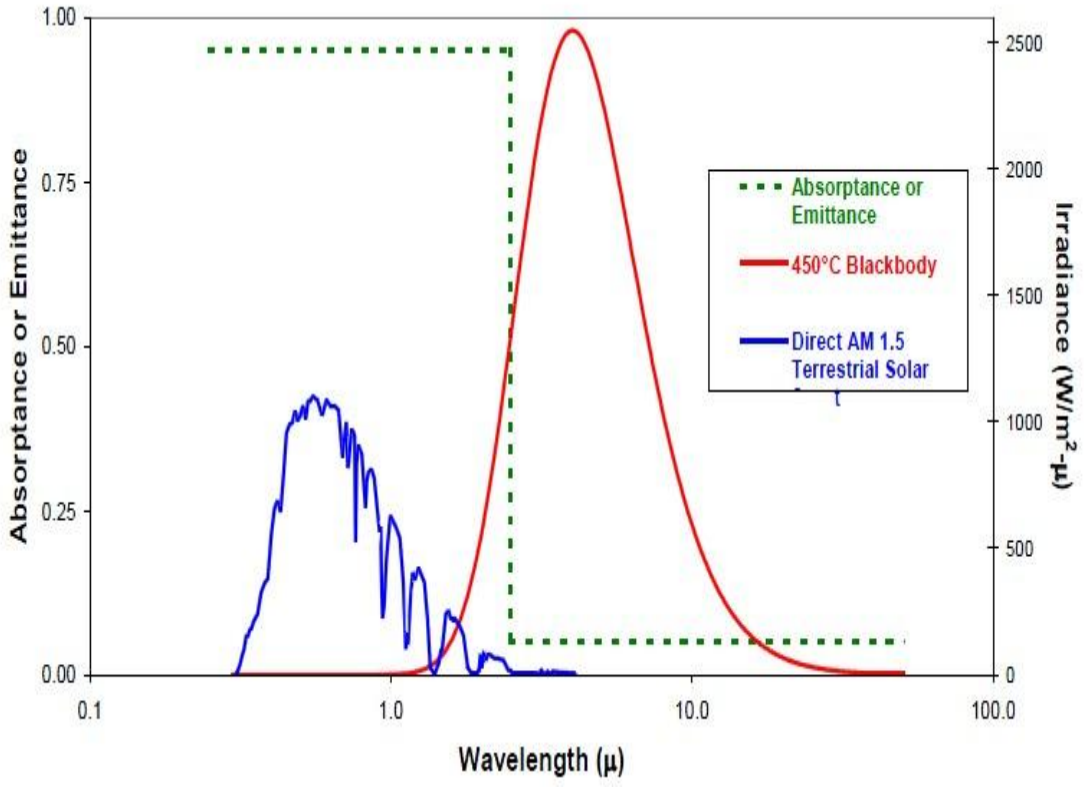

Figure2.2 Spectral performance of an ideal selective solar absorber [6].

.

2.2 Development of the Solar Selective Surface

Since the 1950's, the solar selective surfaces has become a popular topic in the solar energy applications and attracted much research. This has resulted in plenty of work in the materials selection, structures and fabrications [6] [17-19]. Due to the different principles and structures used, the solar selective surfaces can be categorized into five types, semiconductor coatings, multilayer absorbers, metal-dielectric composite coatings, textured surfaces, and selectively solar-transmitting coating on a blackbody-like absorber. In addition, there are various techniques for preparing the solar selective surface such as physical vapour deposition (PVD), electrochemistry, chemical vapour deposition (CVD), spraying and sol-gel process, etc.

2.2.1 Types of the Solar Selective Surfaces

Semiconductor Coatings

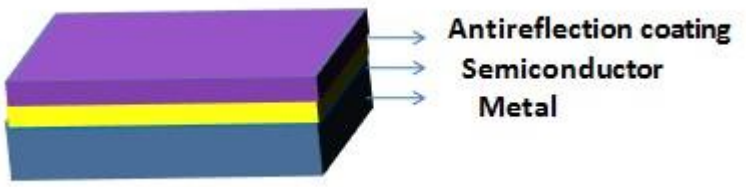

Figure2.3 Schematic design of semiconductor coating.

Semiconductors usually have band gaps from 0.5eV (2.5μm) to 1.26eV (1.0μm). Some semiconductors with low band gaps can absorb the solar radiation. More specifically, the semiconductor coatings absorb the photons with energy greater than the band gap energy, which results in exciting electrons in the material's valence band into the conduction band. The photons with energy less than the band gaps are directly transmitted through the semiconductor coatings. Thus, some semiconductors with low band gaps are suitable for the solar selective coating, such as silicon(1.1eV),

germanium (0.7eV), and lead sulfide (PbS)(0.4eV) [20].

To achieve a high solar absorptance, the refractive index of the solar selective surface needs to be as low as possible. However, the semiconductor coatings have high refraction index, which lead to the large reflectance losses. There exist some approaches to reduce the reflectance, one of which is to obtain a destructive interference interface by controlling the thickness of the coating, while another is to add an antireflection coating on the top of the semiconductor coating to reduce reflectance. An example, a $SiO_2/Si_3N_4/Si/Cr_2O_3/Ag/Cr_2O_3$ selective coating is made by chemical vapour deposition on stainless steel, which has antireflection coatings SiO_2/Si_3N_4. An absorptance of 0.85 and thermal emittance of 0.07 at 500 ℃ are achieved [21]. Improvements can be suggested by adding a thin layer of germanium to increase the solar absorptance. The absorptance of 0.5μm Ge layer and 2.0μm Si layer with a Si_3N_4 antireflection coating reaches 0.89 and its thermal emittance at 500 ℃ is 0.0545 [22]. Alternatively, an evaporated PbS semiconductor coating on aluminum gives α/ε(100 ℃) = 0.93-0.99/0.21-0.038 [23]. But the PbS coating is only stable below the temperature 300 ℃ [24]. In general, the silicon, germanium, lead sulfide can be deposited by gas and vacuum evaporation, chemical vapour deposition as semiconductor coatings for solar absorber application.

Multilayer Absorbers

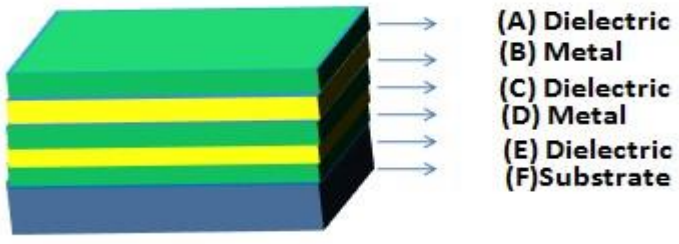

Figure2.4 Schematic design of Multilayer absorbers

The optical characters of multilayer absorbers are determined by interference effects of reflected light between different interfaces and the incident light. The typical structure of multilayer absorber is shown in the Figure (2.4). The selective effect is caused by the multiple reflections when the light passes through the layers A-E and has no relation to the selectivity of the bottom dielectric layer (E). The thin metal layer (D), acts a infrared reflecting layer which has high reflectance in the infrared region and less reflectance at visible region. It separates two quarter-wave dielectric layers (C and E). The upper dielectric layer (C) reduces the reflectance in the visible region. Another metal layer (B) further reduces the visible reflectance and the dielectric layer (A) increases the absorption in the visible region. The multilayer absorbers have high solar absorption, low thermal emittance, which can be optimized by computer modeling [25-26]. Some metals (e.g., Mo, Ag, Cu, Ni) and dielectric materials (e.g., Al_2O_3, SiO_2, CeO_2, ZnS) have been applied for high-temperature multilayer absorbers [27].

Metal-Dielectric Composite Coatings

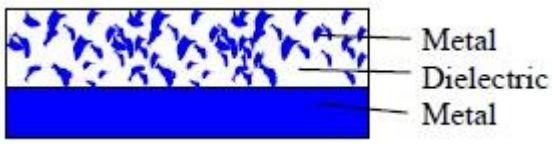

Figure2.5 Schematic design of metal-dielectric composite coatings [6].

Metal-dielectric composite coatings are surfaces consisting of fine metal particles in a dielectric matrix, deposited on the highly IR-reflective metal substrate. The metal particles are usually transition metal and could either be uniformly embedded in the matrix or gradually increasing the metal volume fraction from the surface of the film. These types of the coatings are transparent in the thermal infrared region and strongly absorbing in the solar region because of interband transitions in the metal and the small particle resonance [15]. The optical properties of metal-dielectric composite coatings can be optimized by changing coating thickness, metal volume fraction, and particle size, shape, orientation. Therefore, the design of composite coating is rather flexible.

Typically, the composite coatings range from 0.5 to 1.0 μm in thickness, 0.3 to 0.4 metal volume fraction, and have a solar absorptance of 0.94 to 0.97, a thermal emittance of around 0.1 to 0.2 [28-31]. Some metal-dielectric composite coatings including Mo-Al_2O_3, Ni-NiO_x, Cr-Cr_2O_3, Ni-Al_2O_3, Ni-AlN and Ni-pigmented alumina, have been commercially applied in solar collectors [32-35].

Textured Surfaces

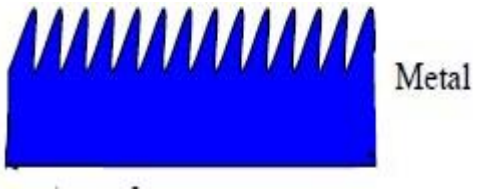

Figure2.6 Schematic design of textured surfaces [6].

Textured surface can be produced by creating texture with suitable scale on highly reflective metal substrate. The textured surfaces have different effects in the short and long wavelength radiation. For short wavelength radiation, the surface looks rough and absorbs solar energy by trapping the light through the geometric effects of multiple reflection and absorption. While, for long wavelength radiation, the surface seems smooth, therefore the mirror-like surface reflects the light to achieve low emittance.

A dendrite structure of rhenium, nickel and tungsten made by chemical vapour deposition and rough copper, nickel, and stainless steel produced by sputter etching are both examples of texture surfaces [15][36-39]. Al-Si Alloy (20 vol.% Si) prepared by co-evaporation of two electron-beam sources on a glass substrate and then chemically etched in a NaOH solution to form an texture surfaces caused from the preferential etching of the aluminum phase [40]. Consequently, the microstructure of the texture surface can be understand as comprising of top absorbing layer of air filled metal and highly reflecting metal substrate.

Selectively Solar-Transmitting Coating on a Blackbody-like Absorber

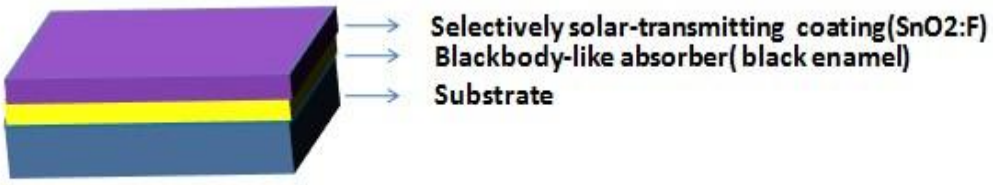

Figure2.7 Schematic design of selectively solar-transmitting coating on a blackbody-like absorber.

A blackbody-like absorber usually has high absorption and emittance. A selectively solar–transmitting coating has high reflectance in the infrared thermal region and transparent in the solar region. Therefore, a selectively solar-transmitting coating deposited on a blackbody-like absorber can achieve high absorption and low thermal emittance. A selectively solar-transmitting coating can be a highly doped semiconductor, for example, SnO_2: F, SnO_2: Sb, In_2SO_3: Sn. Some low temperature solar collector use black enamel as the absorber, which has absorptance of 0.91 an emittance of 0.14 at 300 ℃ [41].

2.2.2 Fabrication Techniques

Physical Vapour Deposition (PVD)

Sputtering and evaporation are two basic methods of thin film deposition. They are widely deployed and require high vacuum systems.

(1)Evaporation

The principle of evaporation is to heat the source material up to a sufficiently high temperature to vaporise it, and let it condense on the substrate to form a layer of thin film. Evaporation is widely used in thin film deposition, which has advantages including high deposition rate, simple process and low cost. However the thin films deposited by the evaporation do not bond well with the substrate. It is also hard to

evaporate the materials with high melting points such as platinum (Pt) and molybdenum(Mo). For the solar selective surfaces, PbS/Al coating deposited by evaporation has the absorption of 0.975 and the emittance of 0.15[24].

(2)Sputtering

Sputtering is a process that the atoms are ejected due to the bombardment of energetic particles on the source material and then deposited on the substrate to form a thin film. Compared with the evaporation, sputtering is easier to control the accuracy. In addition, the thin film by sputtering is more uniform and has better bonding with the substrate than the films deposited by evaporation. Magnetron sputtering has been applied on the solar selective coating due to its better control of the composition and thickness of the thin film, regardless of higher cost. The solar selective coatings prepared by sputtering include Al_2O_3/M-Al_2O_3 (M, metals include Ni, Co, Mo, Pt), and M-AlN, etc. Zhang Qi-Chu and Mills D. R studied the M-AlN solar selective coating created by d.c. sputtering, and showed that the absorptance is 0.92~0.94, the emittance is 0.08~0.10(350 ℃) [42].

Electrochemical Methods

Electrochemical methods, including Electroplating and the Anodic Oxidation Method, can be used to prepare various kinds of solar selective coatings.

(1)Electroplating

Electroplating refers to the process of moving metal irons in the solution by electric field to coat an electrode. The part to be plated is the cathode of the circuit. The solar selective coatings prepared by electroplating have good optical properties, such as black chrome. However, duo to its high cost, risk of pollution and bad thermal stability in high temperatures, electroplating is only suitable for low temperature solar energy applications.

(2)Anodic Oxidation Method

When the metal substrate is immersed in the phosphoric acid (H_2PO_4) solution and connected with the anode of the circuit, the surface forms a porous oxide layer. Then, the anodized sample is placed in metal salt solution for coloration, which amounts to

depositing the metal particles inside the pores of oxide layer by electrochemical deposition. The whole process described above is called Anodic Oxidation Method. The solar selective coatings made by anodic oxidation are thermally stable so that they can work at high temperature, such as anodizing aluminum coating [43], anodizing steel coating [44]. Usually, their absorptance is above 0.9 and the emissivity is around 0.1.

Painting

The painted coating consists of small particles (pigments) mixed with binders, which have good selective optical properties due to the high absorption of the pigment, well disseminated in the coating, and high reflection of the substrate in the infrared region. The painted coatings are usually painted, or sprayed, or dip-coated on the substrate to form solar selective absorbers. FeMnCuO4/silicon binder, PbS/polyacrylic resin are typical painted coatings. Even though the painting method is a simple, low cost process and suitable large-scale application, the painted coating usually has a high emittance and terrible bonding with the substrate.

Sol-Gel Process

The sol-gel process is a chemical method widely used in the solar selective coating preparation. In the process of sol-gel, the colloidal solution is obtained from some metal alkoxides and metal salts by various forms of hydrolysis and polycondensation reactions. This is then deposited to form a coating. The coatings fabricated by sol-gel process are uniform but easily damaged. The researchers show that the CuFeMnO4 coated on the Al plate by sol-gel process has the absorption of 0.85 and emissivity of 0.07 [45-46].

2.3 Metal-Dielectric Composite Solar Selective Coating

2.3.1 Effective Medium Theory

Effective Medium Theory is employed for the metal-dielectric composite coatings. For composite media consisting of small particles in a dielectric matrix, the dielectric constant is assumed to be equivalent to the dielectric constants of the homogeneous constituents. In effective medium theory, we adopt the quasistatic approximation which requires that the size of the grains is much less than the wavelength of the incident light. Generally, metal-dielectric composite solar selective coating is prepared by sputtering and the particle sizes is less than the wavelength of the solar and infrared region. Thus, the optical properties of the composite coatings can be calculated by Effective Medium Theory.

The most commonly used Effective Medium Theories are the Maxwell-Garnett [47] and Bruggeman [48] models. The Maxwell-Garnett model assumes that composite medium has a separated grain structure (Figure 2.8(a)), while the Bruggeman theory assumes an aggregate microstructure (Figure 2.8(b)).

The calculation can be simplified by using the random unit cell (RUC) of Figure 2.8 (c) (d). The random unit cell specifies that the grains in the composite are spherical and independent [49].

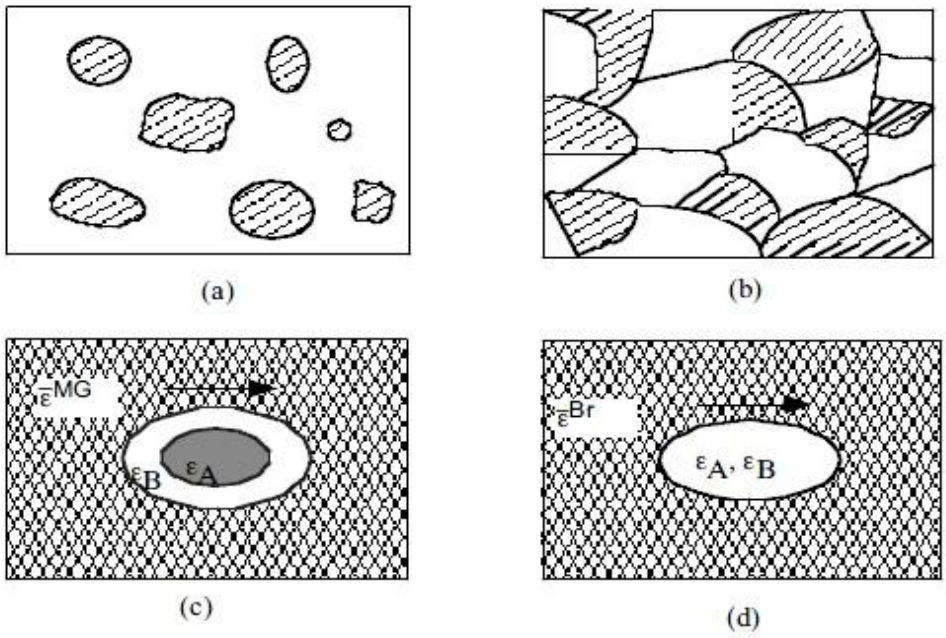

Figure2.8 Microstructures of (a) separated-grain , (b) aggregate structure for a two component composite, (c) and (d) are the random unit cells to derive the effective dielectric function of Maxwell-Garnett model (separated-grain structure) and Bruggeman model(aggregate structure), respectively [15].

Assuming that there are A and B in the composite (A is embedded in the B), the volume fraction (filling factor) of A in the whole composite is f_A and that of B is f_B, where $f_B = 1 - f_A$. The dielectric constants are ε_A and ε_B . According to Electrostatics, we can obtain the following equation [48]:

$$\frac{\varepsilon - \varepsilon_h}{\varepsilon + 2\varepsilon_h} = f_A \frac{\varepsilon_A - \varepsilon_h}{\varepsilon_A + 2\varepsilon_h} + f_B \frac{\varepsilon_B - \varepsilon_h}{\varepsilon_B + 2\varepsilon_h} \qquad (2.8)$$

where ε is the dielectric constant of the composite and ε_h is the dielectric constant of surrounding medium. In Maxwell-Garnett model, when A is embedded in B and B is the surrounding medium ($f_B > f_A$), $\varepsilon_h = \varepsilon_B$. Then the Maxwell-Garnett equation is

$$\frac{\varepsilon - \varepsilon_B}{\varepsilon + 2\varepsilon_B} = f_A \frac{\varepsilon_A - \varepsilon_B}{\varepsilon_A + 2\varepsilon_B} \qquad (2.9)$$

The Bruggeman Model is considered an aggregate structure, in which A or B is embedded in the mixture of A and B, $\varepsilon = \varepsilon_h$. Thus, the Bruggeman equation is given

by:

$$0 = f_A \frac{\varepsilon_A - \varepsilon}{\varepsilon_A + 2\varepsilon} + f_B \frac{\varepsilon_B - \varepsilon}{\varepsilon_B + 2\varepsilon} \qquad (2.10)$$

In terms of the application of the two models, Maxwell-Garnett model is suitable for the composite with high and low filling factor. For middle filling factor, there are clear errors between the real result and Maxwell-Garnett model. Thus, we usually adopt Bruggeman model for calculating the dielectric constant of a composite [48].

2.3.2 Thin Film Optics

2.3.2.1 Reflection and Transmission at a Plane Interface

When the lights travel from one medium with refractive index N_1 to another medium with N_2, reflection and refraction often occur on the plane interface of the two media. (Figure 2.9)

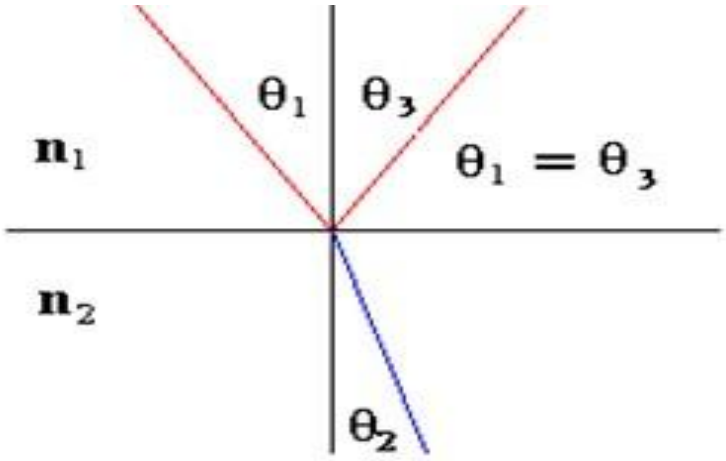

Figure2.9 Reflection and refraction at a plane interface [15].

According to the boundary conditions of the waves in the interface, we can derive the reflection equation:

$$\theta_1 = \theta_3, \qquad (2.11)$$

The law of refraction, Snell's Law, is:

$$N_1 \sin\theta_1 = N_2 \sin\theta_2 \qquad (2.12)$$

The amplitudes of the reflected (r) and transmitted (t) vectors can be derived by the continuity conditions for the Maxwell equations at the interface, which are Fresnel-coefficients:

$$r_s = \frac{N_1 \cos\theta_1 - N_2 \cos\theta_2}{N_1 \cos\theta_1 + N_2 \cos\theta_2} \qquad (2.13)$$

$$r_P = \frac{N_1 \cos\theta_2 - N_2 \cos\theta_1}{N_1 \cos\theta_2 + N_2 \cos\theta_1} \qquad (2.14)$$

$$t_s = \frac{2N_1 \cos\theta_1}{N_1 \cos\theta_1 + N_2 \cos\theta_2} \qquad (2.15)$$

$$t_p = \frac{2N_1 \cos\theta_1}{N_1 \cos\theta_2 + N_2 \cos\theta_1} \qquad (2.16)$$

where the subscript 's' denotes that the vector is perpendicular to the surface and the subscript 'p' denotes that vector is parallel to the interface. Especially for normal incidence ($\theta_1 = \theta_2 = \theta_3 = 0$), the Fresnel Equations can be simplified as:

$$r = \frac{N_1 - N_2}{N_1 + N_2} \qquad (2.17)$$

$$t = \frac{2N_1}{N_1 + N_2} \qquad (2.18)$$

$$R = |r|^2 = \left|\frac{N_1 - N_2}{N_1 + N_2}\right|^2 \qquad (2.19)$$

$$T = \frac{N_2}{N_1}|t|^2 = \frac{N_2}{N_1}\left(\frac{2N_1}{N_1 + N_2}\right)^2 \qquad (2.20)$$

2.3.2.2 Theory of Multilayer Thin Films Optics

The Matrix Method is used in Optics to analyze the propagation of lights through

layered medium [50]. We have known that the reflection of light from a single interface can be described by the Fresnel equations. However, for multiple interfaces, shown in Figure 2.10, matrix method is applied to calculate the reflection coefficient.

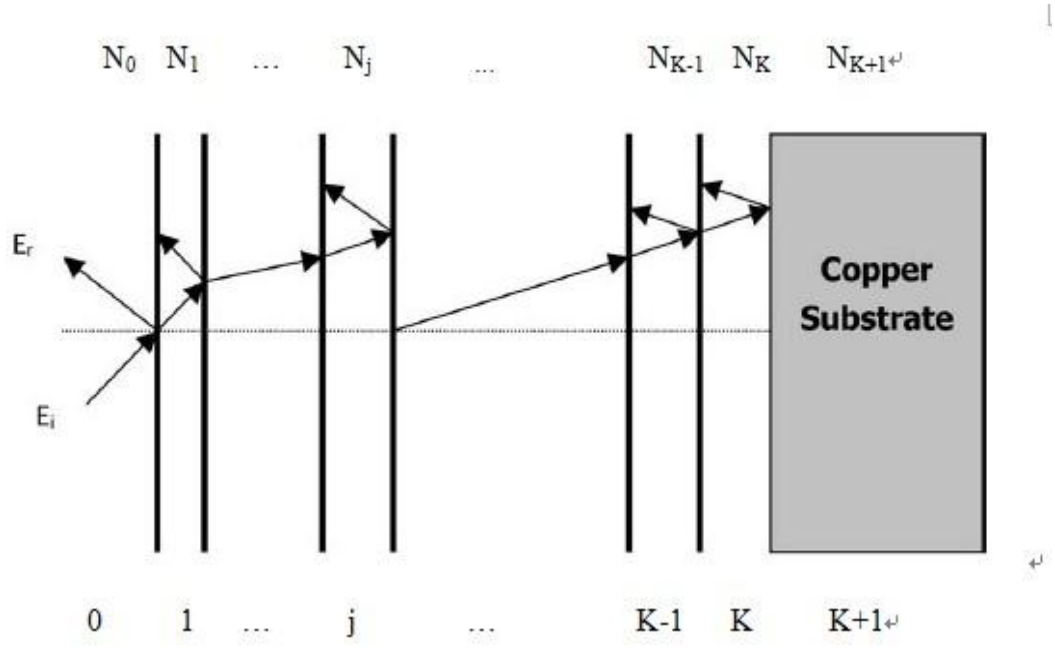

Figure2.10 A multilayer stack scheme of K layers on a metallic substrate [15].

Based on boundary conditions of Maxwell equation, we assume a single layer to be equivalent to an interface. The matrix can be derived:

$$\begin{bmatrix} B \\ C \end{bmatrix} = \begin{bmatrix} \cos\delta_1 & \frac{i}{N_1}\sin\delta_1 \\ iN_1\sin\delta_1 & \cos\delta_1 \end{bmatrix} \begin{bmatrix} 1 \\ N_2 \end{bmatrix} \qquad (2.21)$$

where δ_1 is the thickness of the single layer and $\delta_1 = \frac{2\pi}{\lambda} N_1 d_1$ (for normal incidence). N_1 is the refractive index of the single layer. C/B is the refractive index of the single layer and substrate. Therefore, the reflection equation of equivalent interface is:

$$R = |r|^2 = \left(\frac{N_0 - C/B}{N_0 + C/B}\right)\left(\frac{N_0 - C/B}{N_0 + C/B}\right)^* \qquad (2.22)$$

For K number of layers we can rewrite Eq. (1) as:

$$\begin{bmatrix} B \\ C \end{bmatrix} = \prod_{j=1}^{k} \begin{bmatrix} \cos\delta_j & \frac{i}{N_j}\sin\delta_j \\ iN_j \sin\delta_j & \cos\delta_j \end{bmatrix} \begin{bmatrix} 1 \\ N_{k+1} \end{bmatrix} \qquad (2.23)$$

where C/B is the refractive index of K layers and substrate. The composite films are normally fabricated on metallic substrates, leading to no transmission. We can deduce the absorptance and emittance from the reflectance, which is given by:

$$R = \left(\frac{N_0 - C/B}{N_0 + C/B}\right)\left(\frac{N_0 - C/B}{N_0 + C/B}\right)^* \qquad (2.24)$$

When the system of multilayer thin films includes the absorbing layers, the refractive index of absorbing layer is $N = n - ik$, which can be found in the book [76-78].

2.3.3 M-AlN Solar Selective Coating

A larger number of metal-dielectric composite solar selective coatings have been studied [51-53]. The Zhang's group [54] investigated a series of metal-aluminum nitride (M-AlN) solar selective coatings. They deposited W-AlN, Mo-AlN, and SS-AlN coatings by a direct current (d.c.) magnetron sputtering technology. Generally, the M-AlN cermets are deposited by running aluminum target and metallic target in a gas mixture of argon and nitrogen. The aluminum nitride is deposited by d.c. reactive sputtering while the metallic component by d.c. non-reactive sputtering. To be specific, the partial pressure of reactive nitrogen gas needs to be low enough, which can ensure to form a nearly pure aluminum nitride layer. However, due to its nitriding resistance, for the metallic component an almost pure metallic layer is deposited by d.c. sputtering at this low nitrogen pressure. By rotating the substrates, aluminum nitride and metallic can be alternately sputtered on the substrate, which can be considered as a uniform M-AlN composite layer. In addition, by changing the sputtering rate and rotation speed, the thickness and metal volume fraction of the layer can be controlled [55].

M-AlN solar selective coating with double cermet structure, AlN/M-AlN（LMVF）/M-AlN(HMVF)/Al, consists of an infrared reflector layer Al, double absorbing layers M-AlN（LMVF）/M-AlN(HMVF), and an antireflection layer AlN. In pure argon gas, an Al infrared reflector layer is first deposited on the glass substrate. Then the double M-AlN absorbing layers are deposited in mixed gas of argon and nitrogen. Finally, an AlN antireflection layer is deposited on the M-AlN (LMVF) at a low nitrogen partial pressure. An absorption of 0.92-0.94 and emittance of 0.08-0.10 at 350℃ is acquired for the Metal- AlN solar selective coating [55].

The Peking University and the Sydney University [55] have designed a commercial-scale cylindrical d.c. magnetron sputtering (Figure 2.11) and successfully prepared the SS-AlN solar selective surfaces as above process.

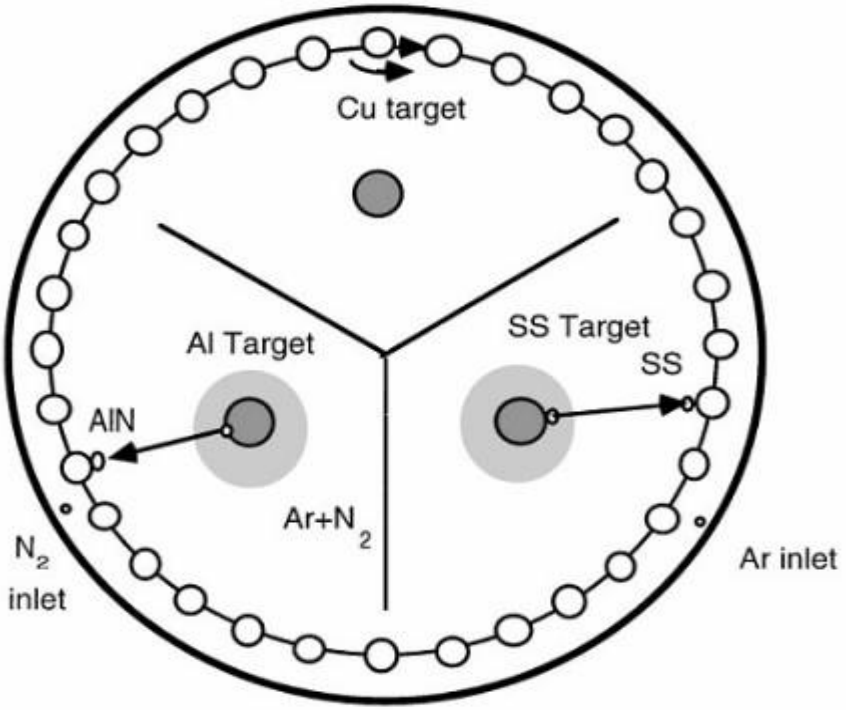

Figure2.11 3-target DC current magnetron sputtering system [55]

Chapter 3 Experimental Methods

3.1 Sample Preparation

3.1.1 Co-precipitation of Particles

“Co-precipitation is carrying down by a precipitate of substances normally soluble under the conditions employed [56]”. It is often applied in chemical analysis and radiochemistry. Co-precipitation is also used as a method of magnetic nanoparticle synthesis [57].

Generally, there are three main mechanisms of co-precipitation, which are absorption, occlusion, and inclusion [58]. An absorption means that an impurity is forced to the surface of the precipitate due to the effects of charge. An occlusion occurs when an adsorbed impurity gets physically trapped inside the crystal as it grows. When the ionic radius and charge of the impurity and carrier are similar, an inclusion happens that the impurity occupies a lattice site in the crystal structure of the carrier and results in a crystallographic defect.

3.1.2 Dip-Coating

Dip-Coating is a simple and low cost method to create a thin film on a substrate. Generally, it can be separated into five stages [59]:

Immersion: The substrate is immersed in the solution of the coating material at a constant speed.

Start-up: After the substrate has remained inside the solution for a while and we start to pull it up.

Deposition: The thin film deposits itself on the substrate while it is pulled up at a constant speed. The speed determines the thickness of the coating

Drainage: Excess liquid will drain from the surface of the substrate.

Evaporation: The solvent evaporates from the liquid to form the thin film on the substrate.

To prepare the Fe_3O_4 nanoparticles solar selective coating, the dip-coating method is employed. The copper substrate was flatly immersed in the Fe_3O_4 nanoparticles solution and left for a while. Then withdrawing was carried out at a constant speed, which determines the thickness of thin film. After that, it took 2 hours to evaporate the solvent and formed a Fe_3O_4 thin layer. This work was carried out in the departmental clean room.

3.1.3 Sputtering of Thin Films

Sputtering is one of the most widely used thin film deposition techniques. The basic principle of the sputtering is that the atoms are ejected due to the bombardment of energetic particles on the source material, then deposit on the substrate to form a thin film. Sputtering offers a flexibility of choosing various materials and substrates to deposit. In addition, the thickness and composition of the thin film deposited by sputtering can be accurately controlled. Thus, sputtering is currently employed for depositing the solar selective coatings in large-scale production [60-61].

The samples of the SS-AlN solar selective absorber in Chapter 4 were prepared by our collaborator, Sunshore Solar Energy Co.,Ltd (China). The sample was deposited by d.c. magnetron sputtering with the structure of AlN/SS-AlN/SS-AlN/AlN/ Cu/ Glass.

3.2 Heat Treatment

Heat treatment refers to a process of heating at certain temperature, time held at such temperature and cooling at a rate, which used to alter the physical, sometimes the chemical properties of materials. Metallic materials consist of a microstructure of small crystals called grains. The grain size and composition of the grains affect the overall mechanical behavior of the material. Heat treatment is an efficient way to manipulate the properties of the metallic materials. Annealing, as a kind of heat treatment, includes heating a metallic material to specific temperature and then cooling at a rate, which will produce a refined and uniform microstructure [62-63].

Thermal oxidation furnace situated in the clean room (as shown in Figure3.1) is a device which can be used for annealing. Its temperature range is 0~1000 ℃。The heat treatments were made in air in this thesis.

Figure3.1 Thermal Oxidation Furnace used for heat treatment

In order to analyze the optical properties of the SS-AlN solar selective coatings after annealing, several annealing temperatures were selected including 100 ℃，200 ℃, 300 ℃, 400 ℃, 500 ℃, 600 ℃, and 700 ℃. The samples of SS-AlN were placed in the thermal oxidation furnace and heated to a selected temperature, and cooled down after remaining for one hour at the given temperature.

3.3 Optical Characterization

The optical properties of the solar absorbers are often investigated using spectrometers. For the solar selective coatings, the spectrometers are of interest especially when they cover the wavelength range of solar spectrum (0.3~2.5um) and the infrared region are of interest. The Filmetrics F10-RT in our lab covers 0.2~1.1μm and Equinox 55 FT-IR spectrometer in our chemistry department covers 1.25~20μm.

3.3.1 Filmetrics F10-RT Spectroscopy

The Filmetrics F10-RT (Figure3.2) is used to measure the reflectance and transmittance of thin films, which covers the wavelength range of 0.2~1.1μm. When considering reflectance measurement, the way that light is reflected from the sample depends on its characteristics, such as thickness, optical constants, and roughness. The Filmetric F10-RT is capable of determining the characteristics of the sample by measuring the amount of light reflected from the sample and analyzing the data by comparing it to a series of calculated reflectance spectra [64]. The basic steps for the F10-RT measurement consist of taking a baseline measurement and then making the measurement of the sample.

Before the sample measurement, the baseline measurement is necessary, which mainly includes measuring a reference sample and taking a “dark” reading. The purpose of measuring the reference sample with known reflectance characteristics is to calibrate the whole optical system. The reference sample does not have to be the same as the substrate on which films are measured. After the reference measurement, a “dark” reading is taken. A non-zero dark level is due to current leakage of photodiodes, which causes each photodiode in the array to slowly charge up even when no light enters the spectroscopy machine [64]. For subtracting this “dark” current contribution, the “dark” reading is taken, which measures the magnitude of the dark current for a given

integration time. When a “dark” measurement is made, a spectrum is measured that is equal to the result of a sample of zero reflectance. Moreover, the baseline measurement should be periodically taken because of the drift in the light source and the temperature of the spectrometer electronics. Generally, the baseline should be repeated every 20-30minutes.

Figure3.2 Filmetrics F10-RT spectroscopy

3.3.2 Equinox 55 Fourier Transform (FT-IR) spectroscopy

IR spectroscopy is a classical technique, which depends on the interaction of infrared radiation with the vibrating dipole moments of molecules. The solar selective coating spectra in the region of 1.2~20μm are collected by the Bruker instruments Equinox 55 FT-IR spectrometer. This spectrometer is equipped with a Taguchi Gas Sensor (TGS) and an MCT detector with liquid nitrogen cooling, enabling high sensitivity measurements in the MIR and NIR with resolution of 0.5cm^{-1}. To calibrate the system before measurement, copper thin film is applied as a background. 256 scans are acquired to be background spectrum. When measuring the sample, the spectrum is formed by co-adding 128 scans.

Figure3.3 Equinox 55 Fourier Transform (FT-IR) spectroscopy

3.4 Non-Optical Characterization

3.4.1 Scanning Electron Microscopy （SEM）

Scanning Electron Microscopy （SEM） is a type of electron microscopy for surface profile analysis. As a focused electron beam is scanned over the sample, those electrons interact with atoms of the sample and the matter causes the emission of backscattered electrons, auger electrons, x-rays, and secondary electrons. In the signals of SEM, the secondary electrons are detected and focused on screen by cathode ray tube (CRT), in order to generate the topography image. Moreover, the resolution of SEM image can be improved by increasing beam acceleration voltage.

SEM is one of the most fundamental instruments for materials surface science. Firstly, one of the major advantages of SEM is that the analyzable area of the sample is quite large due to the large depth of field. Secondly, the electromagnetic focusing lenses can

be adjusted at an extremely fine level, which allows precise focusing of the image. Thus, more information of a certain part of the sample is available. However, when the sample is maintained in the vacuum chamber, the high energy electron beam would ionize carbohydrate floating in the air and cause carbon contamination on the sample. Also for non-conducting samples, a very thin gold-palladium film is applied to reduce the charging effects on the sample.

3.4.2 Transmission Electron Microscopy (TEM)

TEM is another widely used type of electron microscopy, the principle of which is quite different from SEM generating image from secondary electrons. TEM has a much higher accelerated electron beam transmitting through an ultra-thin specimen and interacting with the specimen to form an image. The image is magnified and focused onto an imaging device such as CCD camera or fluorescent screen.

TEM is capable of achieving extremely high resolution. In fact, TEM is the only type of microscope that can image single atom or atom array of examined material. Therefore, TEM, as a major analysis method, is applied in a wide range of scientific fields, such as material science, and biological science.

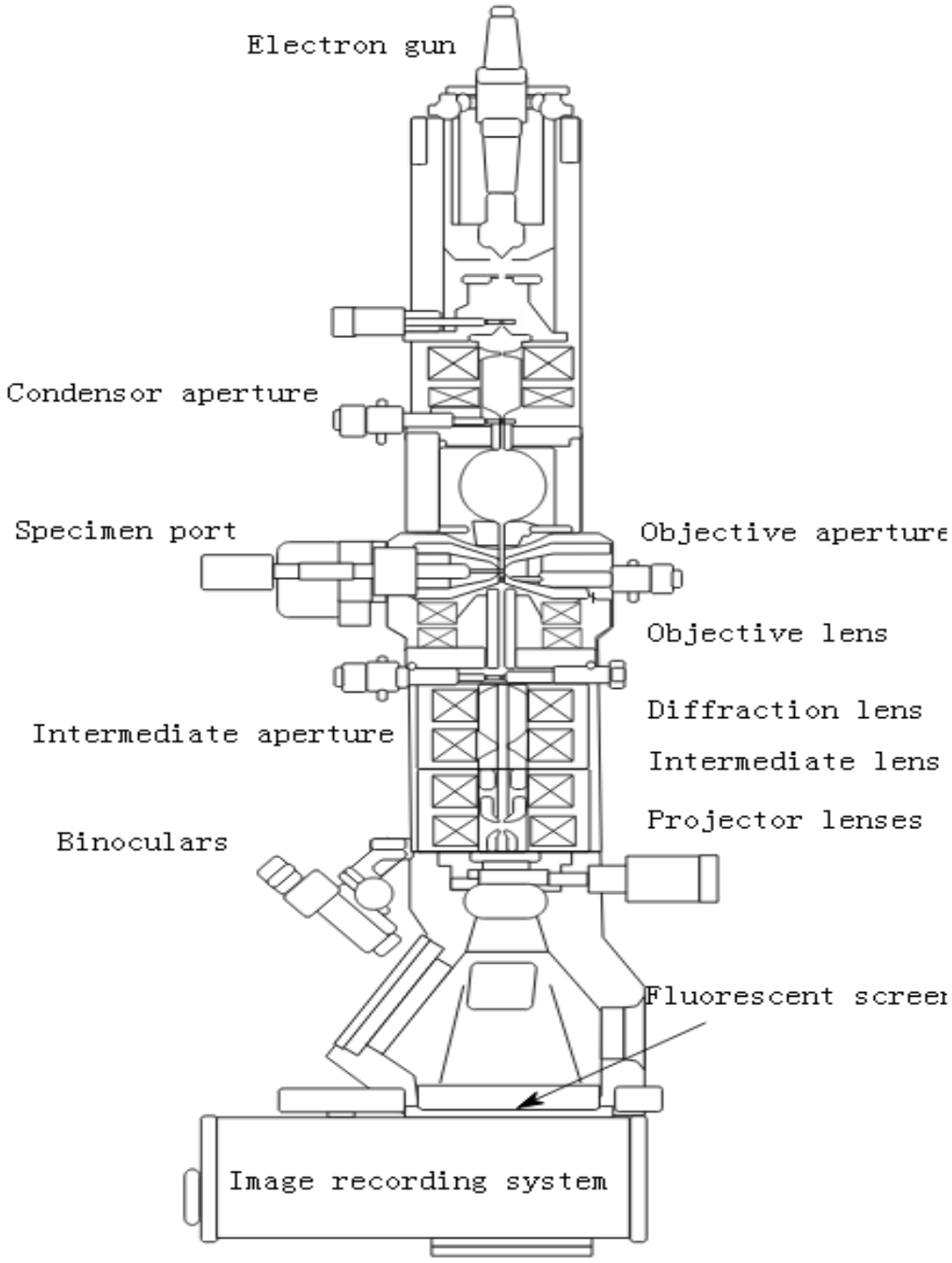

Figure3.4 Layout of components in a basic TEM [65].

A typical TEM (Figure3.4) is composed of several major components, including electron source, vacuum tube, electromagnetic lenses and electrostatic aperture plates.

Electron Source is usually positioned at the top of the TEM. It is formed with a filament, a Wehnelt cap and an anode. The filament can be made of tungsten or LaB6,

and is connected to a negative power supply. When heated up, electron beams would be pumped out from the filament surface and form the electron cloud. The Wehnelt cylinder is a metal cap shaped to cover the filament. As it is also heavily negative biased, the aperture in the middle can help focus the electron cloud to form an electron beam with a small crossover diameter. The anode plate works like an electron extractor since it is grounded or positively biased comparing to the filament. Below is a diagram for tungsten filament electron sources. LaB6 filament sources are of a slightly different design. Simply speaking it uses heating coil to heat the LaB6 rod to generate electrons. This type of filament generates more electrons at the same temperature, hence offers a brighter image at high resolution. However, the cost tends to be an order of magnitude more expensive.

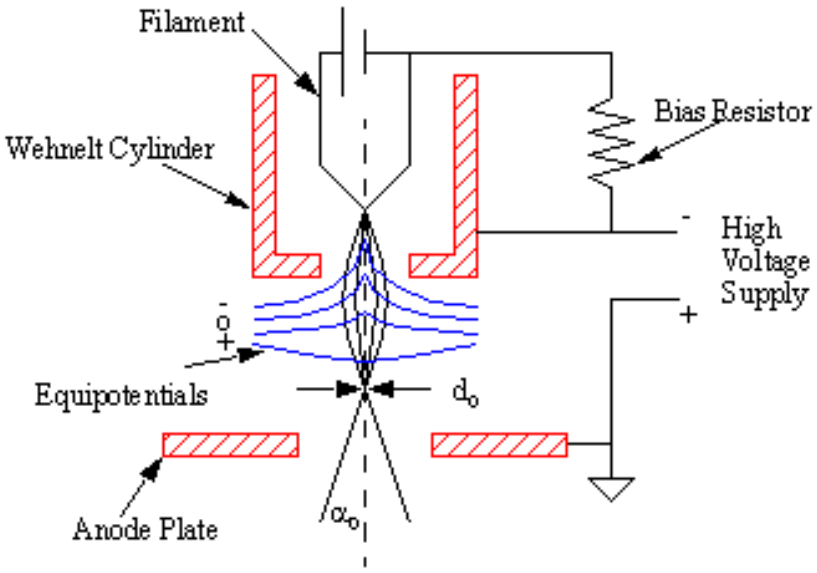

Figure3.5 Tungsten filament electron source [66].

Vacuum tube is made to reduce the mean free path of the electron gas interaction; good vacuum also prevents arc generated between positive anode plates to the ground. The specimen loading and unloading requires the TEM vacuum tube to have the mechanism of multi stage airlock to maintain the quality of the vacuum when replacing specimens. The vacuum level requirement mostly depends on the electron-beam voltage of the TEM. High voltage TEMs generally require UHV environment to prevent electrical arc at the cathode, and sometimes has an independent pumping

system for the electron gun isolated from the main tube.

Electromagnetic lenses and electrostatic apertures offer the operator fine adjustment of beam focusing and tilting. Different from optical lenses, these lenses utilize electromagnetic coils to produce a radially symmetric magnetic field. During operation, current passes through the coils and generates quite a lot of heat. Therefore, not only these lenses must be insulated from any other component, but also have water cooling system to maintain the temperature.

3.4.3 Alpha-step Profiler

Tencor alpha-step 100 profiler (Figure3.6) is employed to measure the thickness of the coating. This instrument scans sample surface with a diamond stylus and plots the results in the strip chart. The operation is described in the following steps. The first step is to position the sample to be measured on the X-Y table. Then lower the stylus, adjust to zero on the meter, and engage the auto test feature. The parameters of tencor alpha-step100 profiler are as shown belows.

Range = 1000Å - 1000KÅ; Resolution = 50Å; Accuracy = 1% of range

Figure3.6 Tencor alpha-step profiler

3.5 Simulation of the Multilayer Solar Selective Coating

3.5.1 Calculation of the Multilayer Solar Selective Coating

- **Determine the optical constant of each layer**

Generally, the optical constant of an absorbing layer can be expressed as

$$N = n - ik \tag{3.1}$$

where n is the refractive constant, and k is the extinction constant. The optical constants of common materials can be found in the book [76-78].

For a metal-dielectric composite layer in solar selective coating, Effective Medium Theory (Bruggeman model) is generally adopted for calculating the dielectric constant of the composite layer as follows:

$$0 = f_A \frac{\varepsilon_A - \varepsilon}{\varepsilon_A + 2\varepsilon} + f_B \frac{\varepsilon_B - \varepsilon}{\varepsilon_B + 2\varepsilon} \tag{3.2}$$

where the ε is the dielectric constant of the composite. ε_A and ε_B are the dielectric constants of metal and dielectric, respectively. f_A is the filling factor of metal, and $f_B = 1 - f_A$. The optical constant is related to dielectric constant as: $\varepsilon = N^2$

- **Reflection calculation of multilayer coatings**

Matrix Method is employed to calculate the reflectance of multilayer coatings.

Given a system of K layers, the K-layer coating can be characterized by the feature matrix (we assume that the light is vertical incidence) below:

$$\begin{bmatrix} B \\ C \end{bmatrix} = \prod_{j=1}^{k} \begin{bmatrix} \cos\delta_j & \frac{i}{N_j}\sin\delta_j \\ iN_j\sin\delta_j & \cos\delta_j \end{bmatrix} \begin{bmatrix} 1 \\ N_{k+1} \end{bmatrix} \tag{3.3}$$

where i^2=-1, N_j is the optical constant of the jth layer, and δ_j is the phase thickness of the jth layer. The reflectance of the system of K layers is calculated using:

$$R = \left(\frac{N_0 - C/B}{N_0 + C/B}\right)\left(\frac{N_0 - C/B}{N_0 + C/B}\right)^* \tag{3.4}$$

In which, $N_0 = 1$ is the optical constant of air. Because the optical constant corresponds to a given wavelength, the reflectance varies with wavelength. Thus, a reflectance spectrum against wavelength can be achieved.

- **Calculation of solar absorptance and thermal emittance**

Solar absorption of the solar selective coating is calculated by their reflectance spectrum $R(\lambda)$ and the solar radiation spectrum $G(\lambda)$ as below:

$$\alpha = \frac{\int_{\lambda_1}^{\lambda_2}[1 - R(\lambda)]G(\lambda)d\lambda}{\int_{\lambda_1}^{\lambda_2} G(\lambda)d\lambda} \qquad (3.5)$$

If the solar spectral distribution is divided into fifty bands of equal energy, then the selected ordinates method can be used to simplify the equation (3.) as:

$$\alpha = 1 - \frac{\sum_{i=1}^{50} R_{\Delta\lambda_i}}{50} \qquad (3.6)$$

To calculate the solar absorptance, the reflectance was taken on the 50 selected ordinates [67] for air mass (AM) 1.5

Similarly, the hemispherical emittance at a given temperature T is calculated by the reflectance spectrum $R(\lambda)$ and the blackbody radiation spectrum $G(\lambda)$:

$$\varepsilon(T) = \frac{\int_{\lambda_1}^{\lambda_2}[1 - R(\lambda, T)]B(\lambda, T)d\lambda}{\int_{\lambda_1}^{\lambda_2} B(\lambda, T)d\lambda} \qquad (3.7)$$

The spectral emittance is evaluated using the Planck blackbody spectral distribution for 373 K at selected ordinates for thermal emittance [68].

3.5.2 MATLAB Simulation Program

MATLAB® version 7.30 (Figure3.7) is a numerical computing environment, which was employed to do the calculation of multilayer solar selective coatings. MATLAB allows the matrix manipulation and produces the required graphs. Based on the Matrix Method, the reflectance spectrum can be achieved. Then, the absorptance and the emittance are evaluated from the reflectance spectra by combining the solar radiation

spectrum and blackbody radiation spectrum at a given temperature.

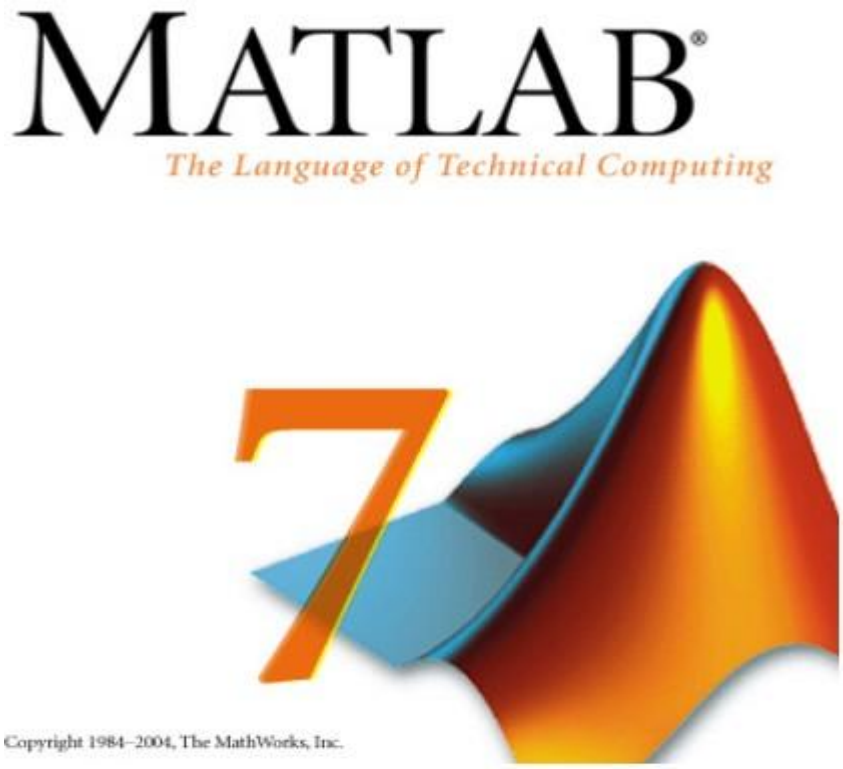

Figure3.7 Working environment of MATLAB software

The simulation studies of multilayer solar selective coating are carried out by using MATLAB. Considering a SS-AlN solar selective coating (Figure3.8) as an example, the simulation program was made as the following steps.

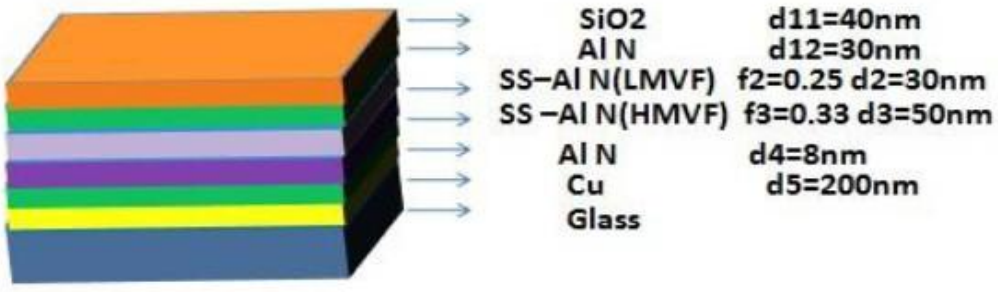

Figure3.8 A structure of SS-AlN solar selective coating

MATLAB CODE: SS-AIN Solar Selective Coating

```
clear, clc, close all
% parameters
theta=pi/2;                              % angle of incidence

k=4;                                    % number of layers

d0=0.04;                                % Al2O3 layer thickness
d1=0.03;                                % AlN layer thickness
d2=0.03;                                % SS-AlN (LMVF) layer thickness
d3=0.05;                                % SS-AlN (HMVF) layer thickness
d4=0.008;                               % AlN layer thickness

% volume fraction of SS-AlN (LMVF)
f2=0.25;
% volume fraction of SS-AlN (HMVF)
f3=0.33;

lamda=linspace(0.25, 8, 50);            % wavelength range
```

- **Determine the optical constants of the layers**

```
% determine optical constants of different layers
% AlN %
Nain=1.9*ones(1,20);

% Cu %
load('cu.mat')
pncu=polyfit(lamdacu,ncu,5);            % refractive index of Cu
pkcu=polyfit(lamdacu,kcu,5);            % extinction coefficient
Ncu=polyval(pncu,lamda)-sqrt(-1)*polyval(pkcu,lamda);

% stainless steel %
load('ss.mat')
pnss=polyfit(lamdanss,nss,5);           % refractive index of SS
pkss=polyfit(lamdakss,kss,5);           % extinction coefficient
Nss=polyval(pnss,lamda)-sqrt(-1)*polyval(pkss,lamda);

% SS-AlN (LMVF) %
N2=eval(solve('0.25*(Nss^2-N^2)/(Nss^2+2*N^2)+(1-0.25)*(1.9^2-N^2)/(1
.9^2+2*N^2)','N'));

% SS-AlN (HMVF) %
```

```
N3=eval(solve('0.33*(Nss^2-N^2)/(Nss^2+2*N^2)+(1-0.33)*(1.9^2-N^2)/(1
.9^2+2*N^2)','N'));
```

- **Reflectance calculation**

```
% reflectance calculation of coating
for i=1:length(lamda)

    % phase thickness of different layers
    eta0=2*pi/lamda(i)*1.48*d0;
    eta1=2*pi/lamda(i)*1.9*d1;
    eta2=2*pi/lamda(i)*N2(1,i)*d2;
    eta3=2*pi/lamda(i)*N3(1,i)*d3;
    eta4=2*pi/lamda(i)*1.9*d4;

    % matrix method

z0=[cos(eta0),sqrt(-1)/1.48*sin(eta0);sqrt(-1)*1.48*sin(eta0),cos(eta
0)];

z1=[cos(eta1),sqrt(-1)/1.9*sin(eta1);sqrt(-1)*1.9*sin(eta1),cos(eta1)
];

z2=[cos(eta2),sqrt(-1)/N2(1,i)*sin(eta2);sqrt(-1)*N2(1,i)*sin(eta2),c
os(eta2)];

z3=[cos(eta3),sqrt(-1)/N3(1,i)*sin(eta3);sqrt(-1)*N3(1,i)*sin(eta3),c
os(eta3)];

z4=[cos(eta4),sqrt(-1)/1.9*sin(eta4);sqrt(-1)*1.9*sin(eta4),cos(eta4)
];

    Z=z0*z1*z2*z3*z4*[1;Ncu(i)];
    Y=Z(2)/Z(1);
    R(i)=(1-Y)/(1+Y)*conj((1-Y)/(1+Y));   % reflectance
end

plot(lamda,R)                    % plotting reflectance spectrum
xlabel('Wavelength(\mum)')
ylabel('Reflectance')
grid on
```

- **Calculation of solar absorptance and thermal emittance**

```
% calculation of solar absorptance and thermal emittance
% solar absorptance %
pr=polyfit(lamda,R,5);
% load 50 selected ordinates for AM 1.5
load('solarlamda.mat')
SR=polyval(pr,solarlamda);
Ab=1-mean(SR);                  % solar absorptance

% thermal emittance %
% load selected ordinates for black body radiation at 373K
load('bblamda2.mat')  ER=polyval(pr,bblamda2);
load('bb2.mat')
beight=sum(bb2.*(ones(1,31)-ER));
aeight=(1-ER(31))*(1-sum(bb2));
Em=beight+aeight;               % thermal emittance
```

Chapter 4 Nanostructured SS-AlN Solar Selective Coating

The all-glass evacuated solar collector tubes, which are coated with Metal-aluminum nitride (M-AlN) solar selective surfaces, have been mass-produced in the market. The M-AlN solar selective coatings are deposited by d.c. sputtering technology, which is suitable for large-area thin film production and has less environmental pollution compared to electrochemical methods, and lower cost than radio-frequency (rf) sputtering technology [55]. As a typical M-AlN solar selective coating, Stainless steel-aluminum nitride (SS-AlN) is investigated in this chapter.

The samples (Figure 4.1) were prepared by our industry collaborator, Sunshore Solar Energy Co.,Ltd in China. As shown in Figure 4.2, the structure is recommended by the industrial process. To study the morphology and structure of the sample, it was measured by Scanning Electron Microscope (SEM) and Transmission Electron Microscope (TEM). JEOL SEM with Tungsten Filament operated at 5-20kV and FEI/Philips CM-20 TEM with LaB6 filament operated at 200kV. Cross-sectional TEM specimens were prepared by using a FEI Quanta 3D FEG dualbeam Focused ion beam (FIB). A typical recipe recommended by FEI company was used to prepare the cross-sectional specimen. Additionally, the optical characteristics of the samples also are carried out by spectrometers. To improve the properties of the SS-AlN solar selective coating, the samples were annealed at different temperatures in the furnace. Finally, a Matlab program has been made for the optical calculations on the multilayer coatings and the optimization of the structures of the SS-AlN solar selective coating.

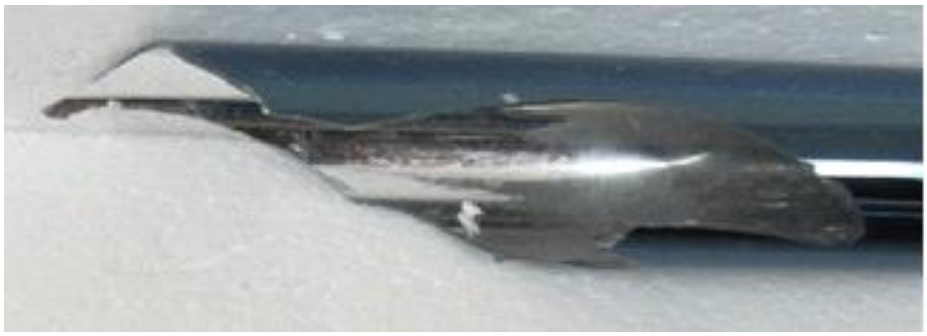

Figure4.1 Pieces of the sunshore's all-glass evacuated solar collector tubes with SS-AlN solar selective coating.

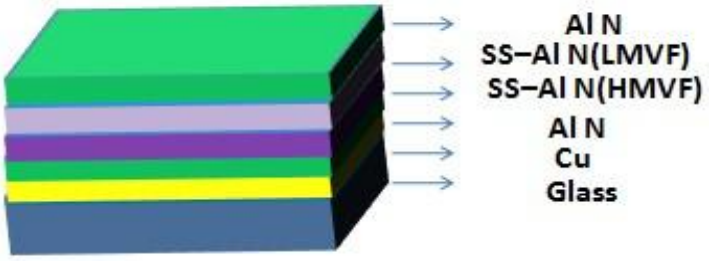

Figure4.2 Structure scheme of the sunshore's SS-AlN solar absorber. LMVF is low metal volume fraction; HMVF is high metal volume fraction.

4.1 Morphology and structure

Scanning Electron Microscopy (SEM) pictures of a SS-AlN solar selective coating sample are shown in Figure 4.3. The surface morphology of the sample is overall uniform, even though there are some holes. The distribution of these holes is irregular and their sizes vary between 100 and 800 nanometers (Figure 4.3 (b)).

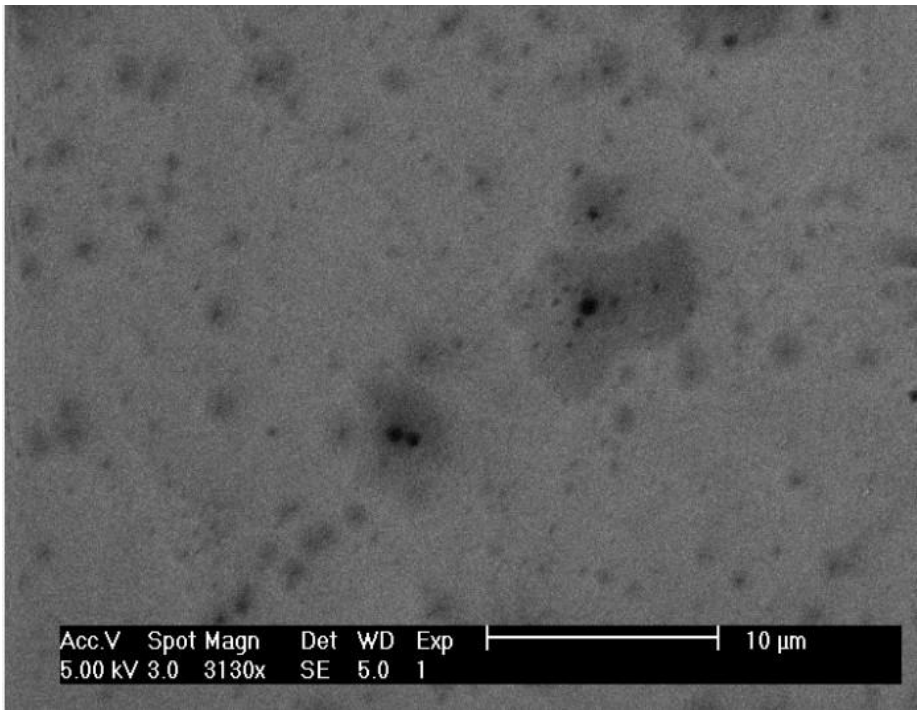

(a)

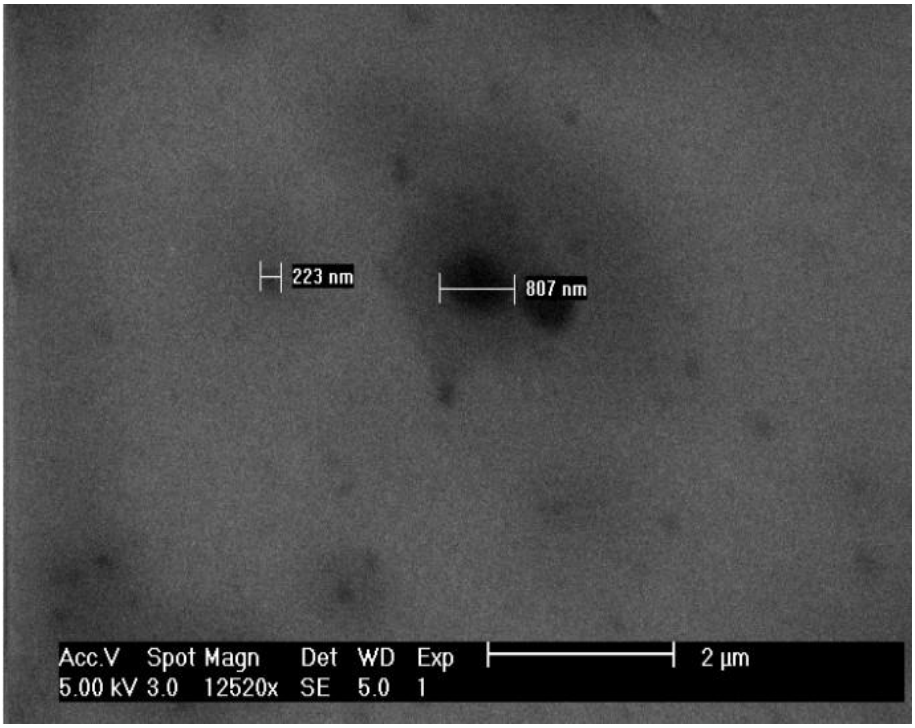

(b)

Figure4.3 SEM images of SS-AlN solar absorber

From the TEM image of the sample (Figure4.4), it can apparently be seen that there are at least three layers (A, B, and C) on the glass substrate. Their thicknesses are about 54nm, 58nm and 73nm, respectively.

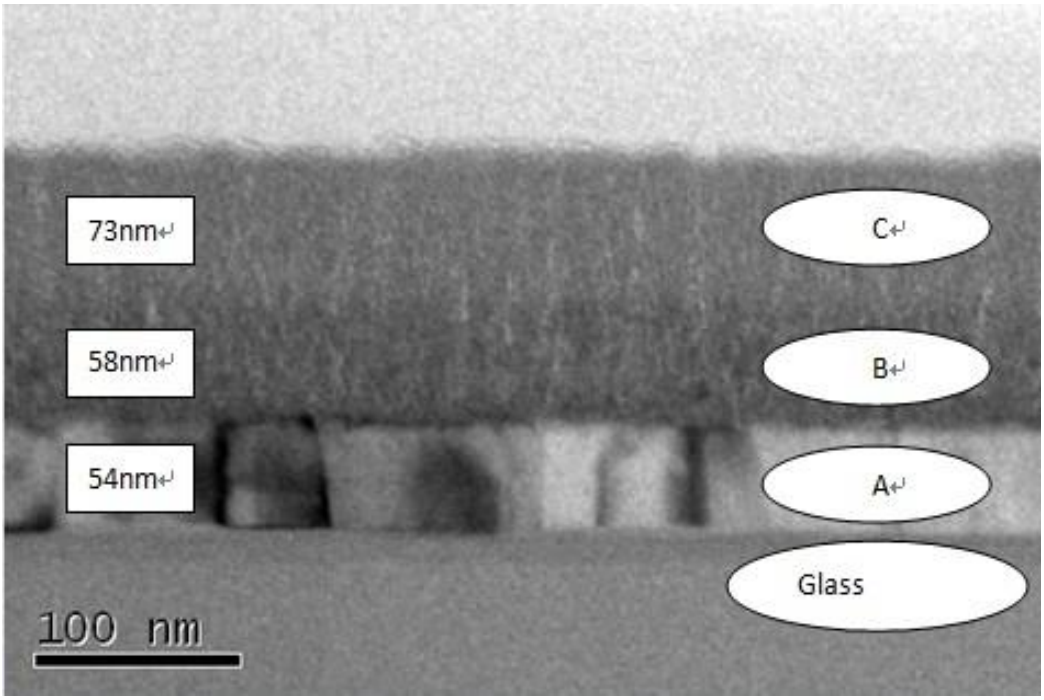

Figure4.4 TEM cross-section image of SS-AlN solar absorber.

Also, the compositions in each layer were analyzed by the EDX and the results are shown in the Figure 4.5 (a). (b). (c). Based on the results in Figure 4.5 (a), it is concluded that layer A is a copper layer. Because Cu, Si, O were found in this layer, while Si and O are most likely from glass substrate.

The layer B, as the result of Figure 4.5 (b), might be the composite of stainless steel and aluminum nitride (SS-AlN), even though little stainless steel was found from EDX results. Perhaps the phenomenon results from the industrial process and the small amount of stainless steel sputtered on the substrate. Additionally, some copper existed in layer B which may be caused by the diffusion from the substrate.

Figure 4.5 (c) shows that the upper layer C constitutes of Al-O-N. The elements in the

layer are Al, O, N, and Cu. The copper is likely from layer A due to diffusion.

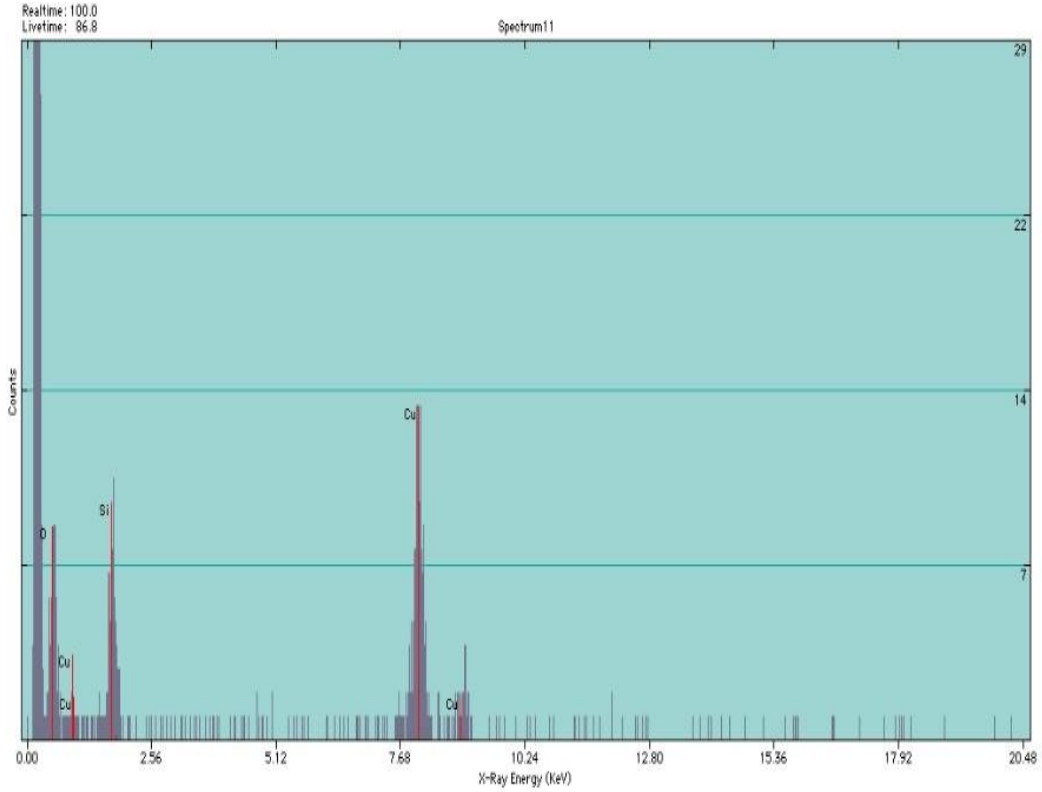

(a)Layer A

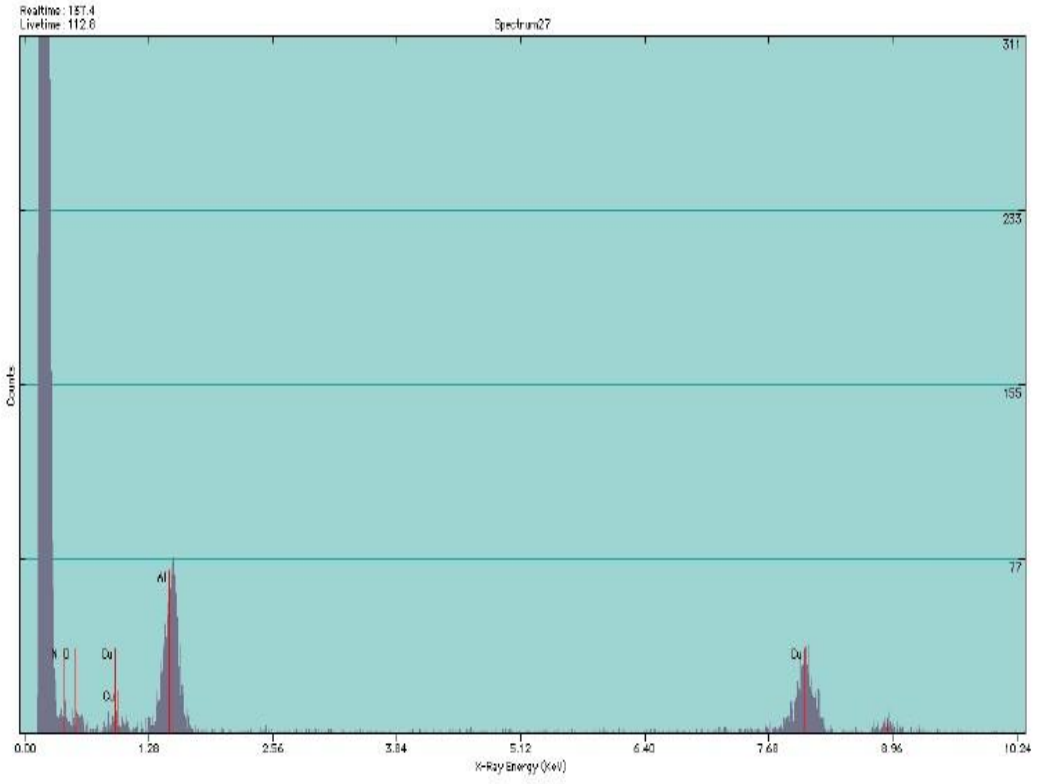

(b)Layer B

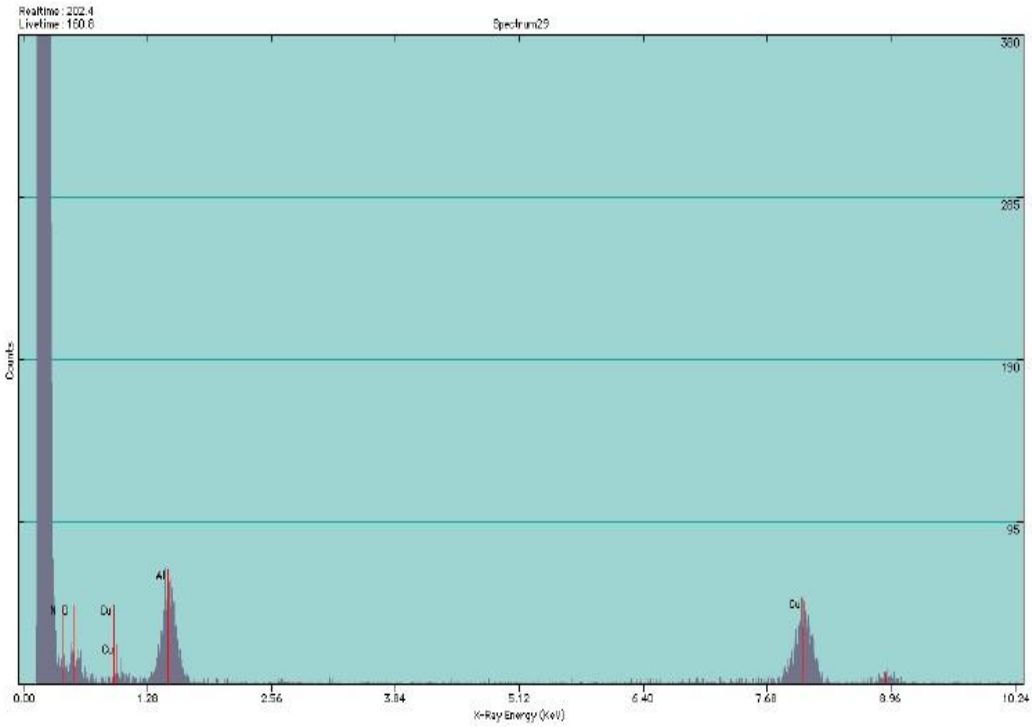

(c)Layer C

Figure4.5 EDS images in A, B, C layers of SS-AlN solar absorber.

In combined with the structure of AlON/SS-AlN(LMVF)/SS-AlN(HMVF)/AlN/Cu /glass, provided by the Sunshore Solar Energy Co.,Ltd, we have further estimated the thickness of the each layer based on the TEM image. The result is shown in Figure 4.6.

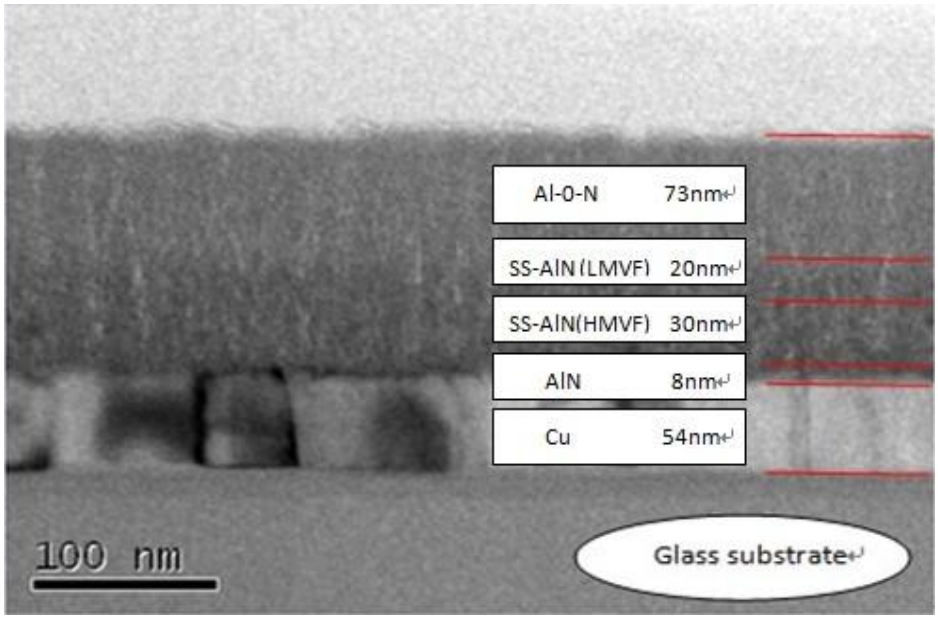

Figure4.6 Estimated structure of SS-AlN samples based on its TEM image.

4.2 Optical Characterization

The SS-AlN solar absorber sample was measured by the Filmetrics F10-RT spectroscopy in the wavelength range of 0.2~1.1μm and Equinox 55 FT-IR spectrometer which covers 1.25~20μm. The whole reflectance spectrum of the sample is shown in the Figure 4.7. The sample has low reflectance in the visible region and high reflectance in the IR region. From the calculation, it shows an absorptance of 0.9033 and an emittance of 0.1317.

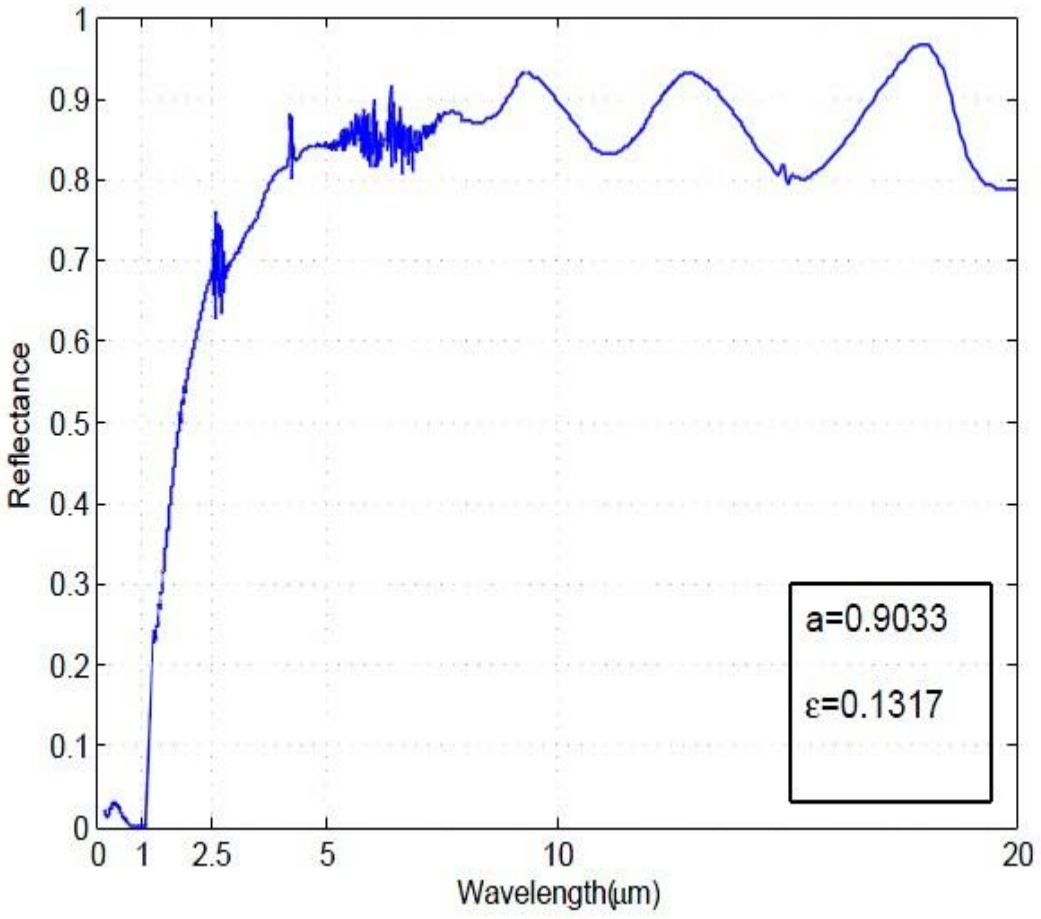

Figure4.7 Measured reflectance spectrum of sunshore's SS-AlN solar absorber.

4.3 Heat Treatment

Heat treatment is the process of heating the sample at a certain temperature, holding at such temperature for a certain time and then cooling down at a rate. This process can be used to alter the physical and chemical properties of materials. Metallic materials consist of a microstructure of small crystals called grains. The grain size and composition of the grains affect the overall mechanical behavior of the material. Heat treatment is an efficient way to manipulate the properties of the metallic materials. The annealing process can produce a refined and uniform microstructure under a certain conditions.

To further investigate the SS-AlN solar selective coating, the changes of the samples after annealing and unannealed have been compared. The samples were annealed at different temperatures 100 ℃, 200 ℃, 300 ℃, 400 ℃, 500 ℃, 600 ℃, 700 ℃ for one hour, and then cooled down. The surface morphologies and optical properties of the sample after annealing are studied by SEM and Spectrometers.

4.3.1 Surface Morphology

SEM images (Figure 4.8) shows the surface morphologies of the unannealed and annealed SS-AlN solar absorber samples with different annealing temperatures (100 ℃, 200 ℃, 300 ℃, 400 ℃, 500 ℃, 600 ℃, 700 ℃). After annealing below 500 ℃, the surfaces of the annealed sample became more refined and uniform. Fewer holes can be seen from the surface SEM images. However, if annealing carried out above 500 ℃, the surfaces became gradually rougher, and even some cracks were found, which shows the samples to be damaged by the process.

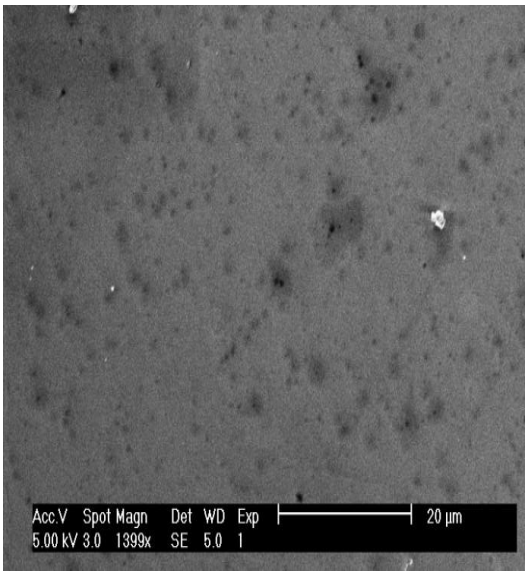

(a) unannealed

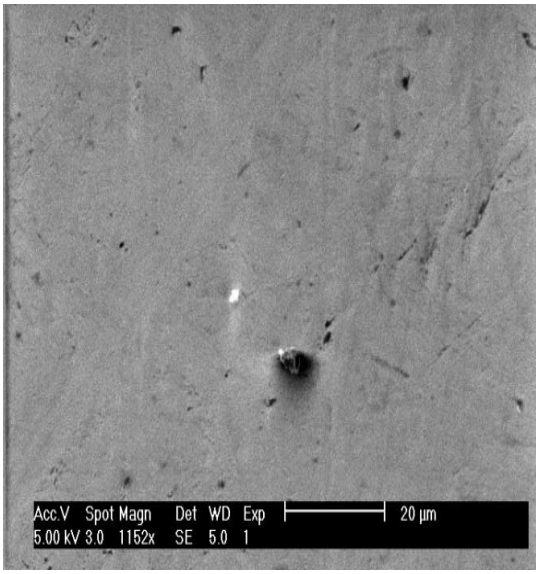

(b)100 ℃

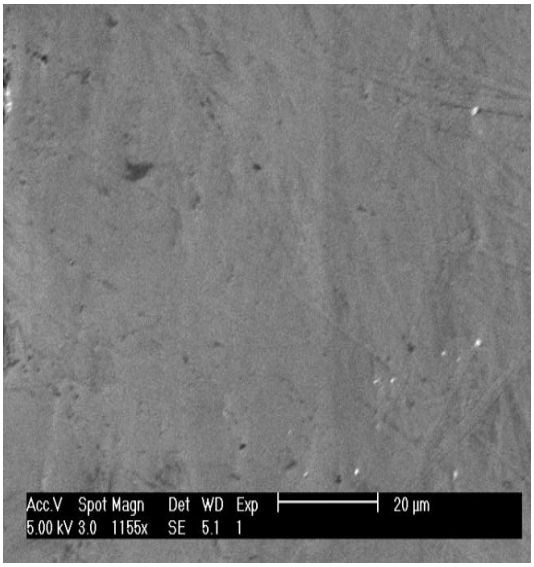

（c）200 ℃

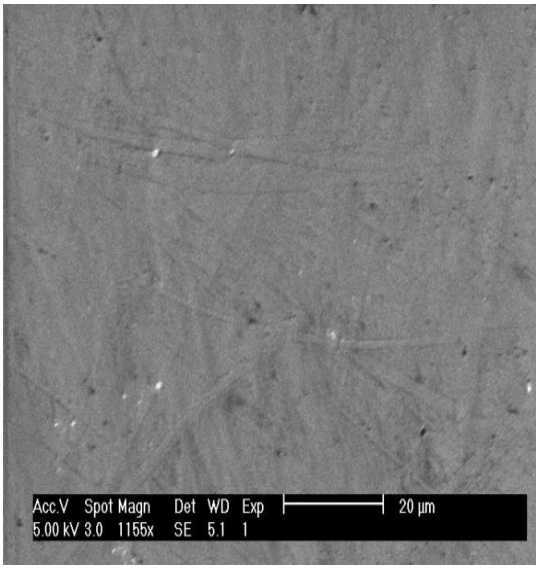

(d) 300 ℃

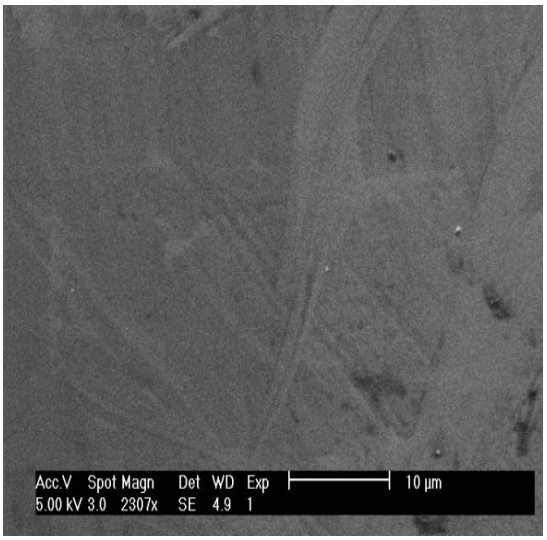

(e) 400 ℃

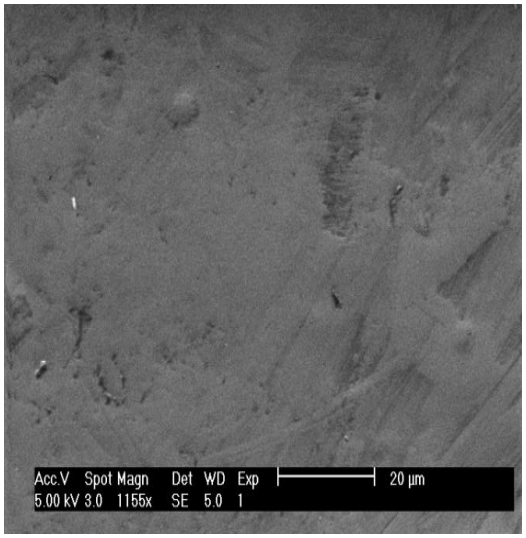

(f) 500 ℃

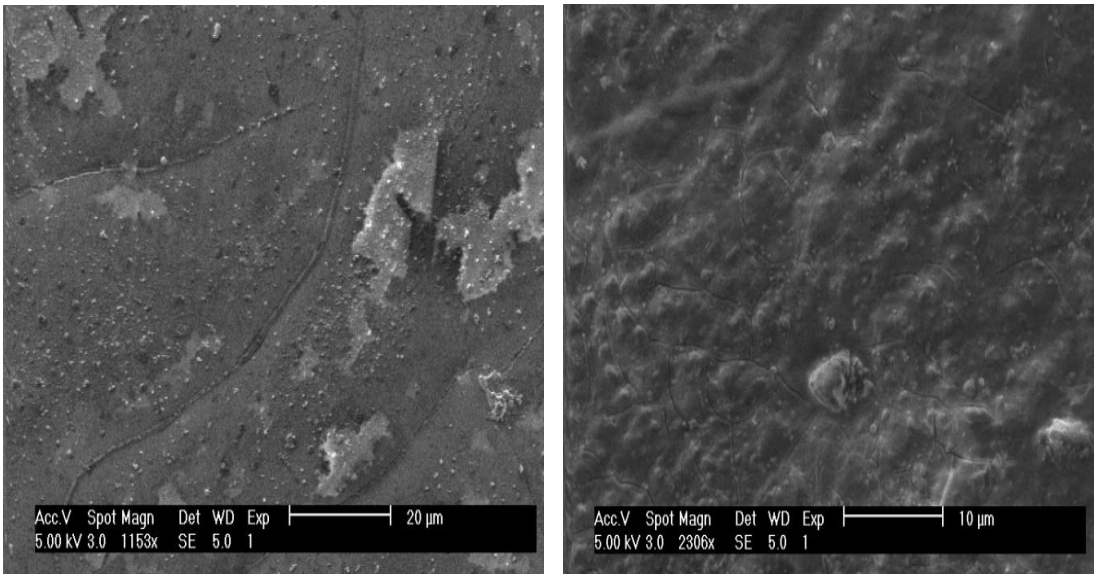

(g) 600 ℃ (h) 700 ℃

Figure4.8 SEM images of SS-AlN solar absorbers after annealing at different temperatures.

4.3.2 Optical properties

- **Annealed below 500 ℃**

The reflectance spectra of unannealed SS-AlN sample and those after annealing in 100 ℃, 200 ℃, 300 ℃, 400 ℃ are shown in Figure 4.8. We can see from the spectra that after annealing the sample has lower reflectance in the solar region than unannealed sample, which gives rise to a higher absorptance. When the annealing temperature is between 200 ℃ and 300 ℃, the reflectance of the sample in the infrared region increases so that less energy would be emitted. Annealing at 100 ℃ and 400 ℃, the reflectance in the infrared region did not change a lot.

In order to further analyze the optical properties of the samples, the absorptance and emittance were calculated, which are shown in Table 4.1. Annealed below 500 ℃, the sample has a higher absorptance and a lower emittance than unannealed sample. Annealing between 200 ℃ and 300 ℃, the absorptance increases and the emittance decreases, which improves the sample a lot compared with the unannealed sample.

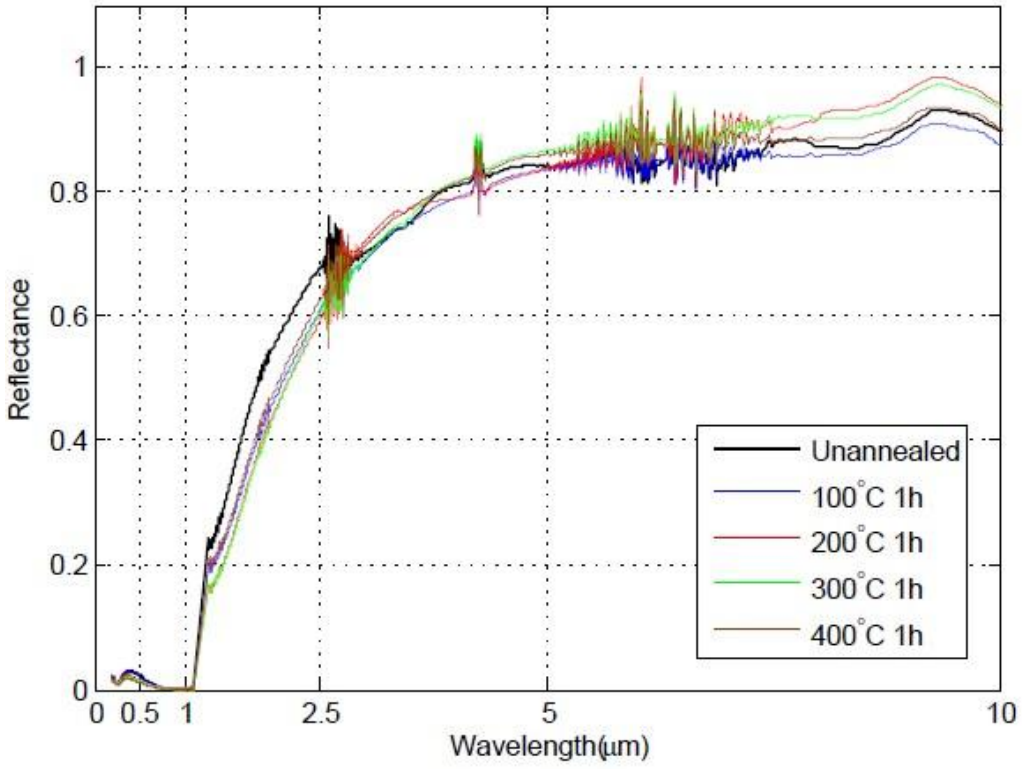

Figure4.9 Reflectance spectra of unannealed and annealed SS-AlN coatings with different annealing temperature (100 ℃, 200 ℃, 300 ℃, 400 ℃)

Table4.1 Absorptance and emittance of unannealed and annealed SS-AlN coatings with different annealing temperature (100 ℃, 200 ℃, 300 ℃, 400 ℃)

	unannealed	100 ℃	200 ℃	300 ℃	400 ℃
Absorptance(a)	0.9033	0.9243	0.9359	0.9378	0.9260
Emittance(ε)(373K)	0.1317	0.1347	0.1202	0.11	0.1304

The improvement of the optical properties of the SS-AlN samples annealed at 100 ℃-400 ℃ is probably due to the diffusion of oxygen atoms diffusion and stainless steel diffusion. After annealing, the oxygen atoms not only disperse in the antireflection layer Al-O-N, but also diffuse deeper, which leads to an increase in the antireflection layer thickness. Moreover, the stainless steels diffuse in the layer after annealing, which helps to form a graded absorbing SS-AlN layer. Consequently, because the thickness of the antireflection layer increases and the absorbing layer

become more graded, the optical properties of the SS-AlN solar selective coating have been improved after annealing.

- **Annealed above 500 ℃**

The transmittance spectra of coatings after annealing above 500 ℃ are shown in the Figure 4.10. For unannealed sample, the transmittance is almost zero. However, after annealing at 500 ℃, 600 ℃, 700 ℃, the transmittance of the samples gradually rises, which indicates the coatings were damaged at different level. Especially annealing at 700 ℃, the maxima of the transmittance is up to 40 percent at wavelength of 1100 nm.

Furthermore, the images of the unannealed sample and annealed samples are shown in Figure 4.11, in which the surfaces of the samples (b)(c)(d) annealled at 500 ℃, 600 ℃, 700 ℃ were damaged and the apparent colour changed, compared with that of unannealed sample(a). Therefore, the SS-AlN samples annealled above 500 ℃ could not work anymore.

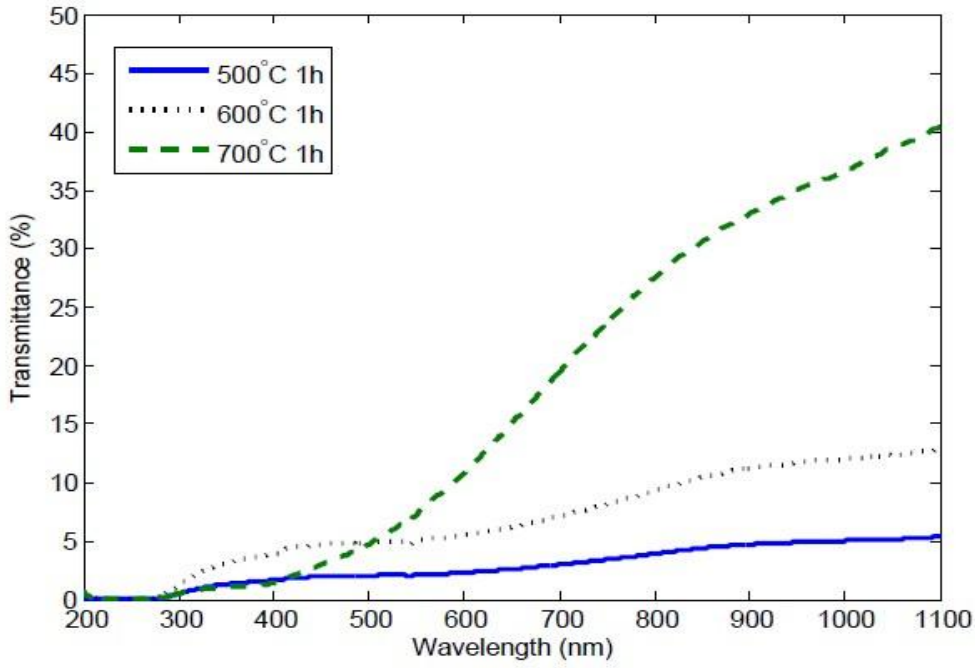

Figure4.10 Transmittance spectra of annealed SS-AlN sample at 500 ℃, 600 ℃ and 700 ℃.

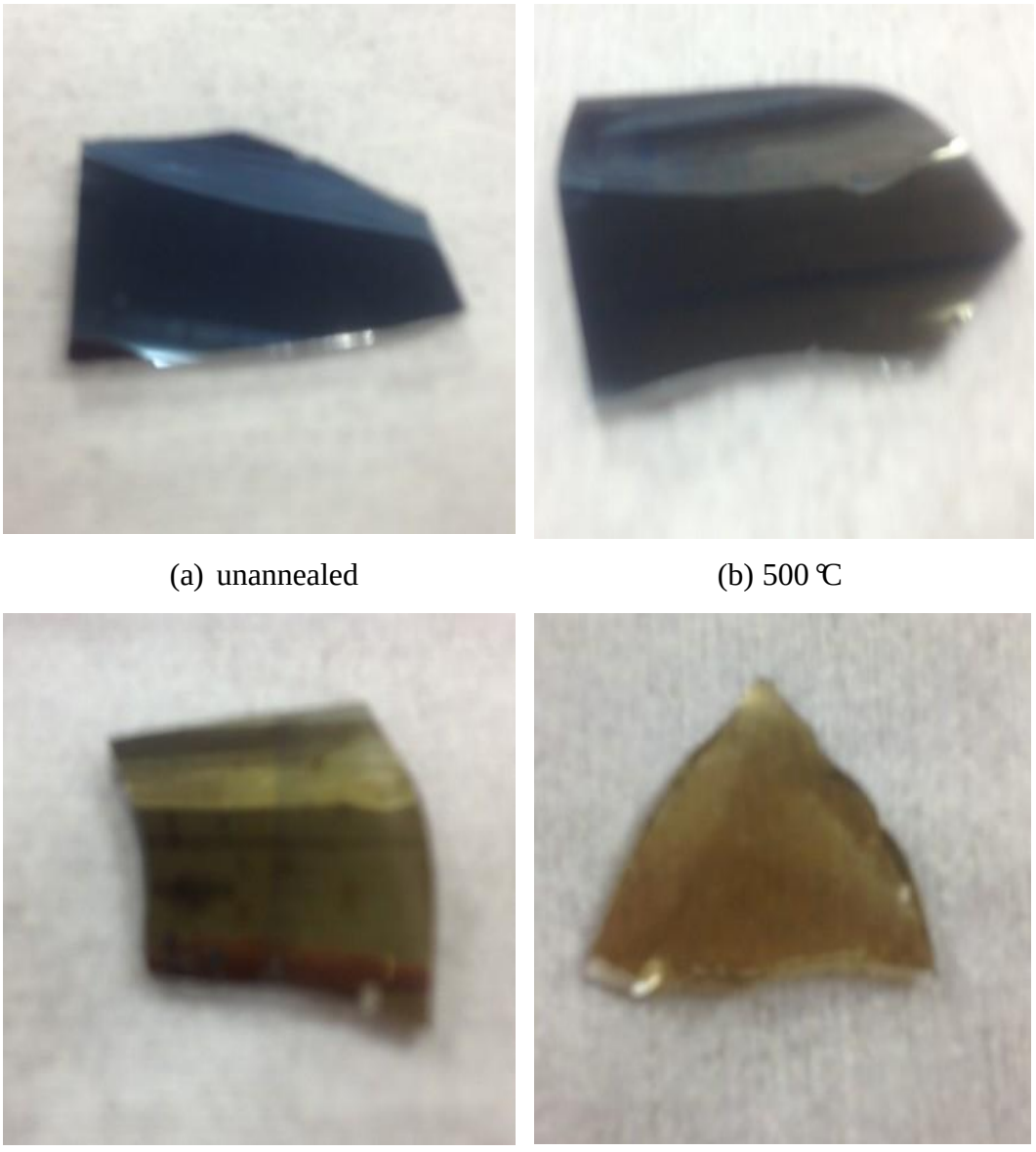

(a) unannealed (b) 500 ℃

(c) 600 ℃ (d) 700 ℃

Figure4.11 Images of unannealed and annealed sample at 500 ℃, 600 ℃, 700 ℃.

4.4 Calculation Optimization

In order to optimize the SS-AlN solar selective coating, the multilayer coatings were simulated by using MATLAB. The simulation program of multi-layer coatings employs the matrix method to calculate the reflectance. Specifically, the system of K layers is characterized by the feature matrix below (assuming that the light has vertical incidence):

$$\begin{bmatrix} B \\ C \end{bmatrix} = \prod_{j=1}^{k} \begin{bmatrix} \cos\delta_j & \frac{i}{N_j}\sin\delta_j \\ iN_j\sin\delta_j & \cos\delta_j \end{bmatrix} \begin{bmatrix} 1 \\ N_{k+1} \end{bmatrix} \qquad (4.1)$$

where i^2=-1, N_j is the refractive index of the jth layer, and δ_j is the phase thickness of the jth layer. The reflectance of the system of K layers can be calculated as:

$$R = \left(\frac{N_0 - C/B}{N_0 + C/B}\right)\left(\frac{N_0 - C/B}{N_0 + C/B}\right)^* \qquad (4.2)$$

where N_0 is the refractive index of air. For multilayer coatings, the absorptance and emittance can be calculated by combining the reflectance spectra, the solar spectra and the blackbody radiation spectra at certain temperature. Additionally, for a composite layer, such as SS-AlN layer, effective medium theory (Bruggeman model) is applied [47-49]. The optical constants of compositions can be found in the book [76-78].

The structure of the sample is shown as Figure 4.12(a). The homogenous SS-AlN absorbing layers sandwiched with AlN antireflection layer and a Cu base layer. According to the industrial process, the stainless steel volume fraction can be estimated for low metal volume fraction (LMVF) layer is 0.25 and high metal volume fraction (HMVF) layer is 0.33. The optical properties of the multilayer coating are simulated with such a structure using the MATLAB program. Figure 4.12(b) shows the calculated reflectance spectrum of the SS-AlN sample. By calculation, the absorptance of the whole system is 0.899 and the emittance is 0.047. The results are similar to the measured optical properties of the sample (a=0.9033, ε=0.1317). The small inaccuracy is unavoidable due to the control of industrial process and degradation of the coating.

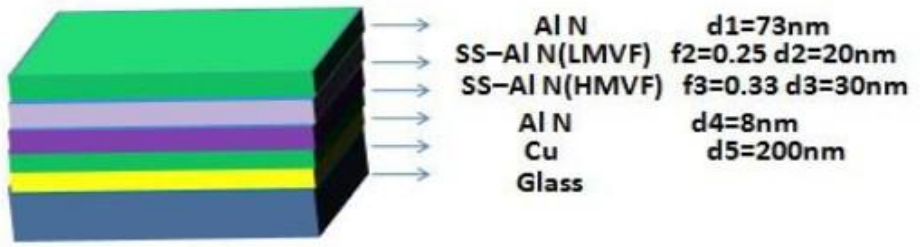

(a)

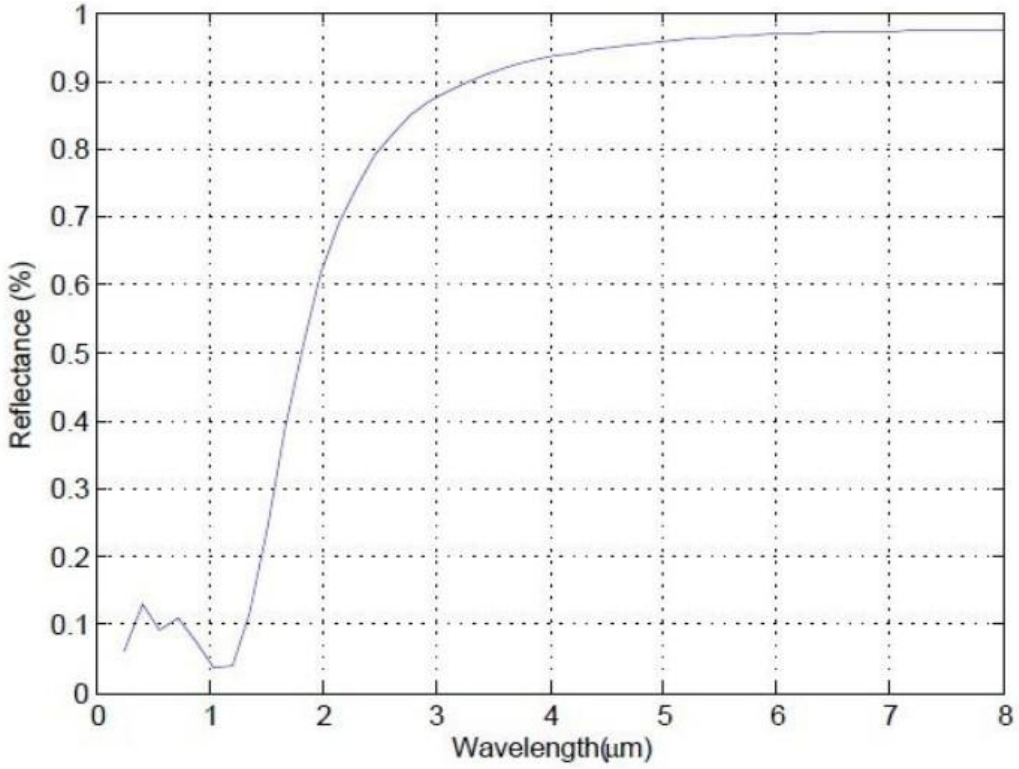

(b)

Figure4.12 Structure (a) and calculated reflectance spectrum (b) of the SS-AlN solar absorber sample

We further study the optical properties of the SS-AlN solar selective coating by optimizing structure and thickness. In the simulation program, there are changes to the total thickness of SS-AlN absorbing layers d2, d3 (a); the thickness of HMVF SS-AlN layer d3 (b); the thickness of LMVF SS-AlN layer d2 (c); and the design of the double antireflection layers.

4.5.1 Optimization of the Absorbing Layers

(a)Optimization of the total thickness of absorbing layers (d2, d3)

h: AlN(73nm)/ SS-AlN(f2=0.25, d2=20nm)/ SS-AlN(f3=0.33, d3=30nm)/AlN(8nm)/Cu
i: AlN(73nm)/ SS-AlN(f2=0.25, d2=40nm)/ SS-AlN(f3=0.33, d3=50nm)/AlN (8nm)/Cu

Table4.2 Absorptance and emittance of calculated SS-AlN coating with different thickness of absorbing layer.

	H	I
Absorptance (a)	0.8990	0.9678
Emittance (ε)(373K)	0.0469	0.0529

The reflectance spectrum named i is the result after adding thickness. After increasing the total thickness of the absorbing layers, the absorptance increases from 0.899 to 0.9678. The emittance in the infrared region also increased from 0.0469 to 0.0529.

Thus, when the thickness of absorbing layer is increased, the absorptance is improved, but the emittance rises at the same time.

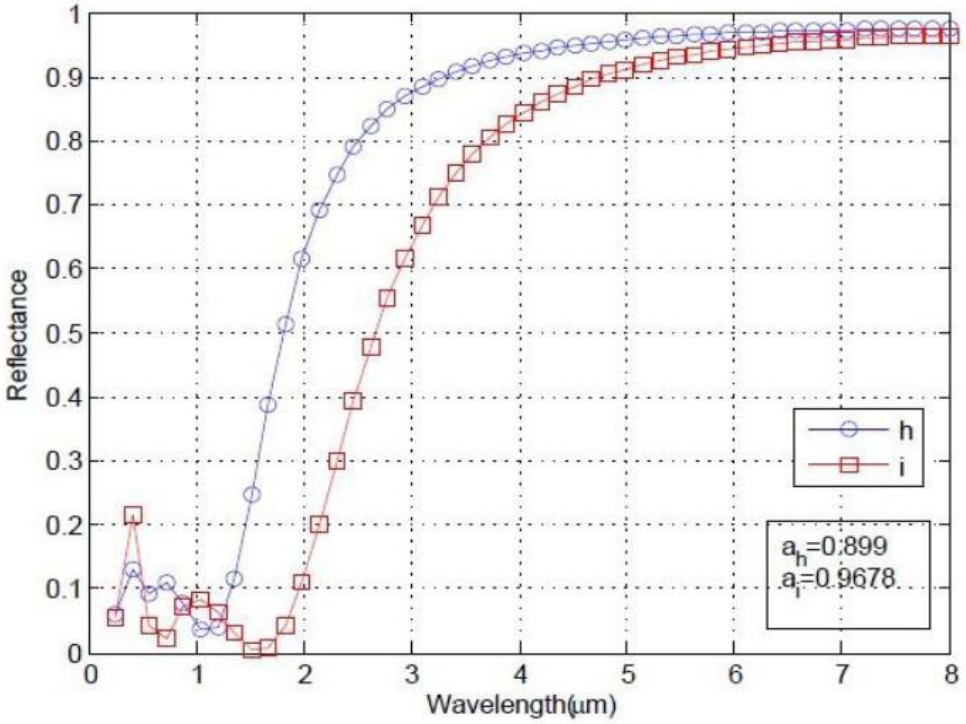

Figure4.13 Calculated spectra of SS-AlN soalr absorbers with different thickness of the absorbing layers.

（b）Optimization of the thickness of HMVF SS-AlN layer (d3)

h: AlN(73nm)/ SS-AlN(f2=0.25, d2=20nm)/ SS-AlN(f3=0.33, d3=30nm)/AlN(8nm)/Cu
j: AlN(73nm)/ SS-AlN(f2=0.25, d2=20nm)/ SS-AlN(f3=0.33, d3=50nm)/AlN(8nm)/Cu
k: AlN(73nm)/ SS-AlN(f2=0.25, d2=20nm)/ SS-AlN(f3=0.33, d3=65nm)/AlN(8nm)/Cu

Table4.3 Absorptance and emittance of calculated SS-AlN coating with different thickness of HMVF SS-AlN layer.

	H	J	K
Absorptance (a)	0.8990	0.9655	0.9693
Emittance (ε)(373K)	0.0469	0.0507	0.0553

Figure 4.14 shows that, when the thicknesses of other layers are kept as constants, the area of high absorption (low reflectance) drifts towards the long wavelengths with the increasing thickness of d3, which results in improvements of the absorptance. While the emittance rises to some extent.

Thus, it can be said that increasing the thickness of d3 can improve the absorptance.

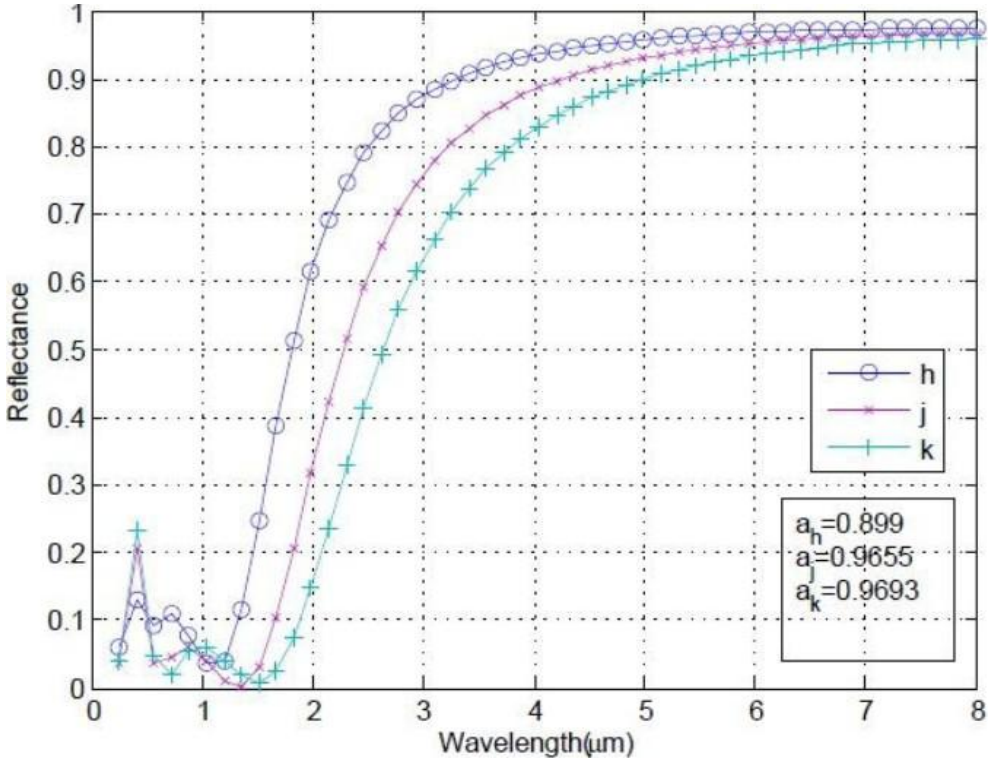

Figure4.14 Calculated spectra of SS-AlN solar absorbers with different thickness of HMVF SS-AlN layer.

(c)Optimization of the thickness of LMVF SS-AlN absorbing layer (d2)

i: AlN(73nm)/ SS-AlN(f2=0.25, d2=40nm)/ SS-AlN(f3=0.33, d3=50nm)/AlN(8nm)/Cu
j: AlN(73nm)/ SS-AlN(f2=0.25, d2=20nm)/ SS-AlN(f3=0.33, d3=50nm)/AlN(8nm)/Cu
l: AlN(73nm)/ SS-AlN(f2=0.25, d2=30nm)/ SS-AlN(f3=0.33, d3=50nm)/AlN(8nm)/Cu

Table4.4 Absorptance and emittance of calculated SS-AlN coating with different thickness of LMVF SS-AlN layer.

	I	J	L
Absorptance (a)	0.9678	0.9655	0.9703
Emittance (ε)(373K)	0.0529	0.0507	0.0516

The reflectance spectra of SS-AlN solar absorber with different d2 thickness are shown in Figure 4.15. The absorptance does not linearity vary with the thickness d2 and has a maximum 0.9703 when d2 is 30nm. However, the emittance increases with the raised thickness.

Thus, the thickness of LMVF absorbing layer (d2) is optimized to be 30nm when the thickness of HMVF absorbing layer (d3) is 50nm.

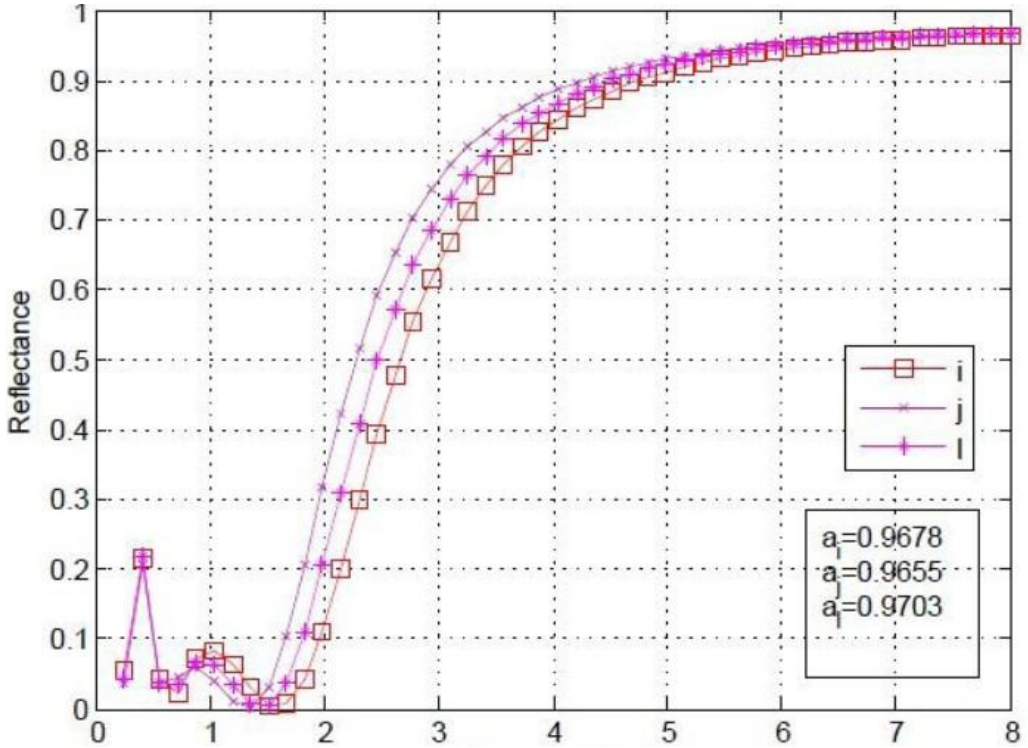

Figure4.15 Calculated spectra of SS-AlN solar absorrs with different thickness of LMVF SS-AlN layer

4.5.2Optimization of the Antireflection Layer

Based on the above thickness optimization of absorbing layers, an optimum structure is chosen:

l: AlN(73nm) / SS-AlN(f2=0.25, d2=30nm)/ SS-AlN(f3=0.33, d3=50nm)/AlN(8nm)/Cu

Then, further research of the antireflection layer is carried out. A double antireflection layer is employed, which is made of a SiO_2 layer and an AlN layer, shown in Figure 4.16

m: SiO_2 (40nm)/AlN(30nm) / SS-AlN(f2=0.25, d2=30nm)/ SS-AlN(f3=0.33, d3=50nm)/AlN(8nm)/Cu

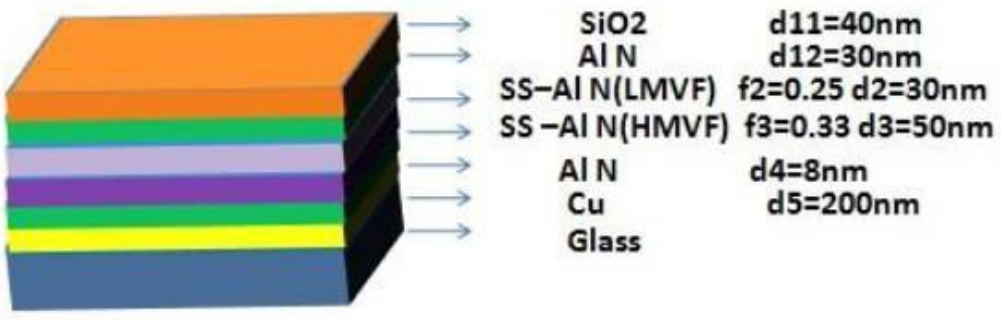

Figure4.16 Optimized structure of SS-AlN solar absorbers with double antireflection layers

Table4.5 Absorptance and emittance of calculated SS-AlN coating with single antireflection layer and double antireflection layers

	L	M
Absorptance (a)	0.9707	0.9703
Emittance (ε)(373K)	0.0513	0.0512

The refractive index of SiO2 layer is closer to that of air, which will help to improve the absorption. The calculated reflectance spectra are shown in the Figure 4.17. The

absorptance is improved from 0.9703 to 0.9707 and the emittance rises from 0.0512 to 0.0513. This illustrates that the double antireflection layers can increase absorptance, especially in short wavelength region and has few influence on the emittance.

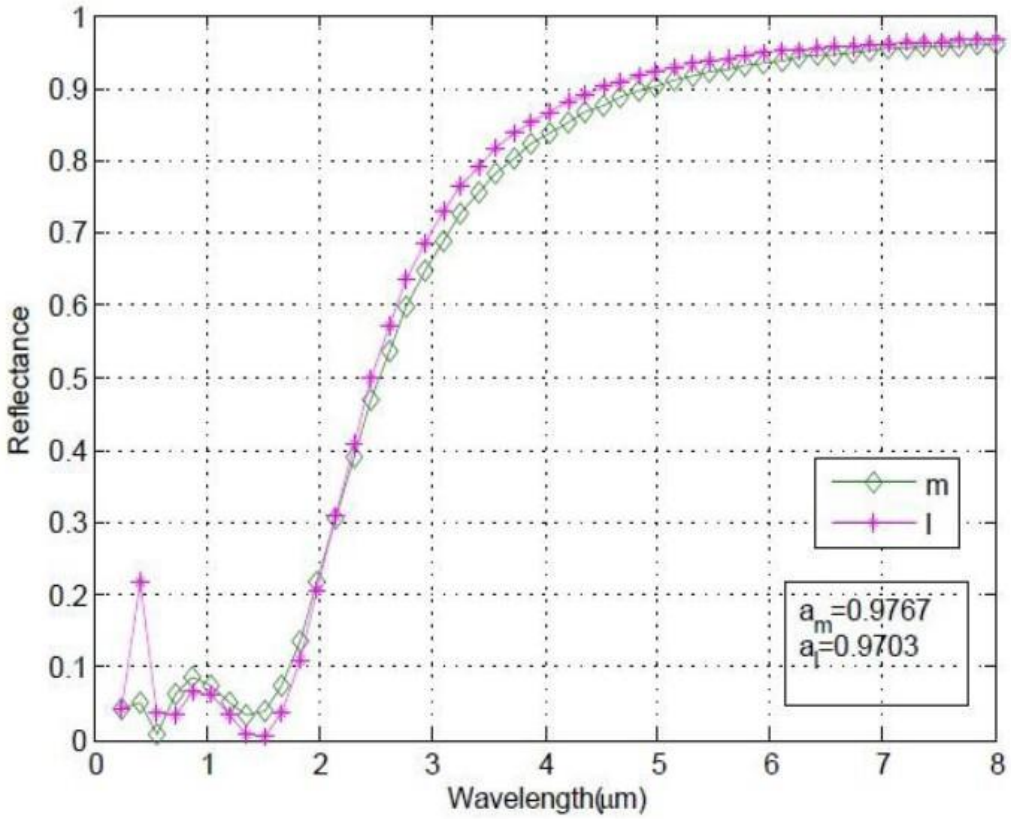

Figure4.17 Optimized reflectance spectrum of SS-AlN soalr absorber with double antireflection layers (m) and reflectance spectrum of SS-AlN solar absorber with single antireflection layer (l).

4.6 Summary

As a typical commercial solar absorber, nanostructured SS-AlN solar selective coating deposited by sputtering is studied. The structure and optical properties are analyzed by SEM, TEM and spectrometers. We also compare the unannealed sample and annealed samples at 100℃, 200℃, 300℃, 400℃, 500℃, 600℃, 700℃ for 1 hour. Furthermore, calculation optimization is made by MATLAB program. We conclude that:

- The surface morphology of SS-AlN solar selective coating is overall uniform, even though there are some holes 100-800 nanometers wide. The structure is estimated by TEM pictures :

  AlN (73nm)/ SS-AlN (LMVF)(20nm)/ SS-AlN(HMVF)(30nm)/AlN(8nm)/Cu.

  The absorptance of 0.9033 and the emittance of 0.1317 are measured by spectrometers
- Annealed below 500℃ for 1 hour, the sample has a higher absorptance and a lower emittance than unannealed sample. Especially, annealed between 200℃ and 300℃，its absorptance raises up and the emittance drops down, which improves it greatly, compared with the optical properties of the unannealed sample.
- The SS-AlN samples annealed above 500℃ are damaged and could not work anymore.
- By calculation, the optimized structure of SS-AlN solar selective coating is:

  SiO2(40nm)/AlN(30nm)/SS-AlN(f2=0.25,d2=30nm)/SS-AlN(f3=0.33, d3=50nm)/AlN(8nm)/Cu

  Double antireflective layers help to improve the absorptance.

Chapter 5 Fe_3O_4 Nanoparticles Solar Selective Coatings

The synthesis and potential applications of Fe_3O_4 nanoparticles are widely researched [69-74]. They have been applied in many areas, such as biomedical, spintronics, plasmonic, and gas sensing, etc. However, the work on Fe_3O_4 nanoparticles solar selective coatings is limited [75]. Fe_3O_4 nanoparticles could potential be an excellent candidate for solar heating as the nanoparticles could enhance the absorption. Therefore, we have studied the coatings of Fe_3O_4 nanoparticles synthesized by a green chemical method and further characterized their structural, optical and morphological properties using various techniques. Finally, the effects of the thickness, substrate roughness and heat treatment on Fe_3O_4 nanoparticles coatings are discussed.

5.1 Fe_3O_4 Nanoparticles Synthesis and Film Formation

- **Preparation of Fe_3O_4 Nanoparticles by Co-precipitation**

Co-precipitation technique is a common method of magnetic nanoparticle synthesis [69-74]. In this work, Fe_3O_4 nanoparticles were synthesized by co-precipitation of ferrous sulphate heptahydrate ($FeSO_4.7H_2O$) and ferric sulphate ($Fe_2(SO_4)_3$). Initially, an aqueous solution of ferrous sulfate with a concentration of 1 mol/l was mixed with another aqueous solution of a ferric sulfate with a concentration of 1 mol/l, at the molar ratio of Fe^{2+} and Fe^{3+} of 1:1.8 at 60 ℃. Then, the ammonia solution (NH_4OH) was added to the iron solution until it reached PH 10 under vigorous stirring for 30 minutes at 60 ℃. After cooling to room temperature, the solution was put close to a magnet so that the sediment powder containing nanoparticles was separated from the suspension, and washed with acetone for three times and de-ionized water for another three times.

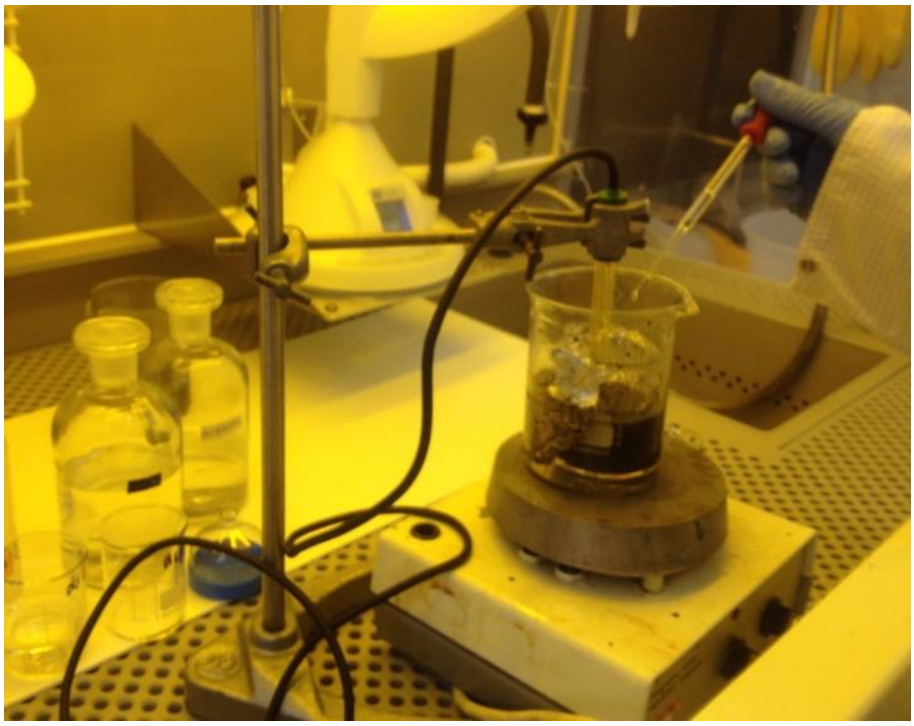

Figure5.1 Fe_3O_4 Nanoparticles preparation

- **Substrate Pretreatment**

Copper sheet of 1 mm thickness was commercially available. The copper sheet was cut into 20mm×20mm small pieces to be the substrates of the Fe3O4 nanopaticles solar selective coatings.

Step 1: Surface roughness

In order to obtain uniform coatings, the copper substrates were polished and roughed by machine in our workshop.

Step 2: Clean process

The polished copper substrates were orderly cleaned by acetone and IPA in the ultrasonic wave cleaner for 5 minutes each. Then the substrates were washed with de-ionized water and dried with gaseous N_2.

- **Dip-Coating**

To prepare for Fe_3O_4 nanoparticles solar selective coating, dip-coating method is employed. We flatly immersed the copper substrate in the Fe_3O_4 nanoparticles solution and maintain this process for a while. Then withdrawing was carried out at a constant speed, which determines the thickness of thin film. After that, it took 2 hours to evaporate the solvent and formed a Fe_3O_4 thin layer.

5.2 Characterization of Fe_3O_4 Nanoparticles

- Particle Size

Figure 5.2 shows the TEM image of Fe_3O_4 nanoparticles. The Fe_3O_4 nanoparticles are needle-like and the average size is estimated around 20 nanometers. Thus, the result confirms that the prepared Fe_3O_4 nanoparticles are nanometric.

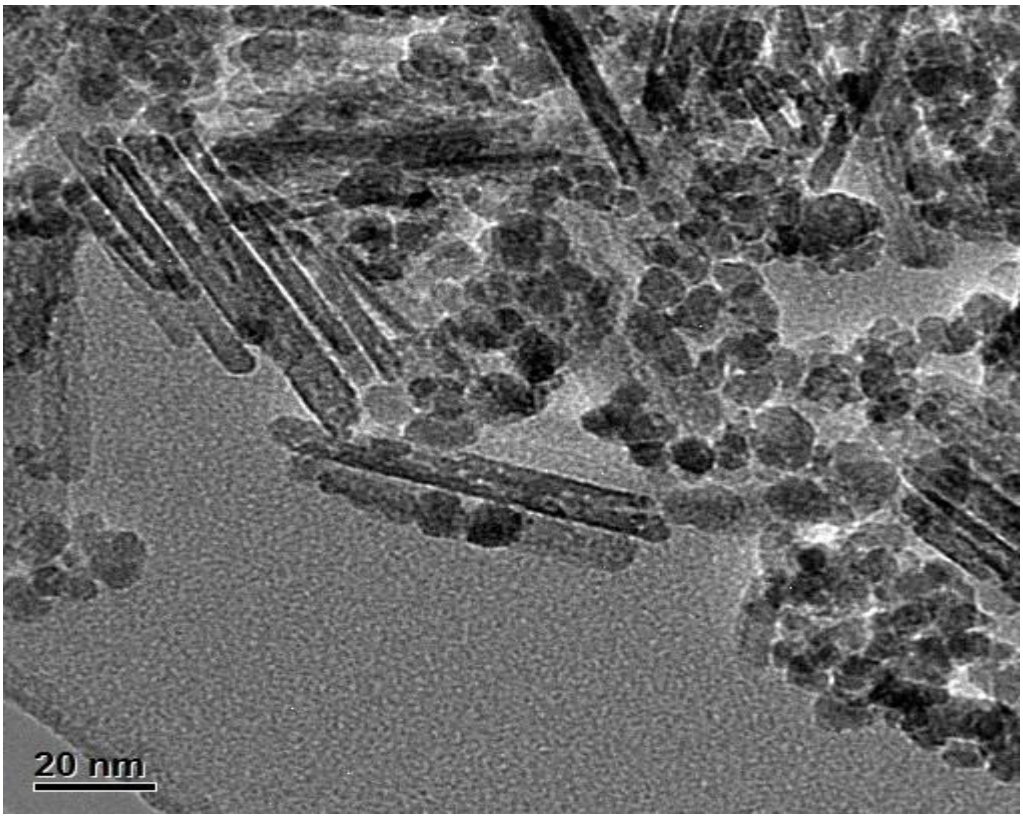

Figure5.2 The TEM image of Fe_3O_4 nanoparticles.

5.3 Thickness Analysis

In order to analyze the performance of the Fe_3O_4 nanoparticles coatings due to different thicknesses, samples with various dip times were made. The Cu substrates are dipped into Fe_3O_4 nanoparticles solution for one time, two times and three times.

5.3.1 Thicknesses Measurement of Coatings with Different Dip Times

The thicknesses of samples are measured by Alpha-step Profiler. The results of Fe_3O_4 nanoparticles coatings with different dip times are shown in Figure 5.3 (a), (b), and (c). It is obvious to see that the thicknesses of coatings with one dip, two dips and three dips are around 5μm, 20μm and 56μm, respectively. With the rise of the number of dips, the thickness of coating increases greatly.

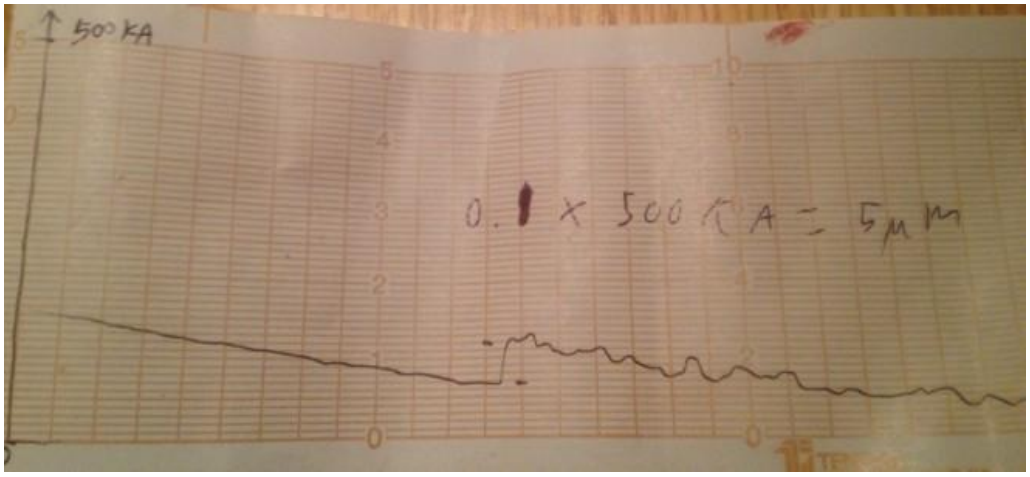

(a) One dip

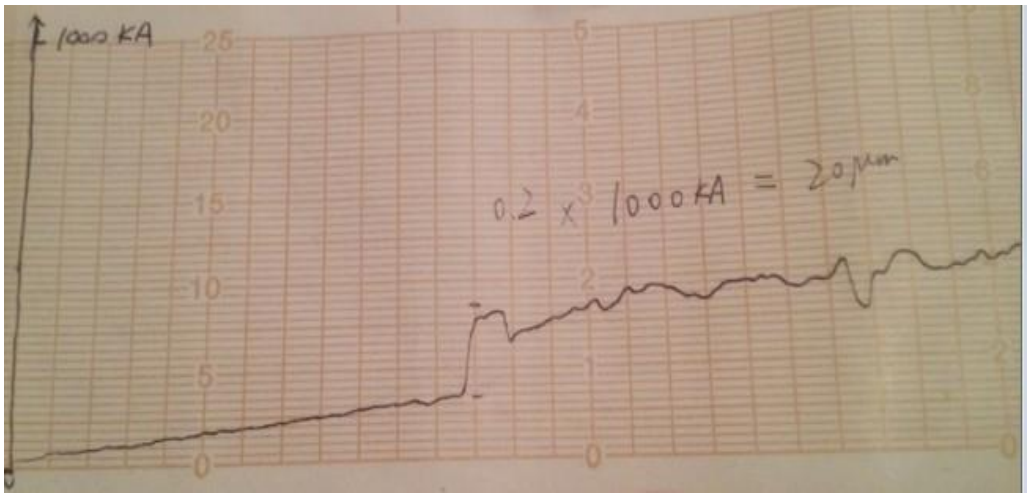

(b) Two dips

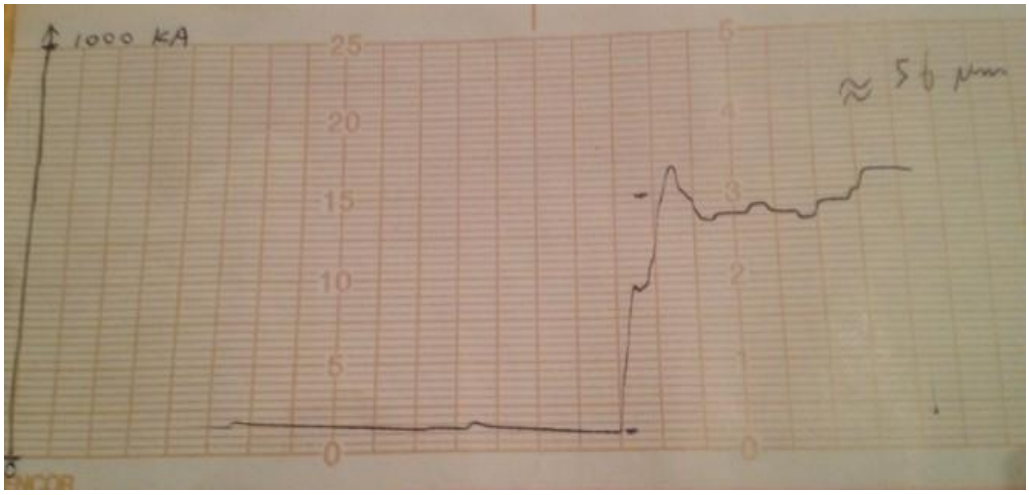

(c) Three dips

Figure5.3 The thicknesses of Fe_3O_4 nanoparticles coatings on polished copper substrate with different dip times. (a) one dip, (b) two dips, (c) three dips. They are measured by Alpha-step Profiler.

5.3.2 Surface Morphology

Figure 5.4 shows surface morphologies of Fe_3O_4 nanoparticles coatings with one dip (a), two dips (b) and three dips (c). The one-dip coating is a granular structure with small cracks (Figure 5.4 (a)). There seems to be more cracks when we the dip number was increased (Figure 5.4 (b), (c)). Moreover, the three-dip coating is detached and damaged (Figure 5.4 (c)). Therefore, increasing the number of dips followed by an increase in thickness, can lead to unfavorable detach of the film [75].

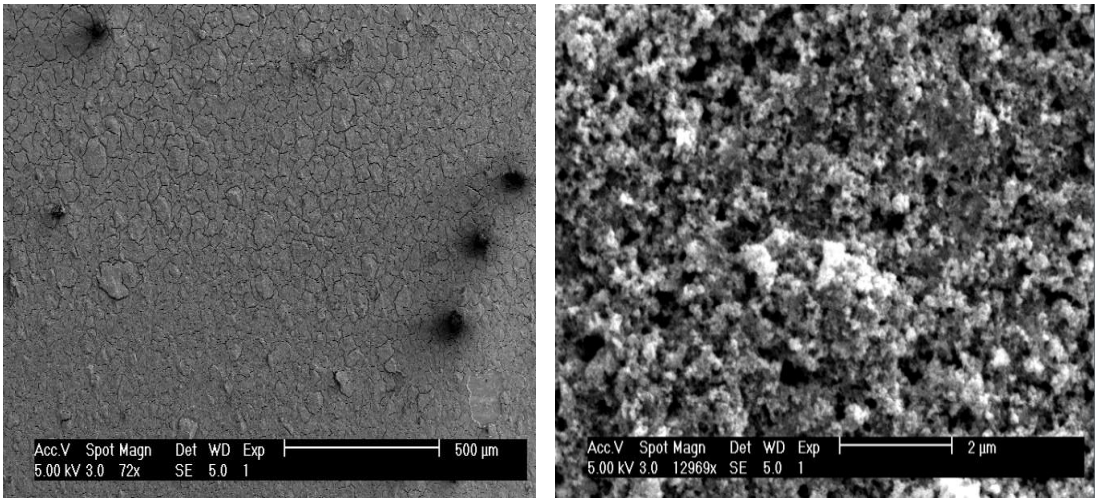

(a) Surface of Fe_3O_4 nanoparticles coatings with one dip

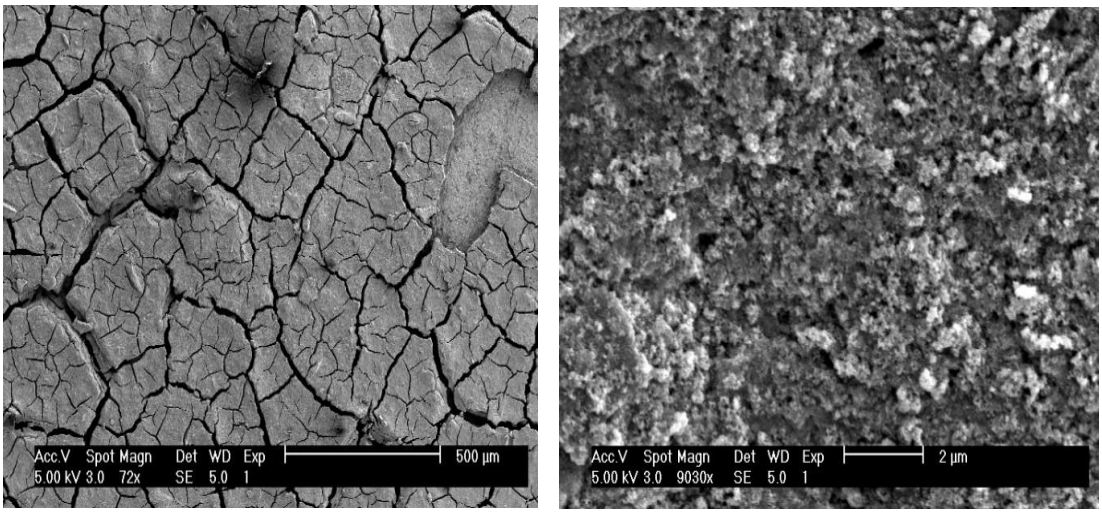

(b) Surface of Fe_3O_4 nanoparticles coatings with two dips

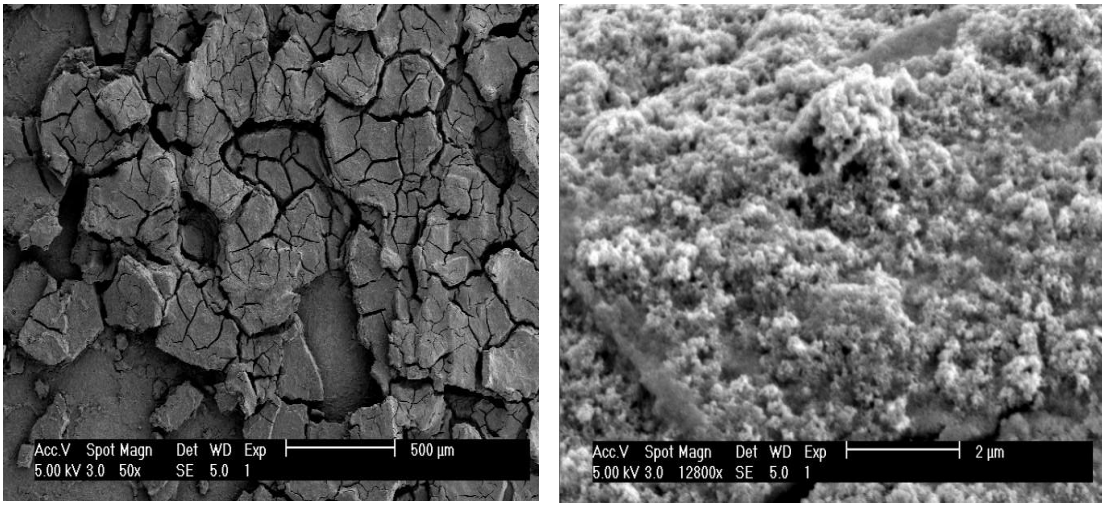

(c) Surface of Fe_3O_4 nanoparticles coatings with three dips

Figure5.4 SEM images of Fe_3O_4 nanoparticles coatings on polished copper substrate with different dip times. (a) coating with one dip, (b) coating with two dips, (c) coating with three dips.

5.4 Substrate Roughness Analysis

We made coatings of Fe_3O_4 nanoparticles with one dip on polished copper and rough copper substrates. These substrates were polished and roughed in the workshop machine, and are shown in Figure 5.5. The surface morphologies and optical properties of these samples are further studied by SEM and Spectrometers.

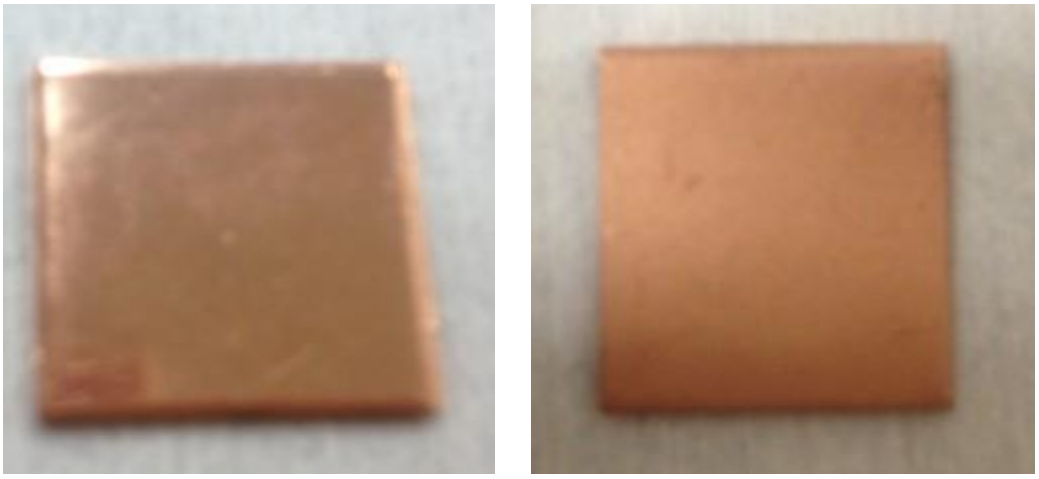

(a) polished (b)rough

Figure5.5 Images of polished and rough copper substrates.

5.4.1 Surface Morphology

Figure 5.6 shows the surface morphologies of Fe_3O_4 nanoparticles coatings on polished and rough copper substrate. The surface of Fe_3O_4 nanoparticles coatings on polished copper substrate has more cracks than that on rough copper substrate. It illustrates that the bonding of coating on the rough substrate is better.

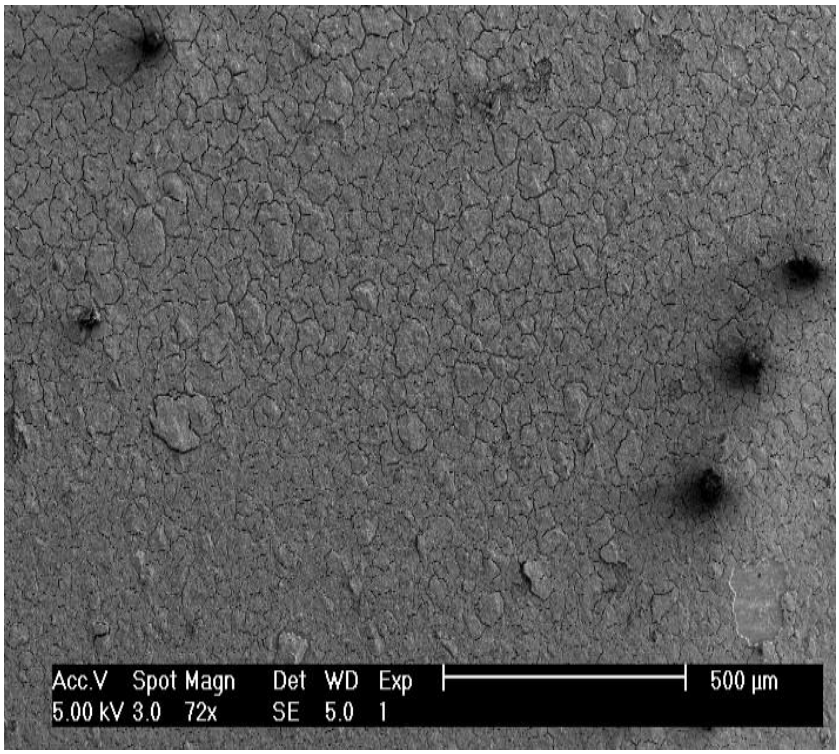

(a) coating on polished copper

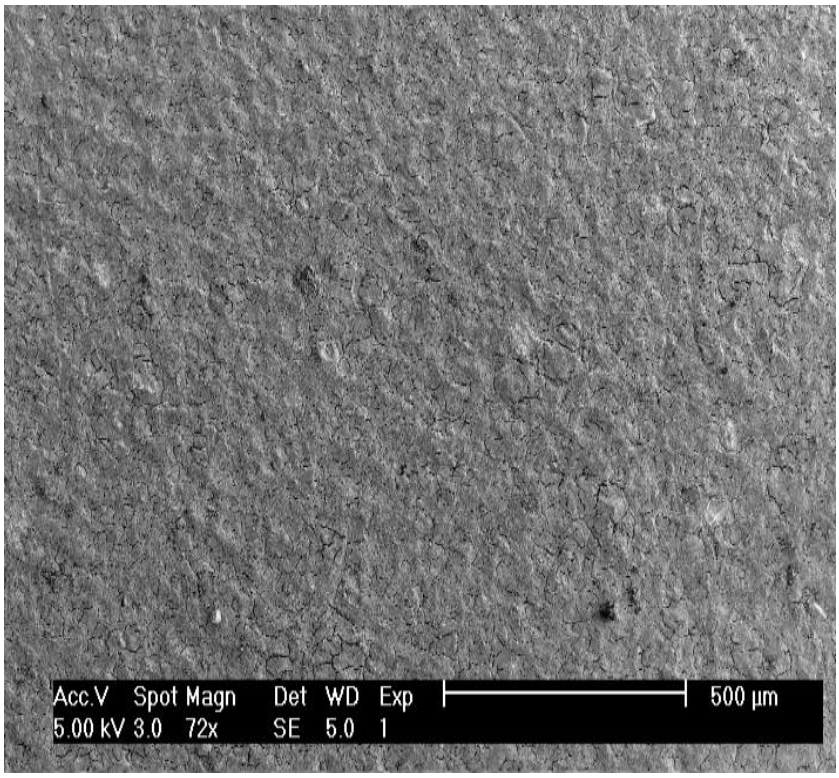

(b) coating on rough copper

Figure5.6 SEM images of Fe_3O_4 nanoparticles coatings on polished copper substrate (a) and rough copper substrate (b).

5.4.2 Optical Characterization

The reflectance spectra of Fe_3O_4 nanoparticles coatings on polished and rough copper substrates are shown in Figure 5.7. We can clearly see that coating on polished substrate has a higher reflectance than that on rough substrate. Even though this reduces the absorption in the solar region (0.3-2.5μm), the change is trivial. More importantly, higher reflectance in infrared region (2.5-10μm) brings smaller the thermal emittance. Therefore, regarding the effects of thermal emittance, the Fe_3O_4 nanoparticles coatings are made on polished copper substrates for further research.

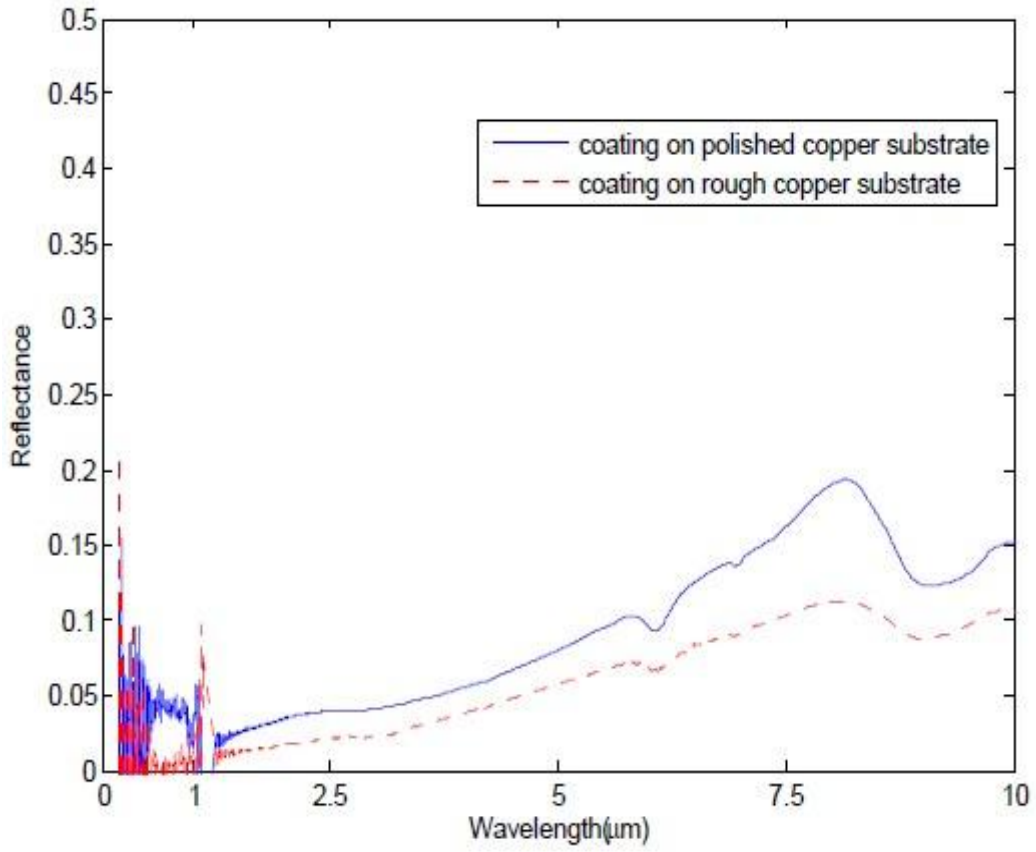

Figure5.7 Measured reflectance Spectra of Fe_3O_4 nanoparticles coatings on polished and rough copper substrates.

5.5 Heat Treatment

The performances of Fe_3O_4 nanoparticles coatings on polished copper substrate after heat treatment are researched in this section. The samples are annealed at 100℃, 200℃, and 300℃ for 1 hour. From the images in Figure 5.8, it was found that the colours of Fe_3O_4 nanoparticles coatings changed from black to yellow then brown with the increase of annealing temperatures. They seem to be further oxidized by annealing. The effects of heat treatment on Fe_3O_4 nanoparticles coatings are further studied by SEM and Spectrometers.

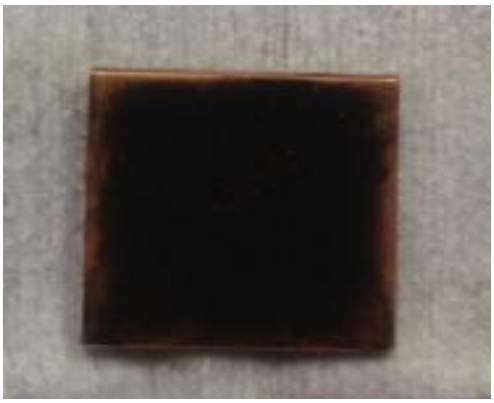

(a) unannealed

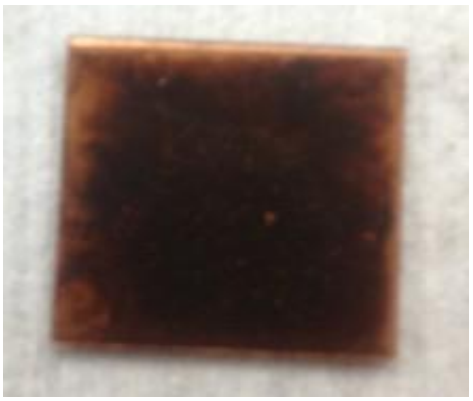

(b) annealed at 100℃ for 1h

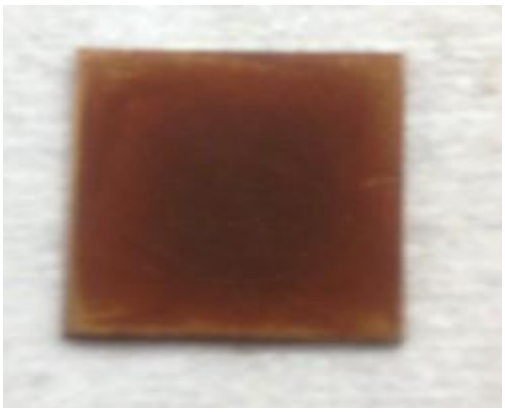

(c) annealed at 200° C for 1h

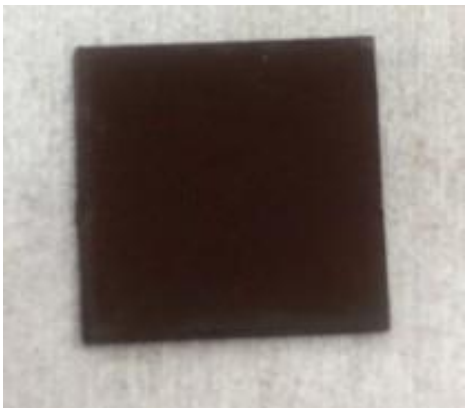

(d) annealed at 300° C for 1h.

Figure5.8 Images of Fe_3O_4 nanoparticles coatings on polished copper substrates: (a) unannealed, (b) annealed at 100℃ for 1 hour, (c) annealed at 200℃ for 1 hour, (d) annealed at 300℃ for 1hour.

5.5.1 Surface Morphology

Figure 5.9 shows the SEM pictures of Fe_3O_4 nanoparticles coating after annealing. The surface of Fe_3O_4 nanoparticles coating after annealing at 100 ℃ for 1 hour (Figure 5.9(b)) is more refined and uniform, compared with that of unannealed sample (Figure5.9 (a)). However, with the rise of annealing temperature, the coating is partly damaged (Figure 5.9(c), (d)).

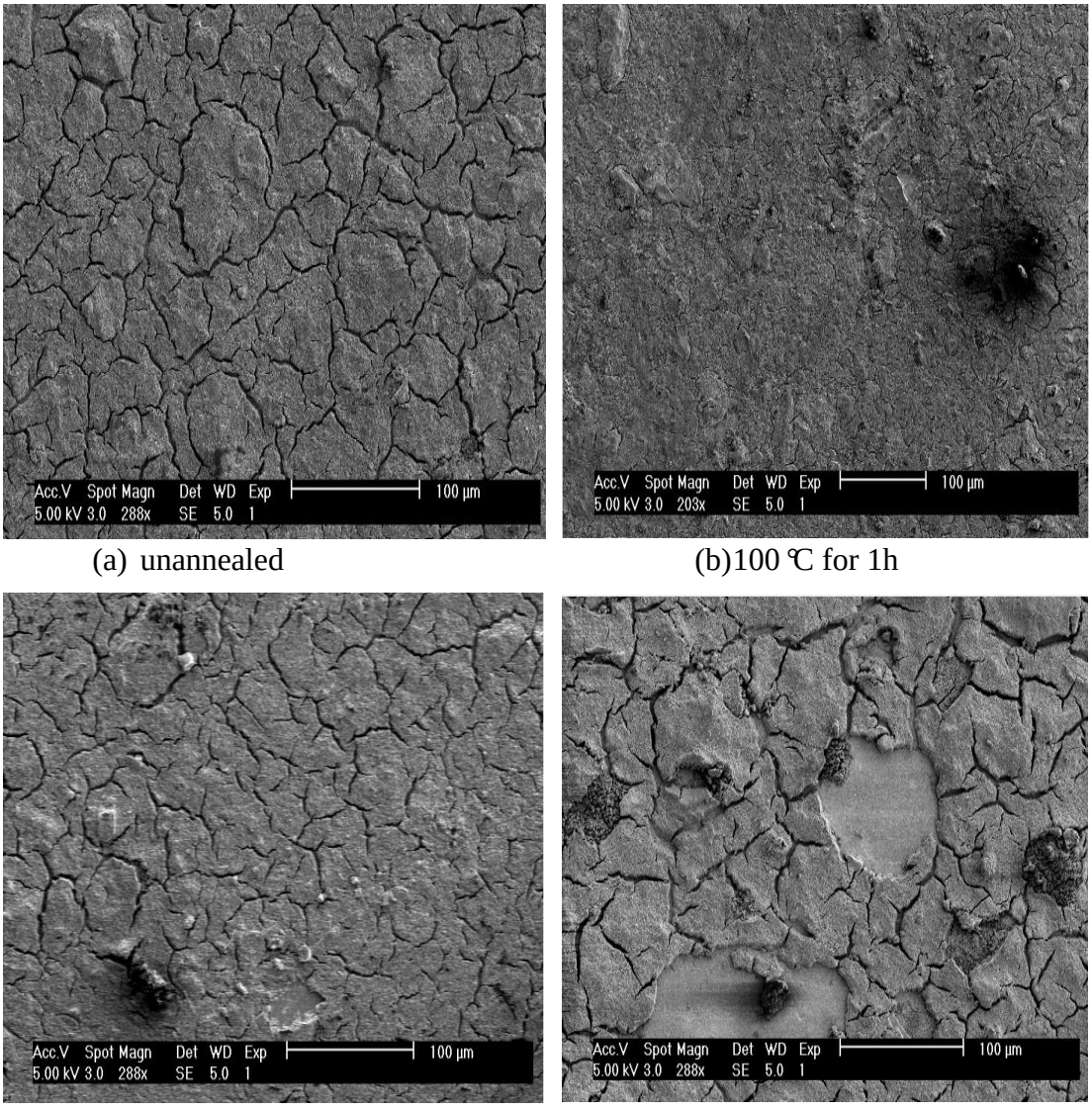

(a) unannealed (b)100 ℃ for 1h

(c) 200 ℃ for 1h (d) 300 ℃ for 1h

Figure5.9 SEM images of Fe_3O_4 nanoparticles coatings on polished copper substrates. (a) unannealed, (b) annealed at 100 ℃ for 1 hour, (c) annealed at 200 ℃ for 1 hour, (d) annealed at 300 ℃ for 1 hour.

5.5.2 Optical Characterization

The reflectance spectra of Fe_3O_4 nanoparticles coating on polished copper substrate and that after annealing are shown in Figure 5.10. The coatings after annealing have a higher reflectance than the unannealed coating, especially in the infrared region, which reduce emittance largely. Specifically, the coating annealed at 100 ℃ has the better optical properties as a solar sbsorber, which has a low reflectance in the solar region (0.3-2.5μm) and high reflectance in infrared region (2.5-10μm).The absorptance of 0.926 and emittance of 0.378, as shown in Table 5.1, are achieved. Annealed after 200 ℃, the coatings have high reflectance in the wavelength range of 1μm and 2.5μm, which decrease the absorptance. Overall, the coatings after annealing reduce emittance and improved the optical properties. However, annealed above 200 ℃, the coatings decrease the absorptance to some extent.

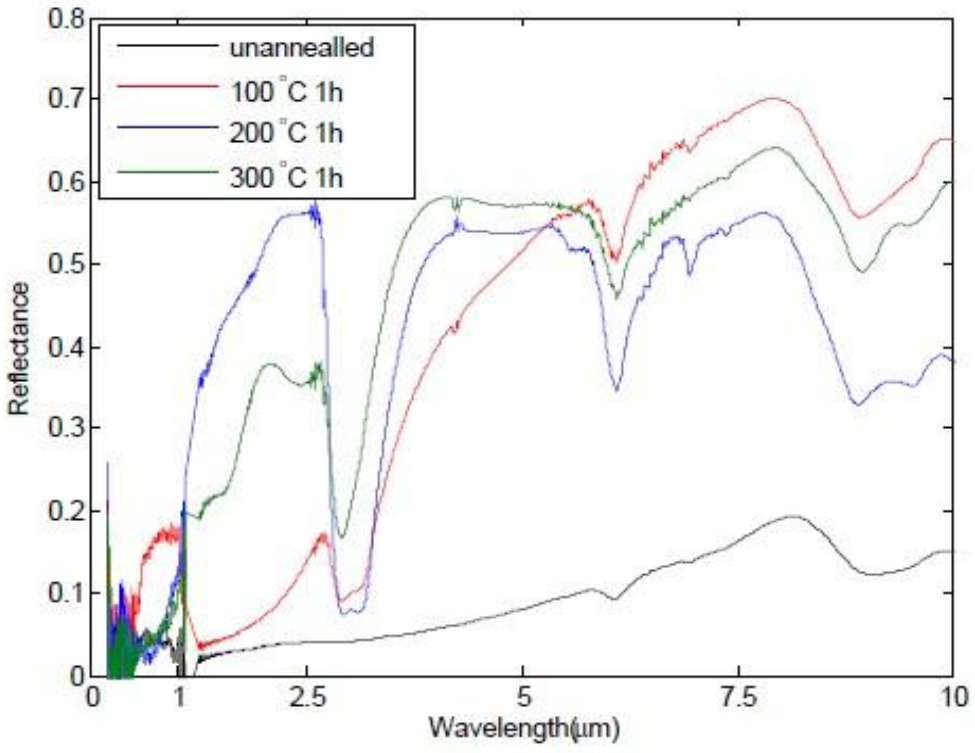

Figure5.10 Measured reflectance spectra of Fe_3O_4 nanoparticles coating on polished copper substrate and that after annealing at 100 ℃, 200 ℃, 300 ℃ for 1 hour.

Table5.1 Absorptance and emittance of Fe3O4 nanoparticles coatings on polished copper substrates and that after annealing.

	Absorptance (a)	Emittance (ε)
Unannealed	0.970	0.911
100 ℃ for 1h	0.926	0.378
200 ℃ for 1h	0.838	0.671
300 ℃ for 1h	0.909	0.460

5.6 Summary

A green chemical method of co-precipitation is employed to make Fe_3O_4 nanoparticles. Then, the coating of Fe_3O_4 nanoparticles is formed by dip-coating process on the copper substrate. The effects of the thickness, substrate roughness and heat treatment on Fe_3O_4 nanoparticles coatings were further studied leading to the following conclusions:

- Fe_3O_4 nanoparticles are needle-like and the average size is estimated around 20 nanometers.
- Increasing the thicknesses of Fe_3O_4 nanoparticles coatings made by increasing the number of dip times, lead to unfavorable detach of the film.
- The Fe_3O_4 nanoparticles coating has a better bonding with rough copper substrate. However, the coating on polished copper substrate has higher reflectance in infrared region than that on rough copper substrate, which helps to reduce thermal emittance.
- The Fe_3O_4 nanoparticles coatings after annealing at 100 ℃, 200 ℃, and 300 ℃ reduce the thermal emittance, compared with unannealed coating. Especially, the optical properties of coating annealed at 100 ℃ are significantly improved, i.e. a=0.926, ε=0.378. Annealed above 200 ℃, the coatings decrease the absorptance to some extent.

Chapter 6 Conclusions and Future Work

6.1 Summary and Conclusions

The nanostructured SS-AlN solar selective coating deposited by sputtering, as a typical commercial solar absorber, has been studied experimentally and theoretically. Also, the Fe_3O_4 nanoparticles were prepared by a green chemical method of co-precipitation and form the coating on copper substrate by dip-coating process. Then, the Fe_3O_4 nanoparticles coatings have been investigated as a potential solar absorber.

- The surface morphology of nanostructured SS-AlN solar selective coating is overall uniform, even if there are some holes with 100-800 nanometers. The structure is estimated by TEM pictures :
  AlN (73nm)/SS-AlN (LMVF) (20nm)/SS-AlN (HMVF) (30nm)/AlN (8nm)/Cu.
  The absorptance (a) of 0.9033 and the emittance (ε) of 0.1317 are measured by spectrometers.

- Annealed below 500 ℃ for 1 hour, the SS-AlN solar selective coating has a higher absorptance and a lower emittance than unannealed sample. Especially, annealed between 200 ℃ and 300 ℃， its absorptance increases and the emittance decreases, to values such as a=0.9378, ε=0.11. However, the SS-AlN samples annealled above 500 ℃ are most likely to be damaged.

- Simulated by the MATLAB programe, the optimized structure of SS-AlN solar selective coating is:
  SiO2 (40nm)/AlN (30nm)/SS-AlN (f2=0.25, d2=30nm)/SS-AlN (f3=0.33, d3=50nm)/AlN (8nm)/Cu.
  Double antireflective layers help to improve the absorptance.

- Fe_3O_4 nanoparticles prepared by co-precipitation are needle-like and the average size is estimated around 20 nanometers. Increasing the thicknesses of Fe_3O_4 nanoparticles coatings by adding the number of dip times, leads, however, to unfavorable detach of the film.

- The Fe_3O_4 nanoparticles coating has a better bonding with rough copper substrate. However, the coating on polished copper substrate has higher reflectance in infrared region than that on rough copper substrate, which helps to reduce thermal emittance. The Fe_3O_4 nanoparticles coatings after annealing at 100 ℃, 200 ℃, and 300 ℃ reduce the thermal emittance, compared with the unannealed coating. Especially, the optical properties of the coating annealed at 100 ℃ are improved greatly with a=0.926 and ε=0.378, which suggests that Fe_3O_4 nanoparticles could potentially used for the solar heating applications.

6.2 Future work

- For better understanding of Fe_3O_4 nanoparticles coatings, there are several directions for the future work: (1) prepare thinner Fe3O4 nanoparticles coatings, less than 1μm; (2) compare the effects of different substrate; (3) improve the bonding with the substrate.

- Study the potential of using some other materials with thermal stability as high-temperature solar absorber, such as Ti, Mo, etc.

Bibliography

1. J. M. Jefferson. “Global Climate Change and the Challenges for Renewable Energy”. *Florence*, Italy, 1998 (Pergamon), P. 1-7
2. N. S. Lewis, G. W. Crabtree, eds., “Basic Research Needs for Solar Energy Utilization: Report of the Basic Energy Sciences Workshop on Solar Energy Utilization”. *US Department of Energy Office of Basic Energy Sciences*, April 18–21, 2005.
3. “Solar Energy Technologies and Applications”. *Canadian Renewable Energy Network*, Retrieved 2007-10-22 by Wikipedia.
4. W. Werner, B. Irene, F. Gerhard. “Markets and Contributions to the Energy Supply”. *International Energy Agency*, 2005.
5. H. Tabor. “Receiver for solar energy collectors”. *U.S. 2917817,* December 22, 1959.
6. C. Kennedy. “Review of mid-to-high temperature solar selective absorber materials”. Technical report, Report No: NREL/TP-520-31267, *National Renewable Energy Laboratory*, 2002.
7. N. Etherden, T. Tesfamichael, G. A. Niklasson, A. E. Wackelgard. “A theoretical feasibility study of pigments for thickness-sensitive spectrally selective paints”. *J Phys D: Appl Phys* 2004; 37: 1115-22.
8. F. Gonz áez, E. Barrera-Calva, L. Huerta and R. Mane. “Coatings of Fe3O4 Nanoparticles as Selective Solar Absorber”. *The Open Surface Science Journal*, 2011, 3, 131-135
9. F. K. Richtmyer and E. H. Kennard. “Introduction to Modern Physics”. 4 th ed.(McGraw-Hill, New York, 1947)
10. J. M. Kendall and C. M. Berdahl. “Two Blackbody Radiometers of High Accuracy”. *Appl. Opt*.9, 1082-1091(1970)
11. J. A. Duffie and W. A. Beckman. “Solar Engineering of Thermal Progresses”. 2nd ed. (Wiley-Interscience, New York,1991)

12. M. Iqbal. “An Introduction to Solar Radiation”. *Academic Press,* Ontario, Canada, 1983.
13. F. Kasten. “A New Table and Approximate Formula for Relative Optical Air mass”. *Arch. Meteorol.* Geophys. Bioklimatol. Ser. B 14, 206-233(1966)
14. M. A. Lind, R. B. Pettit, and K. D. Masterson. “The Sensitivity of Solar Transmittance Reflectance and Absorptance to Selected Averaging Procedures and Solar Irradiance Distributions”. *Trans. ASME* 102,34-40(1980)
15. T. Tesfamichael. “Characterization of Selective Solar Absorbers, Department of Materials Science*”. The Angstrom Laboratory,* Uppsala Univeristy, 2000.
16. H. Tabor. “Solar energy research: program in the new desert research institute in Beersheba”. *Solar Energy*, 1958, 2(1):3-6
17. G. A. Niklasson, C. G. Granqvist. “Review Surface for Selective Absorption of Solar energy: an annotated bibliography 1955-1981”. *Journal of Materials science*. 1983, 18:3475-3534.
18. M. Nejati, V. Fathollahi, M. Khalaji Asadi. “Computer simulation of the optical properties of high-temperature cermet solar selective coating”. *Solar Energy*.2005,78:235-241
19. M. Farooq, Z. H. Lee. “Computations of the Optical Properties of Metal/ Insulator-Composites for Solar Selective Absorbers”. *Renewable Energy*. 2003.
20. O. P. Agnihotri and B. K. Gupta. “Solar Selective Surfaces”. *Wiley-Interscience Pub*, New York, NY, 1981, p.126
21. B. O. Seraphin. “Chemical Vapor Deposition of Thin Semiconductor Films for Solar Energy Conversion”. *Thin Solid Film* 39,87(1976)
22. A. Donnadieu and B. O. Seraphin. “Optical Performance of Absorber-Reflector Combinations for Photothermal Solar Energy Conversion*” J. Opt. Sci. Am*., 68, 292(1978)
23. D. A. Williams, T. A. Lappin, and J.A. Duffie. “Selective Radiation Properties of Particulate Coatings,” *J. Eng. Power*, 85A, 213(1963)
24. T. J. McMahon and D. L. Stierwalt. “Cost-effective PbS-Al Selective Solar-Absorbing Panel”. *SPIE,* 68, 169(1975)

25. A. Andersson, O. Hunderi, and C. G. Granqvist. “Nickel Pigmented Anodic Aluminum Oxide for Selective Absorption of Solar Energy”. *J. Appl. Physics*, 51, 754(1980).
26. M. Born and E. Wolf, Principles of Optics, 6th Ed. (Pergamon, Oxford,1980)
27. R. N. Schmidt, K. C. Park, R. H. Torberg, and J. E.Jensen. “High Temperature Solar Coating” Part I, AST-TDR-63-579, *Honeywell Corporation*, Hopkins, MN,1963
28. G. A. Niklasson and C. G. Granqvist. “Materials Science for Solar Energy Conversion Systems” edited by C. G. Granqvist, *Pergamon Press*, Oxford, 1991, p.70.
29. R. A. Buhrman and H. G. Craighead. Solar Materials Science, edited by L. E. Murr(Academic Press, Inc., New York, 1980), Chap.9.
30. H. Uchino, S. Aso, S. Hozumi, H. Tokumasu, and Y. Yoshioka. “Selective Surface of Color-Anodized Aluminum for Solar Collectors*”. Matsushita Electr. Ind. Natl. Tech*. Rep 25,994(1979).
31. E. Wackelgard, T. Chibuye, and B. Karlsson. “Improved Solar Optical Properties of a Nickel Pigmented Anodized aluminum Selective Surface”. *Univ. of Reading, UK*, 1990 (Pergamon Press, Oxford, UK), p. 177-182.
32. M. Adsten, R. Joerger, K. Jarrendahl, et al. “Optical Characterization of Industrially Sputtered Nickel-Nickel Oxide Solar Selective Surface”. *Solar Energy*, 2000, 4(68): 325-328.
33. S. Suzer, F. Kadirgan, H. M. Sohmen, et al. “Spectroscopic Characterization of Al2O3-Ni Selective Absorbers for Solar Collectors”. *Solar Energy Materials and Solar Cells*, 1998, 52: 55-60.
34. Q. Zhang, Y. Yin, D. Mills. “High Efficiency Mo-Al2O3 Cermet Selective Surfaces for High-Temperature Application”. *Solar Energy Materials and Solar Cells*, 1996, 40 : 43-53
35. T. K. Bostrom, E. Wackelgard, G. Westin. “Anti-reflection Coatings for Solution-chemically Derived Nickel-alumina Solar Absorbers”. *Solar Energy Materials and Solar Cells*, 2004, 84 : 183-191

36. J. J. Cuomo, J. F. Ziegler, J. M. Woodall. “A New Concept for Solar Energy Thermal Conversion”. *Applied Physics Letters*, 1975 (26):557-559.
37. G. L. Harding, M. R. Lake. “Sputter Etched Metal Solar Selective Absorbing Surfaces for High Temperature Thermal Collectors”. *Solar Energy Materials*, 1981 (5):445-464.
38. A. Alejandro, M. Ulises. “Thermally and Air-plasma-oxidized Titanium and Stainless Steel Plates as Solar Selective Absorbers". *Solar Energy Materials & Solar Cells*, 2006, 90: 2556-2568.
39. B. O. Seraphin and A. B. Meinel. “Optical Properties of Solids: New Development”, edited by B.O. Seraphin, *North Holland Publ. Co*., Amesterdam, 1976, Chap. 17.
40. T. Tesfamichael, W. E. Vargas, E. Wackelgard, et al. “A Feasibility Study of Integrally Colored Al-Si as a Solar Selective Absorber”. *Solar Energy Materials and Solar cells* 1998 55 : 251-265
41. C. G. Granqvist. “Spectrally Selective Surfaces for Heating and Cooling Applications”. Series ed. R. F. Potter, Tutorial Texts in Optical Engineering, Vol. TT 1, *SPIE Optical Engineering Press*, Bellingham, WA, 1989, p. 59.
42. Zhang Qi-Chu, Mills D R. “New Cermet Film Structures with Much Improved Selectivity for Solar Thermal Application”. *Appl Plays Lett*, 1992, 60(5):545-547.
43. Y. W. Zhao, H. F. Huang, Y. B. Zhang. “The Optical Properties of Anodizing Aluminum solar selective coating”. *Solar Energy*. 1985, 6(2): 135-141.
44. T. X. Wang, Q. H. Zhao, X. X. Chen. “The Fabrication and Properties of Anodizing steel solar selective coating”. *Solar Energy*, 1991, 12(1): 62-66.
45. L. Kaluza, A. S. Vuk, B. Orel. “Structural and Spectroscopic Analysis of Sol-gel Processed CuFeMnO4 Spinel and CuFeMnO4/silica Films for Solar Absorbers”. *Sol-Gel Science and Technology*, 2001, 20:61-83.
46. L. Kaluza, B. Orel, G, Drazic, et al. “Sol-gel Derived CuCoMnOx Spinel Coatings for Solar Absorbers: Structural and Optical Properties”. *Solar Energy Materials and Solar Cells*, 2001 70: 187-201.
47. J. C. M. Garnett. “Colours in Metal Glassed and in Metallic Films”. *Philos. Trans.*

R. Soc. London, 203, 385-420(1904)

48. G. A. Nikalasson, C. G. Granqvist, and O. Hunderi. “Effective Medium Models for the Optical Properties of Inhomogeneous Materials”. *Appl. Opt*. 20, 26-30(1981).
49. G. A. Nikalasson and C. G. Granqvist. “Optical Properties and Solar Selectivity of Coevaporated Co-Al2O3 Composite Film”. J. Appl. Phys. 55, (1984)
50. H. Han. “Spectrally Selective Tinoxide and Indiumoxide Coatings”. Bibliotheek Technische University, 1989.
51. G. A. Nikalasson and C. G. Granqvist. 1983 J. Materials Science. 18. 3475
52. C. M. Lampert. “Theory and Modeling of Solar Materials Solar Collectors”, *Energy Storage*, 1990, p 904
53. G. A. Nikalasson and C. G. Granqvist. “Selectively Solar-Absorbing Surface Coatings: Optical Properties and Degradation Materials Science for Solar Energy”. Conversion Systems ed C. G. Granqvist, *Pergamon*, P70
54. Q. Zhang. “Recent Progress in High-temperature Solar Selective Coatings”. *Solar Energy Materials and Solar Cells* 62(2000)63-67.
55. Q. Zhang. “Metal –AlN Cermet Solar Selective Coatings Deposited by Direct Current Magnetron Sputtering Technology”. *J. Phys. D: Appl. Phys.* 31(1988) 355-362.
56. P. Patnaik. “Dean's Analytical Chemistry Handbook”, 2nd ed. *McGraw-Hill*, 2004
57. A. H. Lu, E. L. Salabas, F. Schüth, Angew. *Chem., Int. Ed*., 2007, 46,1222–1244
58. D. Harvey. “Modern Analytical Chemistry”. *McGraw-Hill*, 2000.
59. M. N. Rahaman. “Ceramic Processing”. Boca Raton*: CRC Press*.2007; p 242–244
60. P. Sigmund. “Sputtering by Particle Bombardment”. Vol. 47, edited by R. Behrisch, *Springer Verlag*, Berlin 1981, p. 9.
61. B. Chapman, Glow Discharge Processes, *John Wiley & Sons*, New York, 1980.
62. T. V. Rajan, C. P. Sharma, A. Sharma. “Heat Treatment: Principles and Techniques”. *Prentence Hall*. (1992).p. 1.
63. J. L. Dossett. B. Howard (2006). “Practical Heat Treating”. *ASM International*. (2006). pp. 17–22.
64. “Manual of The Filmetrics F10-RT”, Filmetrics, Inc.

65. Wikipedia, “Transmission Electron Microscopy”, Retrieved Nov, 2011,
66. Semitracs. “Transmission Electron Microscopy”, Retrieved Nov, 2011,
67. M. G. Hutchins. Appl. Opt. in Solar Energy II. Czechoslovak National Academy of Sciences, 1987.
68. S. Sargent. “A Compact Table of Blackbody Radiation Function”. Bull. *Am. Meteorol*. Soc. 1972; 53: 360.
69. Y. Kang, S. Risbud, J. Rabolt, Stroeve P. “Synthesis and Characterization of Nanometer-size Fe3O4 and Gamma-Fe2O3 Particles”. *Chem Mater* 1996; 8: 2209-11.
70. D. Zhang, Z. Liu, S. Han, et al. “Magnetite (Fe3O4) Core-shell Nanowires: Synthesis and Magnetoresistance”. *Nano Lett* 2004; 4:2151-5.
71. S. Si, C. Li, X. Wang, D. Yu, Q. Peng, Y. Li. “Magnetic Monodisperse Fe3O4 Nanoparticles”. *Cryst Growth Design* 2005; 5:391-3.
72. R. Chen, G. Song, Y. Wei. “Synthesis of Variable-sized Fe3O4 Nanocrystals by Visible Light Irradiation at Room Temperature”. *J Phys Chem* C 2010; 114: 13409-13.
73. R. Vijayakumar, Y. Koltypin, I. Felner, A. Gedanken. “Sonochemical Synthesis and Characterization of Pure Nanometer-sized Fe3O4 Particles”. *Mater Sci Eng* A 2000; 286: 101-5.
74. Z. Zhou, J. Wang, X. Liu, H. Chan. “Synthesis of Fe3O4 Nanoparticles from Emulsions”. *J Mater Chem* 2001; 11: 1704-9.
75. G. Federico, B. Enrique, H. Lazaro, S. Rajaram. “Coatings of Fe3O4 Nanoparticles as Selective Absorber”. *Open Surface Science Journal*, 2011, 3, 131-135.
76. E. D. Palik. “Handbook of optical constant of solids I", *Academic Press,* 1985.
77. E. D. Palik. “Handbook of optical constant of solids II”, *Academic Press*, 1991.
78. E. D. Palik. “Handbook of optical constant of solids III”, *Academic Press*, 1998.